Impact Factor:						
	ISRA (India)	= 6.317	SIS (USA)	= 0.912	ICV (Poland)	= 6.630
	ISI (Dubai, UAE)	= 1.582	РИНЦ (Russia)	= 3.939	PIF (India)	= 1.940
	GIF (Australia)	= 0.564	ESJI (KZ)	= 8.771	IBI (India)	= 4.260
	JIF	= 1.500	SJIF (Morocco)	= 7.184	OAJI (USA)	= 0.350

SOI: 1.1/TAS DOI: 10.15863/TAS

International Scientific Journal

Theoretical & Applied Science

p-ISSN: 2308-4944 (print) **e-ISSN:** 2409-0085 (online)

Year: 2022 **Issue:** 12 **Volume:** 116

Published: 26.12.2022 **http://T-Science.org**

Issue Article

Denis Chemezov
Vladimir Industrial College
M.Sc.Eng., Corresponding Member of International Academy of Theoretical and Applied Sciences, Lecturer, Russian Federation
https://orcid.org/0000-0002-2747-552X
vic-science@yandex.ru

Andrey Kovalyov
Vladimir Industrial College
Student, Russian Federation

Ivan Chebryakov
Vladimir Industrial College
Student, Russian Federation

Dmitriy Sevrikov
Vladimir Industrial College
Student, Russian Federation

Denis Korkunov
Vladimir Industrial College
Student, Russian Federation

Matvey Sulyakov
Vladimir Industrial College
Student, Russian Federation

Arkhip Babkin
Vladimir Industrial College
Student, Russian Federation

REFERENCE DATA OF PRESSURE DISTRIBUTION ON THE SURFACES OF AIRFOILS HAVING THE NAMES BEGINNING WITH THE LETTER N (THE SECOND PART)

Abstract: *The results of the computer calculation of air flow around the airfoils having the names beginning with the letter N (continuation) are presented in the article. The contours of pressure distribution on the surfaces of the airfoils at angles of attack of 0, 15 and -15 degrees in conditions of the subsonic airplane flight speed were obtained.*

Key words: *the airfoil, the angle of attack, pressure, the surface.*

Language: *English*

Citation: Chemezov, D., et al. (2022). Reference data of pressure distribution on the surfaces of airfoils having the names beginning with the letter N (the second part). *ISJ Theoretical & Applied Science, 12 (116),* 901-990.

Soi: http://s-o-i.org/1.1/TAS-12-116-73 ***Doi***: crossref https://dx.doi.org/10.15863/TAS.2022.12.116.73

Scopus ASCC: *1507.*

Introduction

Creating reference materials that determine the most accurate pressure distribution on the airfoil surfaces is an actual task of the airplane aerodynamics.

Materials and methods

The study of air flow around the airfoils was carried out in a two-dimensional formulation by means of the computer calculation in the *Comsol Multiphysics* program. The airfoils in the cross section were taken as objects of research [1-29]. In this work, the airfoils having the names beginning with the letter *N* were adopted. Air flow around the airfoils was carried out at angles of attack (α) of 0, 15 and -15 degrees. Flight speed of the airplane in each case was subsonic. The airplane flight in the atmosphere was carried out under normal weather conditions. The geometric characteristics of the studied airfoils are presented in the Table 1. The geometric shapes of the airfoils in the cross section are presented in the Table 2.

Table 1. The geometric characteristics of the airfoils.

Airfoil name	Max. thickness	Max. camber	Leading edge radius	Trailing edge thickness
NACA 67A018	17.99% at 50.0% of the chord	0.0% at 0.0% of the chord	1.6466%	0.0%
NACA 6-H-10	10.02% at 40.0% of the chord	4.51% at 40.0% of the chord	0.8057%	0.0%
NACA 6-H-15	15.58% at 40.0% of the chord	4.51% at 40.0% of the chord	1.274%	0.0%
NACA 6-H-20	19.95% at 40.0% of the chord	6.13% at 40.0% of the chord	2.1369%	0.0%
NACA 77 A	9.5% at 30.0% of the chord	0.0% at 0.0% of the chord	1.014%	0.2%
NACA 8-H-12	11.98% at 30.0% of the chord	3.54% at 30.0% of the chord	1.0409%	0.0%
NACA 97	14.32% at 30.0% of the chord	8.37% at 40.0% of the chord	2.8886%	0.13%
NACA BR 63-55-12	11.9% at 30.0% of the chord	3.98% at 40.0% of the chord	1.1658%	0.0%
NACA M10	6.19% at 30.0% of the chord	1.91% at 30.0% of the chord	0.7135%	0.39%
NACA M11	8.15% at 30.0% of the chord	1.88% at 30.0% of the chord	0.8615%	0.0%
NACA M12	11.93% at 30.0% of the chord	2.04% at 30.0% of the chord	1.3654%	0.4%
NACA M13	6.21% at 30.0% of the chord	3.91% at 30.0% of the chord	0.6791%	0.44%
NACA M14	8.06% at 30.0% of the chord	3.97% at 30.0% of the chord	0.8406%	0.42%
NACA M15	12.0% at 30.0% of the chord	3.83% at 30.0% of the chord	1.3716%	0.45%
NACA M16	6.15% at 30.0% of the chord	4.11% at 30.0% of the chord	0.6754%	0.56%
NACA M17	8.08% at 40.0% of the chord	4.11% at 30.0% of the chord	0.8194%	0.41%
NACA M18	12.02% at 30.0% of the chord	4.18% at 30.0% of the chord	1.3708%	0.44%
NACA M19	6.17% at 30.0% of the chord	6.03% at 30.0% of the chord	0.6482%	0.38%
NACA M2	8.0% at 30.0% of the chord	0.0% at 0.0% of the chord	0.8678%	0.4%
NACA M20	8.15% at 30.0% of the chord	6.13% at 30.0% of the chord	0.8375%	0.47%
NACA M21	11.95% at 30.0% of the chord	6.04% at 30.0% of the chord	1.3832%	0.48%
NACA M22	6.25% at 30.0% of the chord	6.3% at 30.0% of the chord	0.6553%	0.53%
NACA M23	8.14% at 30.0% of the chord	6.38% at 30.0% of the chord	0.7975%	0.54%
NACA M24	11.94% at 30.0% of the chord	6.34% at 30.0% of the chord	1.3453%	0.47%
NACA M25	6.27% at 30.0% of the chord	8.23% at 30.0% of the chord	0.6671%	0.45%
NACA M26	8.3% at 40.0% of the chord	8.25% at 30.0% of the chord	0.7925%	0.48%
NACA M27	11.94% at 30.0% of the chord	8.36% at 30.0% of the chord	1.3042%	0.52%
NACA M3	11.9% at 30.0% of the chord	0.0% at 0.0% of the chord	1.396%	0.4%
NACA M4	6.28% at 30.0% of the chord	2.21% at 30.0% of the chord	0.7059%	0.49%
NACA M5	8.21% at 30.0% of the chord	2.07% at 30.0% of the chord	0.8627%	0.63%
NACA M6	12.01% at 30.0% of the chord	2.21% at 30.0% of the chord	1.3998%	0.52%
NACA M7	6.19% at 40.0% of the chord	5.0% at 30.0% of the chord	0.9013%	0.47%
NACA M8	11.72% at 15.0% of the chord	8.04% at 30.0% of the chord	1.8128%	0.0%
NACA M9	10.4% at 15.0% of the chord	7.18% at 30.0% of the chord	1.4686%	0.0%
NACA/Munk M-10	6.19% at 30.0% of the chord	1.91% at 30.0% of the chord	0.1624%	0.39%
NACA/Munk M-7	6.18% at 40.0% of the chord	5.0% at 30.0% of the chord	0.533%	0.47%
NACA/Munk M-8	11.7% at 15.0% of the chord	8.03% at 30.0% of the chord	1.2388%	0.0%
NACA/Munk M-9	10.39% at 15.0% of the chord	7.17% at 30.0% of the chord	0.8791%	0.0%
NACA0009	9.02% at 30.9% of the chord	0.0% at 0.0% of the chord	0.5385%	0.0%
NACA-0009 9,0% smoothed	9.02% at 30.9% of the chord	0.0% at 0.0% of the chord	0.5385%	0.0%
NACA0012	12.0% at 30.9% of the chord	0.0% at 0.0% of the chord	1.4782%	0.252%
NACA0018	18.01% at 30.0% of the chord	0.0% at 0.0% of the chord	3.1017%	0.378%
NACA1408	8.47% at 32.4% of the chord	1.72% at 37.5% of the chord	0.4195%	0.0%
NACA1410	10.01% at 30.1% of the chord	1.0% at 40.0% of the chord	1.0934%	0.204%
NACA1412	12.01% at 30.1% of the chord	1.0% at 40.0% of the chord	1.3525%	0.243%
NACA2408	8.0% at 30.1% of the chord	2.0% at 40.0% of the chord	0.8684%	0.158%
NACA2410	10.01% at 30.1% of the chord	1.99% at 40.0% of the chord	1.0907%	0.195%
NACA2411	11.0% at 29.8% of the chord	2.5% at 39.6% of the chord	1.2891%	0.0%
NACA2412	12.0% at 30.9% of the chord	2.0% at 40.2% of the chord	1.2273%	0.0%
NACA2415	14.99% at 30.9% of the chord	2.01% at 40.2% of the chord	2.0939%	0.0%
NACA2418	18.0% at 30.0% of the chord	2.0% at 40.0% of the chord	3.1519%	0.0%

NACA3412	11.99% at 30.9% of the chord	3.0% at 40.2% of the chord	0.8527%	0.065%
NACA4309	9.0% at 30.0% of the chord	4.0% at 30.0% of the chord	0.9316%	0.0%
NACA4409	9.01% at 30.9% of the chord	3.97% at 40.2% of the chord	0.7547%	0.0%
NACA4412	12.02% at 30.0% of the chord	4.0% at 40.0% of the chord	1.4734%	1.13%
NACA4415	15.0% at 30.0% of the chord	4.0% at 40.0% of the chord	2.2447%	0.32%
NACA4418	18.02% at 30.0% of the chord	4.0% at 40.0% of the chord	3.2207%	0.38%
NACA5412	12.01% at 30.0% of the chord	5.0% at 40.0% of the chord	1.4857%	0.065%
NACA6306	6.0% at 30.0% of the chord	6.0% at 30.0% of the chord	0.6401%	0.0%
NACA-64	15.73% at 30.0% of the chord	7.87% at 30.0% of the chord	1.8013%	2.25%
NACA6409	9.01% at 30.0% of the chord	6.0% at 39.6% of the chord	0.8992%	0.0%
NACA6409 9%	9.01% at 30.0% of the chord	6.0% at 39.6% of the chord	0.8992%	0.0%
NACA6412	12.07% at 30.2% of the chord	6.02% at 44.8% of the chord	1.6785%	0.22%
NACA6509	9.1% at 40.0% of the chord	6.55% at 40.0% of the chord	1.5216%	0.0%
NACA-66	11.8% at 30.0% of the chord	5.9% at 30.0% of the chord	1.0984%	1.7%
NACA-69	7.58% at 30.0% of the chord	3.79% at 30.0% of the chord	0.6916%	1.15%
NACA-CYH	11.7% at 30.0% of the chord	5.85% at 30.0% of the chord	1.2661%	0.2%
NACA-K6E	14.91% at 33.9% of the chord	3.73% at 55.1% of the chord	0.8796%	0.0%
NACA-K6M	13.44% at 32.1% of the chord	3.39% at 41.3% of the chord	1.0958%	0.0%
NACA-K6S	95.49% at 200.0% of the chord	28.75% at 300.0% of the chord	1.158%	0.0%
NACA-LANGLEY SYMMETRICAL, SUPERCRITICAL	10.96% at 40.0% of the chord	0.0% at 0.0% of the chord	1.9204%	0.0%
NACA-M1	6.16% at 30.0% of the chord	0.0% at 0.0% of the chord	0.7497%	0.4%
NACA-NASA/AMES/Hicks 63(1)-212 MOD A	11.96% at 41.1% of the chord	2.45% at 21.4% of the chord	3.0061%	0.0%
NACA-NASA/AMES/Hicks 63(1)-212 MOD B	12.05% at 35.1% of the chord	1.49% at 10.1% of the chord	1.3903%	0.0%
NACA-NASA/AMES/Hicks 63(2)-215 MOD B	15.04% at 32.5% of the chord	1.49% at 10.0% of the chord	1.3861%	0.0%
NACM14	8.08% at 30.0% of the chord	4.97% at 30.0% of the chord	0.8423%	0.42%
Narramore JN153	17.57% at 29.9% of the chord	8.35% at 38.0% of the chord	3.8093%	0.0%
NASA NLF1015	14.99% at 40.3% of the chord	4.7% at 61.1% of the chord	0.9583%	0.0%
NASA GA [W] 1-12 17	11.98% at 40.0% of the chord	1.52% at 60.0% of the chord	1.306%	0.5%
NASA NLF(1)-0115	14.96% at 40.6% of the chord	1.83% at 30.8% of the chord	1.2803%	0.0%
NASA NLF(1)-1015	14.99% at 40.3% of the chord	4.7% at 61.1% of the chord	0.9583%	0.0%
NASA RC(4)-10	9.98% at 37.8% of the chord	2.13% at 30.3% of the chord	1.4162%	0.1582%
NASA RC(5)-10	9.96% at 40.1% of the chord	2.21% at 25.3% of the chord	1.0539%	0.1583%
NASA SC(2)-0010	10.0% at 37.0% of the chord	0.0% at 0.0% of the chord	1.8764%	0.5%
NASA SC(2)-0012	12.0% at 37.0% of the chord	0.0% at 0.0% of the chord	2.2548%	0.6%
NASA SC(2)-0402	2.0% at 34.0% of the chord	0.16% at 79.0% of the chord	1.3878%	0.19%
NASA SC(2)-0403	3.0% at 36.0% of the chord	0.39% at 81.0% of the chord	1.3792%	0.24%
NASA SC(2)-0404	4.01% at 37.0% of the chord	0.47% at 80.0% of the chord	1.3801%	0.285%
NASA SC(2)-0406	6.02% at 35.0% of the chord	0.35% at 79.0% of the chord	1.4316%	0.39%
NASA SC(2)-0410	9.97% at 38.0% of the chord	1.18% at 85.0% of the chord	1.8758%	0.49%
NASA SC(2)-0412	12.0% at 37.0% of the chord	1.35% at 83.0% of the chord	2.294%	0.55%
NASA SC(2)-0414	14.0% at 36.0% of the chord	1.52% at 84.0% of the chord	2.8516%	0.6%
NASA SC(2)-0503	3.01% at 32.0% of the chord	0.21% at 79.0% of the chord	1.3802%	0.24%
NASA SC(2)-0518	17.98% at 35.0% of the chord	1.48% at 82.0% of the chord	4.3098%	0.69%
NASA SC(2)-0606	6.0% at 34.0% of the chord	0.37% at 75.0% of the chord	1.4337%	0.41%
NASA SC(2)-0610	9.98% at 38.0% of the chord	1.02% at 80.0% of the chord	1.8743%	0.49%
NASA SC(2)-0612	12.0% at 37.0% of the chord	1.13% at 81.0% of the chord	2.2923%	0.58%
NASA SC(2)-0614	13.99% at 36.0% of the chord	1.25% at 80.0% of the chord	2.8472%	0.66%
NASA SC(2)-0706	6.0% at 34.0% of the chord	0.38% at 77.0% of the chord	1.4343%	0.39%
NASA SC(2)-0710	9.98% at 37.0% of the chord	0.95% at 80.0% of the chord	1.8738%	0.49%
NASA SC(2)-0712	11.99% at 37.0% of the chord	1.03% at 79.0% of the chord	2.2897%	0.6%
NASA SC(2)-0714	13.96% at 37.0% of the chord	1.5% at 80.0% of the chord	2.8264%	0.7%
NASA SC(2)-1006	6.0% at 30.0% of the chord	0.03% at 13.0% of the chord	1.428%	0.39%
NASA SC(2)-1010	10.0% at 32.0% of the chord	0.02% at 16.0% of the chord	1.8782%	0.61%
NASA/AMES	7.73% at 30.0% of the chord	0.55% at 65.0% of the chord	2.5812%	0.7%
NASA/AMES/Hicks A-01	10.28% at 35.0% of the chord	1.41% at 15.0% of the chord	1.2997%	0.599%
NASA/AMES/Hicks A-02	7.73% at 30.0% of the chord	0.55% at 65.0% of the chord	2.5812%	0.7%
NASA/AMES/Kennelly A-03	10.0% at 37.5% of the chord	1.21% at 17.5% of the chord	0.8628%	0.6%
NASA-AMES 63A108 MOD C	7.73% at 30.0% of the chord	0.55% at 65.0% of the chord	2.5812%	0.7%
NASA-AMES A-01	10.28% at 35.0% of the chord	1.41% at 15.0% of the chord	1.2997%	0.599%
NASA-AMES A-02	7.74% at 30.0% of the chord	0.55% at 65.0% of the chord	2.5809%	0.7%
NASA-AMES A-03	10.0% at 37.5% of the chord	1.21% at 17.5% of the chord	0.8638%	0.6%
NASA F G8	10.04% at 20.0% of the chord	3.67% at 30.0% of the chord	2.0782%	0.58%
NASA F PG 7	8.9% at 20.0% of the chord	3.41% at 20.0% of the chord	1.3069%	0.0%
NASA-LANGLEY 64-012	11.96% at 40.0% of the chord	0.0% at 0.0% of the chord	0.7718%	0.0%
NASA-LANGLEY LS(1)-0013	12.86% at 40.0% of the chord	0.0% at 0.0% of the chord	1.2655%	0.604%

NASA-LANGLEY LS(1)-0413 (GA(W)-2)	12.93% at 37.5% of the chord	2.14% at 62.5% of the chord	1.4792%	0.55%
NASA-LANGLEY LS(1)-0413MOD	13.02% at 35.0% of the chord	1.99% at 32.5% of the chord	1.3564%	0.51%
NASA-LANGLEY LS(1)-0417 (GA(W)-1)	16.98% at 40.0% of the chord	2.17% at 65.0% of the chord	2.9706%	0.709%
NASA-LANGLEY LS(1)-0417MOD	17.0% at 30.2% of the chord	2.33% at 20.2% of the chord	3.5598%	0.732%
NASA-LANGLEY LS(1)-0421	20.89% at 40.0% of the chord	2.14% at 62.5% of the chord	4.1137%	0.902%
NASA-LANGLEY LS(1)-0421MOD	20.96% at 32.5% of the chord	2.08% at 25.0% of the chord	4.1897%	0.9%
NASA-LANGLEY MS(1)-0317	17.01% at 37.5% of the chord	1.51% at 70.0% of the chord	2.7082%	0.722%
NASA-LANGLEY MS(1)-0413	13.14% at 37.5% of the chord	1.58% at 65.0% of the chord	1.5702%	0.5583%
NASA-LANGLEY NLF 0414F	14.17% at 43.6% of the chord	2.41% at 51.3% of the chord	1.4857%	0.0392%
NASA-LANGLEY NLF(1)-0215F	14.95% at 41.6% of the chord	3.95% at 41.6% of the chord	1.2778%	0.0%
NASA-LANGLEY NLF(1)-0416	15.95% at 32.3% of the chord	2.44% at 32.3% of the chord	1.3631%	0.0%
NASA-LANGLEY NLF(2)-0415	15.02% at 46.1% of the chord	2.96% at 73.1% of the chord	0.7186%	0.0%
NASA-LANGLEY RC-08(B)3	8.0% at 37.8% of the chord	1.1% at 34.1% of the chord	0.751%	0.18%
NASA-LANGLEY RC-08(N)1	8.02% at 37.4% of the chord	1.56% at 25.0% of the chord	0.3816%	0.128%
NASA-LANGLEY RC08-64C	8.0% at 40.0% of the chord	1.0% at 35.0% of the chord	3.3467%	0.16%
NASA-LANGLEY RC-10(B)3	9.97% at 37.7% of the chord	1.71% at 34.0% of the chord	1.0679%	0.2%
NASA-LANGLEY RC-10(N)1	10.01% at 37.4% of the chord	1.49% at 25.0% of the chord	0.6105%	0.159%
NASA-LANGLEY RC10-64C	10.0% at 40.0% of the chord	1.0% at 35.0% of the chord	1.0054%	0.2%
NASA-LANGLEY RC-12(B)3	12.0% at 38.0% of the chord	2.22% at 34.3% of the chord	1.2622%	0.25%
NASA-LANGLEY RC-12(N)1	12.02% at 37.4% of the chord	1.38% at 30.0% of the chord	0.8855%	0.19%
NASA-LANGLEY RC12-64C	12.0% at 40.0% of the chord	1.0% at 35.0% of the chord	2.1965%	0.24%
NASA-LANGLEY RC-SC2	9.97% at 40.0% of the chord	0.6% at 65.0% of the chord	1.7584%	0.21%
NASA-LANGLEY SC(2)-0714 SUPERCRITICAL	13.97% at 37.0% of the chord	1.48% at 80.0% of the chord	2.8282%	0.7%
NASANLF1	14.96% at 40.6% of the chord	1.83% at 30.8% of the chord	1.3874%	0.06%
NASA-SC2	13.93% at 37.0% of the chord	1.48% at 80.0% of the chord	2.3052%	0.59%
NAVY-N-9	8.23% at 30.0% of the chord	4.14% at 30.0% of the chord	0.8246%	0.25%
Neelmeyer	8.9% at 30.0% of the chord	4.45% at 30.0% of the chord	1.4817%	0.3%
NEUMANN	9.0% at 25.0% of the chord	7.3% at 40.0% of the chord	1.2396%	0.0%
NLF(1)-0115	14.96% at 40.6% of the chord	1.83% at 30.8% of the chord	1.2803%	0.0%
NLR-1T	8.7% at 38.3% of the chord	1.26% at 22.3% of the chord	0.7321%	0.208%
NLR-7223-43	8.61% at 38.1% of the chord	1.35% at 74.1% of the chord	0.9011%	0.0%
NLR-7223-62	8.61% at 38.1% of the chord	1.25% at 21.5% of the chord	0.9043%	0.0%
NLR-7301	16.52% at 35.0% of the chord	1.66% at 75.0% of the chord	5.2858%	0.11%
NPL	10.67% at 35.8% of the chord	0.84% at 81.8% of the chord	1.4008%	0.0%
NPL 9510	11.08% at 32.0% of the chord	1.62% at 80.0% of the chord	1.8092%	0.488%
NPL 9615	11.3% at 34.0% of the chord	1.01% at 19.4% of the chord	1.3007%	0.026%
NPL 9626	12.06% at 30.8% of the chord	0.73% at 30.8% of the chord	1.7414%	0.252%
NPL 9627	12.16% at 30.8% of the chord	0.9% at 40.2% of the chord	1.6806%	0.252%
NPL 9660	11.3% at 34.0% of the chord	1.01% at 19.4% of the chord	1.3007%	0.26%
NPL transonic airfoil FROM ARC CP 1372	10.67% at 35.8% of the chord	0.84% at 81.8% of the chord	1.4008%	0.0%
NWINGLET	0.0% at 0.0% of the chord	2.41% at 60.0% of the chord	0.7316%	0.0%
NYU-GRUMMAN K-1	11.59% at 31.7% of the chord	1.96% at 75.0% of the chord	3.2522%	0.1%

Note:
NACA 67A018 (Generato da Profili);
NACA 77 A (USA);
NACA 97 (USA);
NACA BR 63-55-12 (USA);
NACA-K6E (Emplanture aile du K6E MPX);
NACA-K6M (mediane aile du K6E MPX);
NACA-K6S (Saumon aile du K6E MPX);
NASA GA [W] 1-12 17 (J. Whitcomb (USA));
NASA/AMES (modification of the NACA 63A-108 airfoil);
NASA/AMES/Hicks A-01 (transonic rotorcraft airfoil);
NASA/AMES/Hicks A-02 (transonic rotorcraft airfoil);
NASA/AMES/Kennelly A-03 (transonic rotorcraft airfoil);
NASA F G8 (F. Gale' (Italy));
NASA F PG 7 (F. Piantanida - F. Gale' (Italy));
Neelmeyer (K. Neelmeyer (Holland)).

Table 2. The geometric shapes of the airfoils in the cross section.

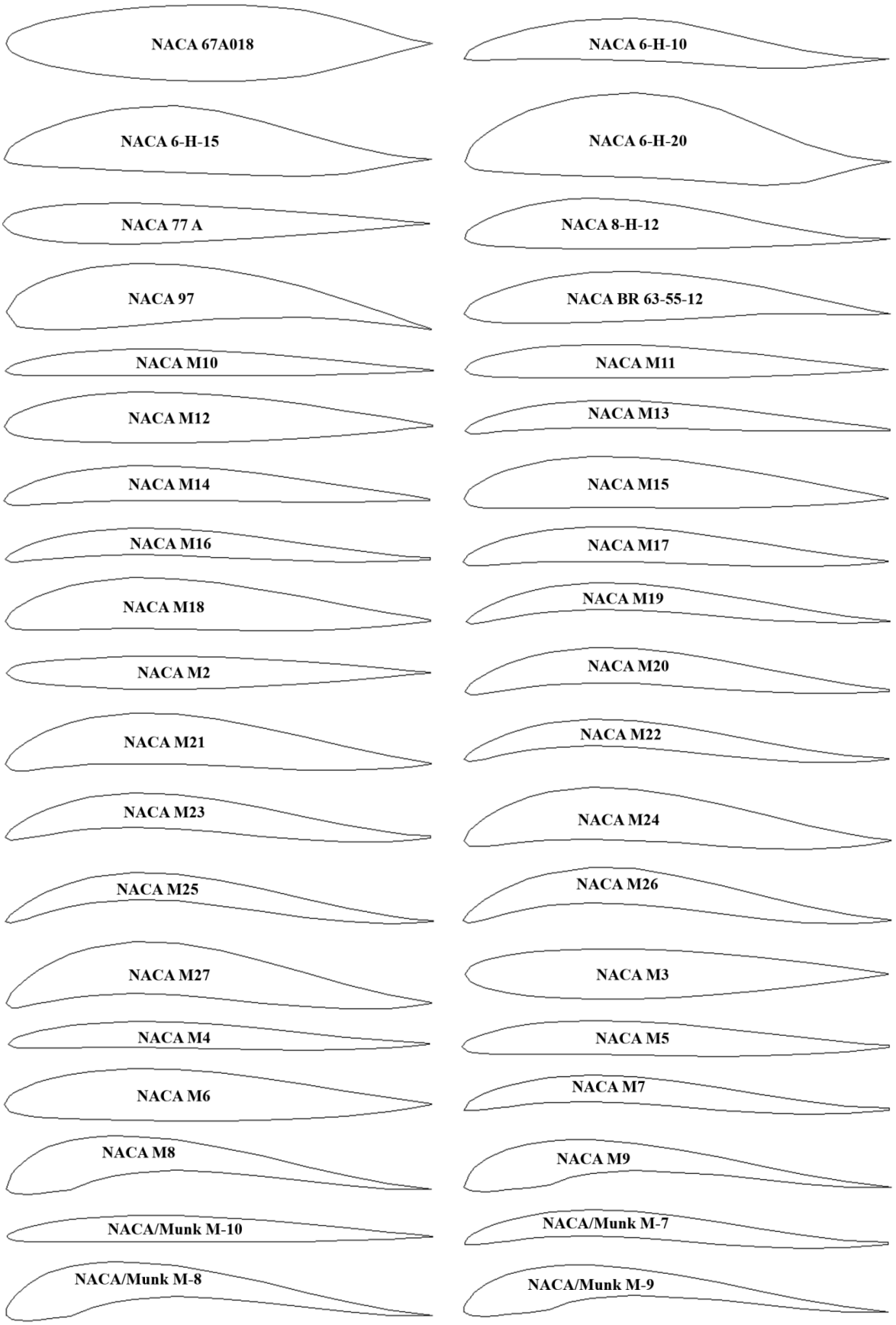

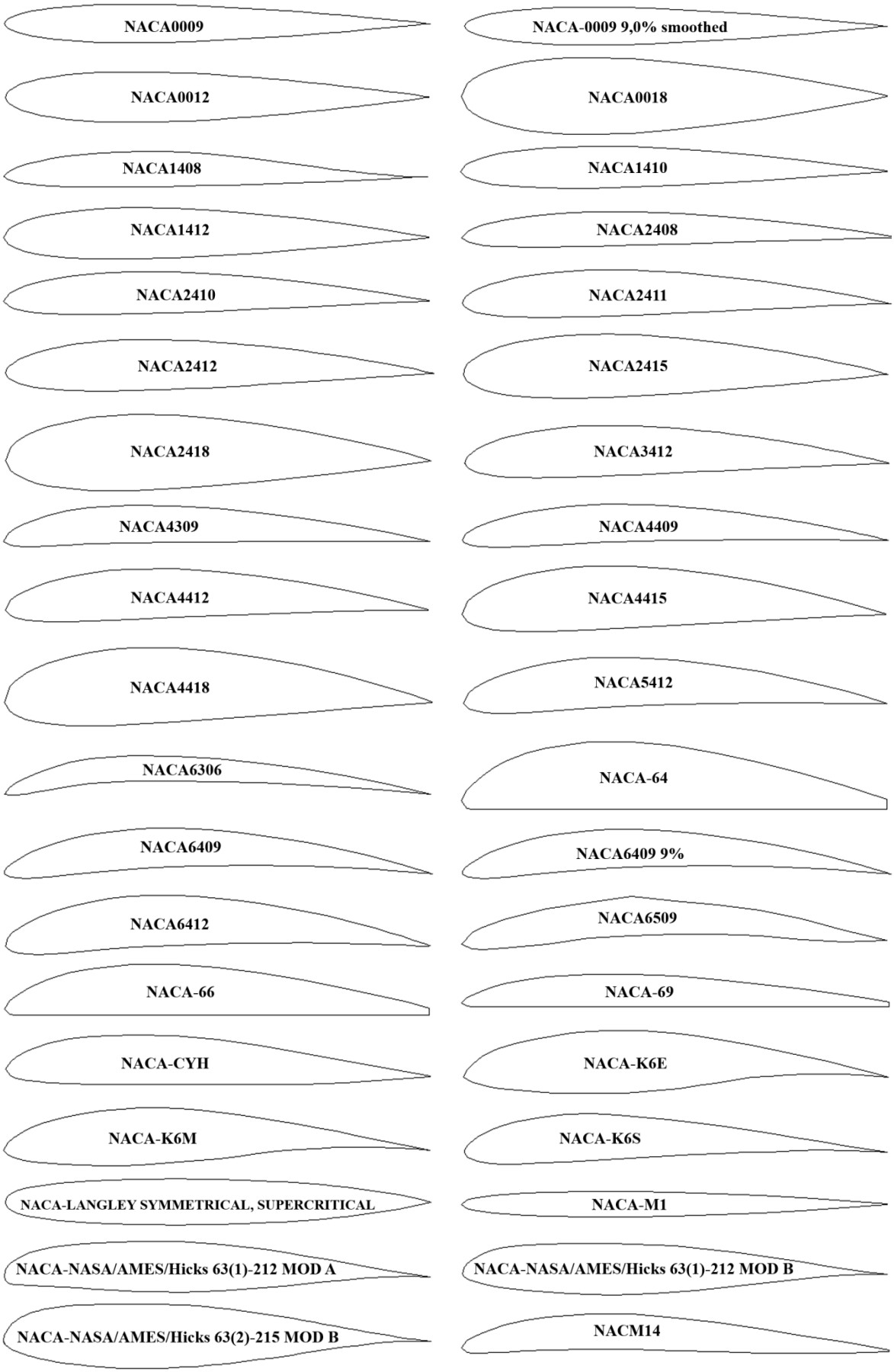
NACA0009
NACA-0009 9,0% smoothed
NACA0012
NACA0018
NACA1408
NACA1410
NACA1412
NACA2408
NACA2410
NACA2411
NACA2412
NACA2415
NACA2418
NACA3412
NACA4309
NACA4409
NACA4412
NACA4415
NACA4418
NACA5412
NACA6306
NACA-64
NACA6409
NACA6409 9%
NACA6412
NACA6509
NACA-66
NACA-69
NACA-CYH
NACA-K6E
NACA-K6M
NACA-K6S
NACA-LANGLEY SYMMETRICAL, SUPERCRITICAL
NACA-M1
NACA-NASA/AMES/Hicks 63(1)-212 MOD A
NACA-NASA/AMES/Hicks 63(1)-212 MOD B
NACA-NASA/AMES/Hicks 63(2)-215 MOD B
NACM14

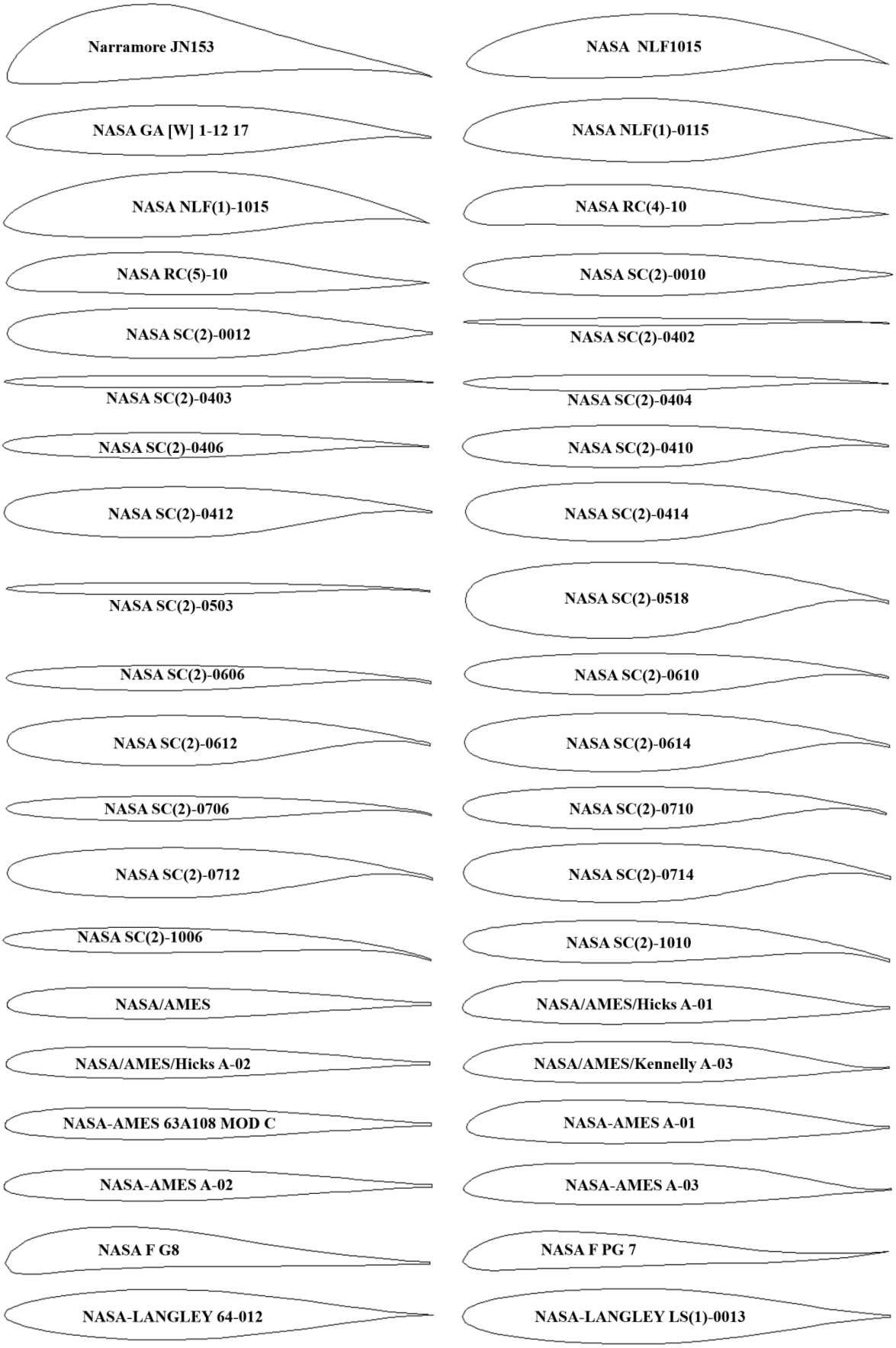
Narramore JN153
NASA NLF1015
NASA GA [W] 1-12 17
NASA NLF(1)-0115
NASA NLF(1)-1015
NASA RC(4)-10
NASA RC(5)-10
NASA SC(2)-0010
NASA SC(2)-0012
NASA SC(2)-0402
NASA SC(2)-0403
NASA SC(2)-0404
NASA SC(2)-0406
NASA SC(2)-0410
NASA SC(2)-0412
NASA SC(2)-0414
NASA SC(2)-0503
NASA SC(2)-0518
NASA SC(2)-0606
NASA SC(2)-0610
NASA SC(2)-0612
NASA SC(2)-0614
NASA SC(2)-0706
NASA SC(2)-0710
NASA SC(2)-0712
NASA SC(2)-0714
NASA SC(2)-1006
NASA SC(2)-1010
NASA/AMES
NASA/AMES/Hicks A-01
NASA/AMES/Hicks A-02
NASA/AMES/Kennelly A-03
NASA-AMES 63A108 MOD C
NASA-AMES A-01
NASA-AMES A-02
NASA-AMES A-03
NASA F G8
NASA F PG 7
NASA-LANGLEY 64-012
NASA-LANGLEY LS(1)-0013

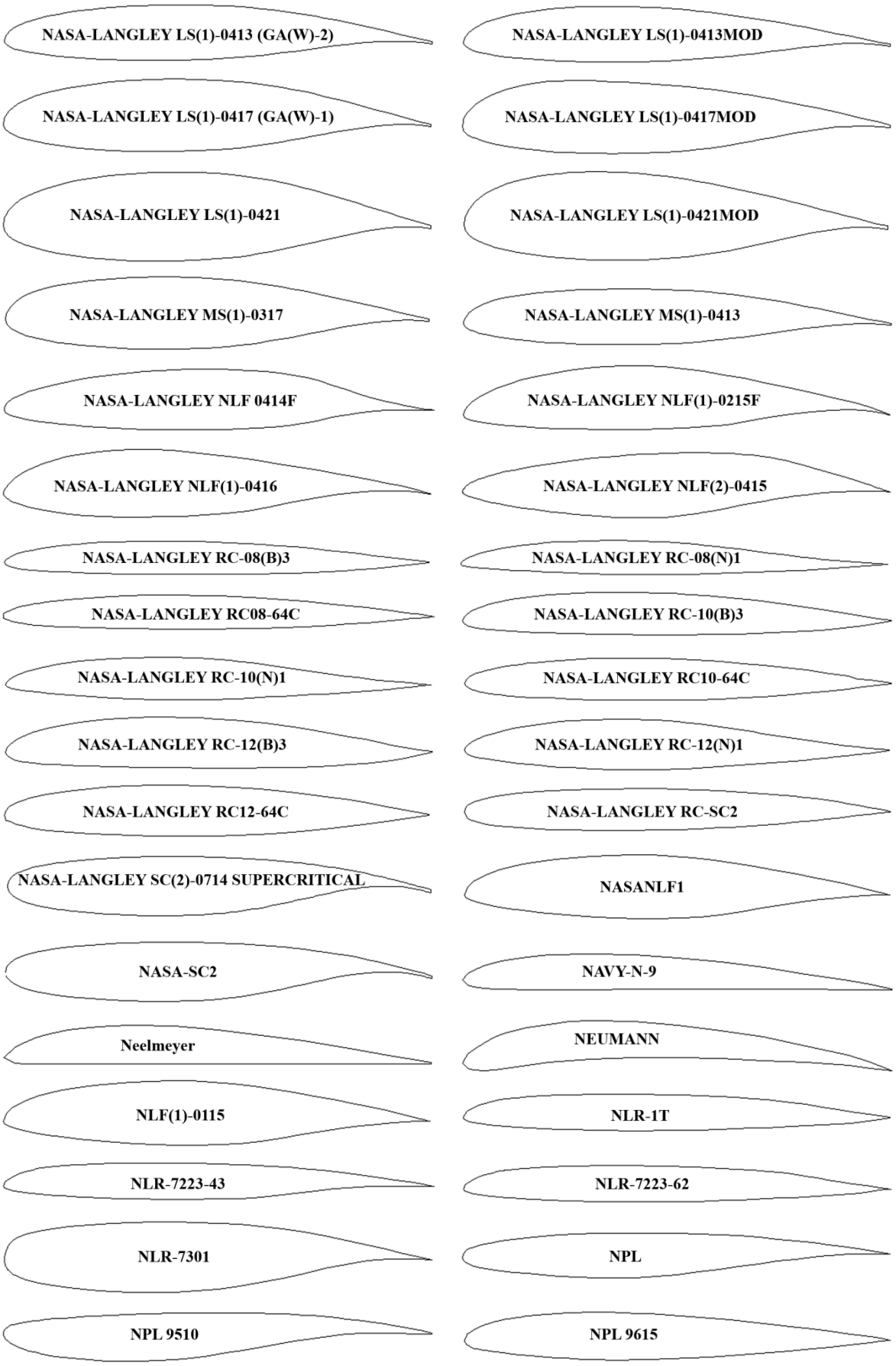
NASA-LANGLEY LS(1)-0413 (GA(W)-2)
NASA-LANGLEY LS(1)-0413MOD
NASA-LANGLEY LS(1)-0417 (GA(W)-1)
NASA-LANGLEY LS(1)-0417MOD
NASA-LANGLEY LS(1)-0421
NASA-LANGLEY LS(1)-0421MOD
NASA-LANGLEY MS(1)-0317
NASA-LANGLEY MS(1)-0413
NASA-LANGLEY NLF 0414F
NASA-LANGLEY NLF(1)-0215F
NASA-LANGLEY NLF(1)-0416
NASA-LANGLEY NLF(2)-0415
NASA-LANGLEY RC-08(B)3
NASA-LANGLEY RC-08(N)1
NASA-LANGLEY RC08-64C
NASA-LANGLEY RC-10(B)3
NASA-LANGLEY RC-10(N)1
NASA-LANGLEY RC10-64C
NASA-LANGLEY RC-12(B)3
NASA-LANGLEY RC-12(N)1
NASA-LANGLEY RC12-64C
NASA-LANGLEY RC-SC2
NASA-LANGLEY SC(2)-0714 SUPERCRITICAL
NASANLF1
NASA-SC2
NAVY-N-9
Neelmeyer
NEUMANN
NLF(1)-0115
NLR-1T
NLR-7223-43
NLR-7223-62
NLR-7301
NPL
NPL 9510
NPL 9615

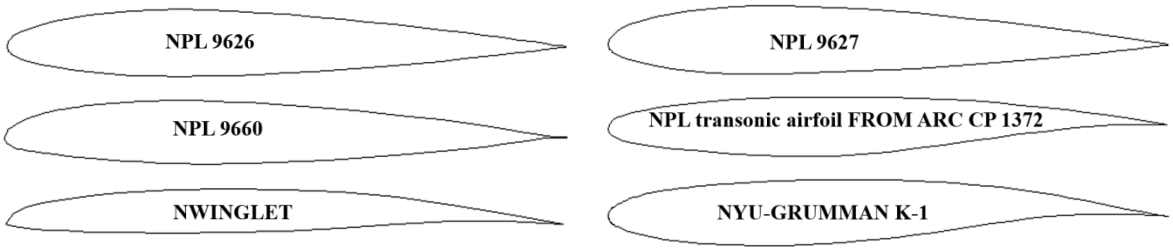

Results and discussion

The calculated pressure contours on the surfaces of the airfoils at different angles of attack are presented in the Figs. 1-158. The calculated values on the scale can be represented as the basic values when comparing the pressure drop under conditions of changing the angle of attack of the airfoils.

158 airfoils of the airplane wings were considered. The studied airfoils were both asymmetrical and symmetrical (for example, NACA 67A018, NACA 77 A, NACA M2, NACA M3, NACA0009, NACA-0009 9,0% smoothed, NACA0012, NACA0018, NACA-LANGLEY SYMMETRICAL, SUPERCRITICAL, NACA-M1, NASA SC(2)-0010, NASA SC(2)-0012, NASA-LANGLEY 64-012 and NASA-LANGLEY LS(1)-0013).

The rational geometry of the airfoil of the airplane wing allows for high lift and low drag coefficient. The geometry analysis allows you to select a number of airfoils for a detailed assessment of the aerodynamic characteristics of the airplane wings. The maximum thickness along the chord is observed for NASA-LANGLEY LS(1)-0421MOD (20.96%), the minimum thickness along the chord is observed for NASA SC(2)-0402 (2.0%) from the considered airfoils. The airfoils of the airplane wings with the camber have the better aerodynamic characteristics. The camber of the NACA 97 airfoil is 8.37%, and the camber of all symmetrical airfoils is 0.0% relative to the chord length, which is the largest and smallest ratios among all the studied airfoils, respectively. Increasing the radius of the leading edge of the airfoil increases drag. The smallest and largest leading edge radii are 0.1624% and 5.2858% for the NACA/Munk M-10 and NLR-7301 airfoils, respectively. The minimum thickness of the trailing edge of some airfoils is 0.0%. The maximum thickness of the trailing edge (2.25%) is determined for the NACA-64 airfoil.

Consideration of the calculation results for each airfoil will lead to a significant increase in the volume of the article. Therefore, let us consider in detail the change in pressure on the surfaces of several proposed airfoils under conditions of changing the angle of attack: NACA 6-H-10, NACA 6-H-20, NACA M22, NACA/Munk M-8, Narramore JN153, NASA SC(2)-0402, NASA SC(2)-0712, NASA F PG 7, Neelmeyer and NWINGLET.

The NACA 6-H-10 airfoil is subjected to maximum loads during the airplane climb. However, pressure decreases by 6 times during the descent airplane, which is due to thickening on the side of the upper surface.

However, with an increase in the thickness of the airfoil, for example, NACA 6-H-20, the lifting force of the airplane wing decreases. Negative pressure increases on the leading edge of the airfoil at a negative angle of attack.

The NACA M22 curved airfoil is characterized by high lift during the climb and minimal pressure on all surfaces during the airplane descent. The pressure difference on the upper and lower surfaces of the airfoil varies by almost 10 times.

The same values of positive and negative pressures are observed at both positive and negative angles of attack of the NACA/Munk M-8 airfoil. The lifting force of the airplane wing is low.

The load increases slightly when air flows around the Narramore JN153 airfoil. This is true both during the climb and during the descent of the airplane. The configuration of the airfoil does not provide high lift of the airplane wing.

The NASA SC(2)-0402 airfoil is effectively used for high-speed movements of the airplane in the horizontal direction. The lifting force of the airplane wing is minimal during maneuvers.

At small angles of attack, the camber in the region of the trailing edge of the NASA SC(2)-0712 airfoil does not affect the overall intensity of pressure formation. The leading edge of the airfoil at an angle of attack of 15 degrees experiences maximum pressure.

A decrease in the thickness of the airfoil contributes to an increase in the pressure difference on the wing surfaces of the airplane. This is confirmed by comparing the NASA F PG 7 and NASA F G8 airfoils. It is noted that for the NASA F PG 7 airfoil at an angle of attack of 15 degrees, the pressure difference on the surfaces changes by 8 times.

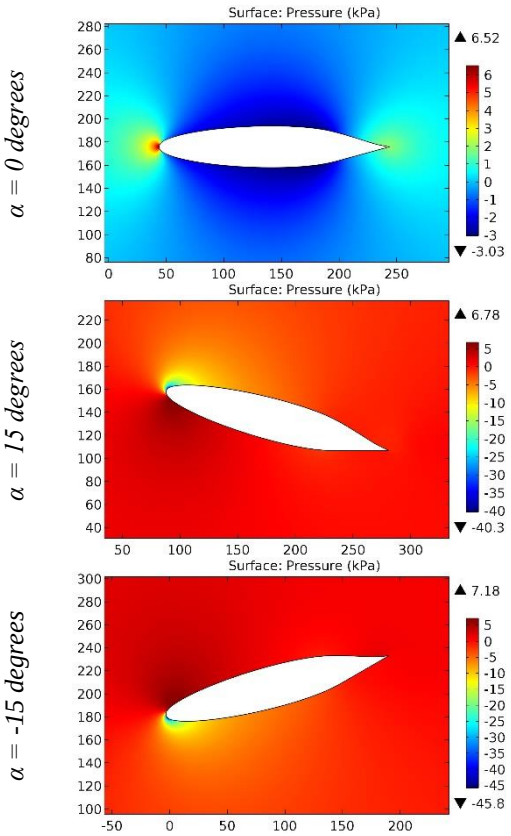

Figure 1. The pressure contours on the surfaces of the NACA 67A018 airfoil.

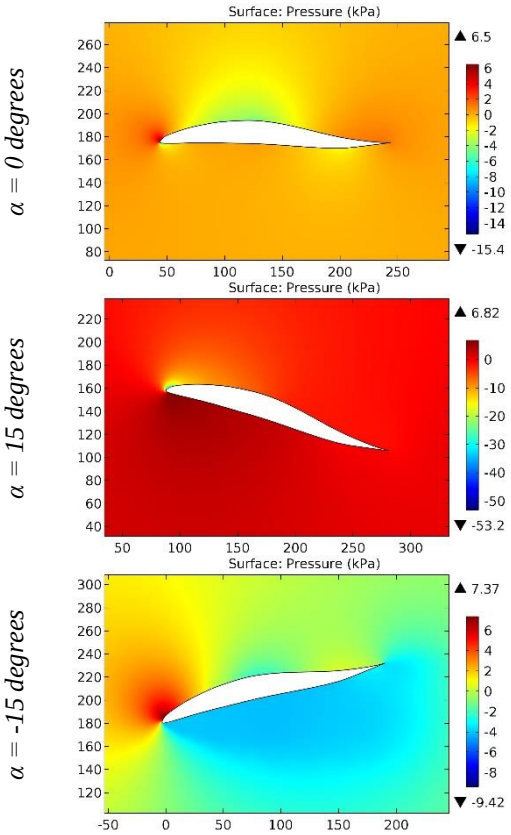

Figure 2. The pressure contours on the surfaces of the NACA 6-H-10 airfoil.

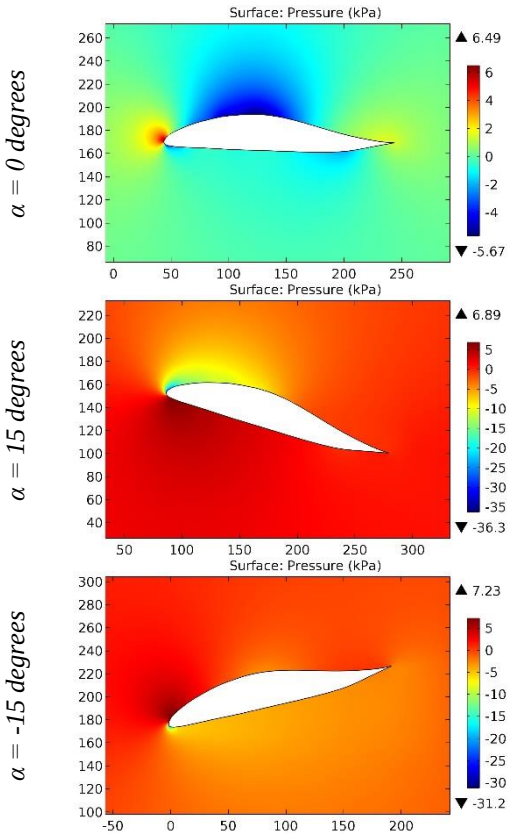

Figure 3. The pressure contours on the surfaces of the NACA 6-H-15 airfoil.

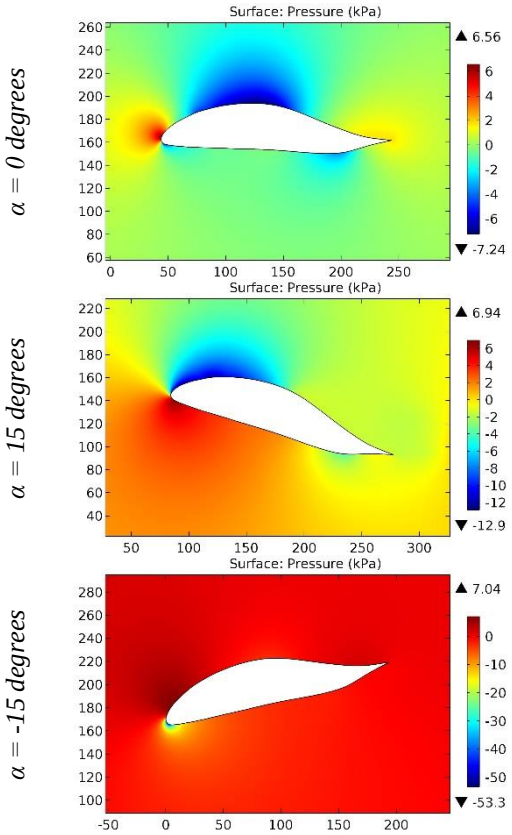

Figure 4. The pressure contours on the surfaces of the NACA 6-H-20 airfoil.

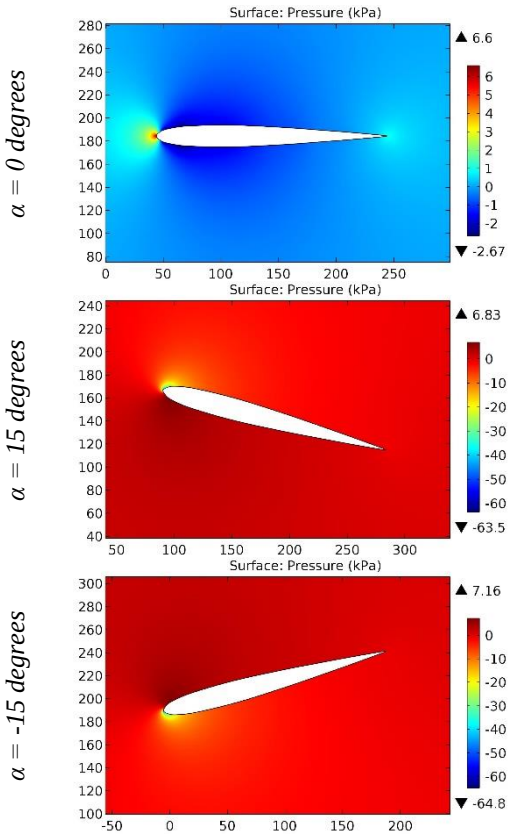

Figure 5. The pressure contours on the surfaces of the NACA 77 A airfoil.

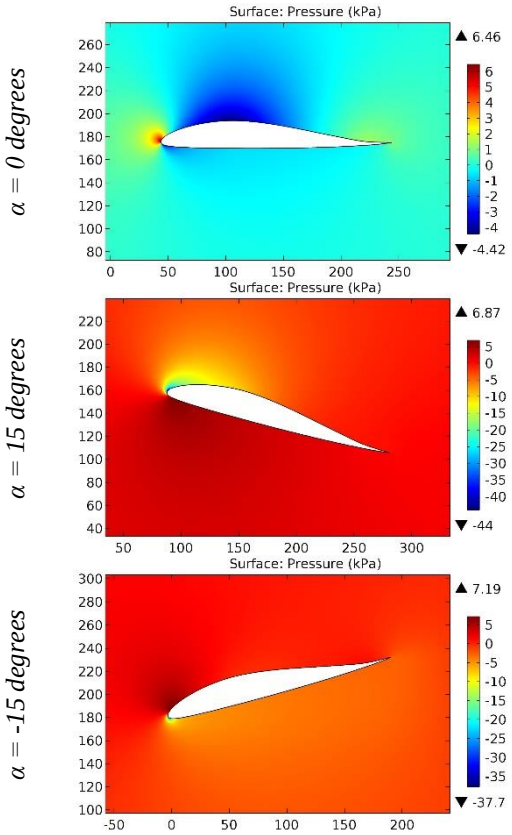

Figure 6. The pressure contours on the surfaces of the NACA 8-H-12 airfoil.

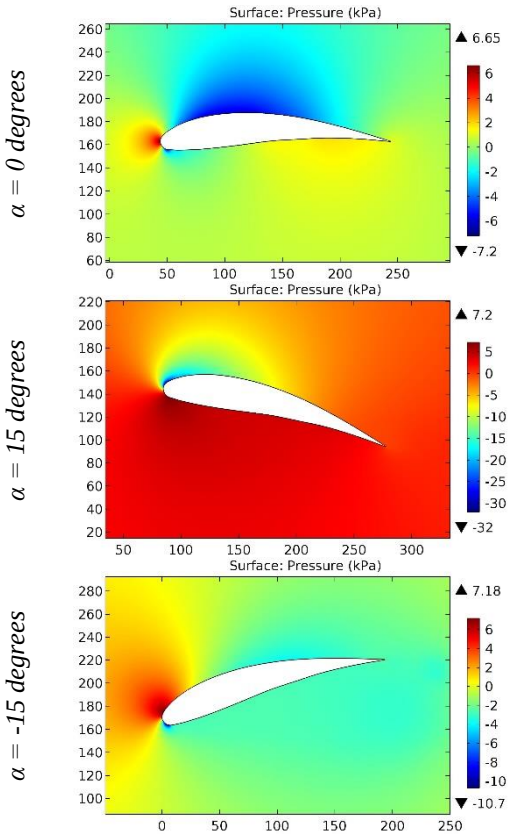

Figure 7. The pressure contours on the surfaces of the NACA 97 airfoil.

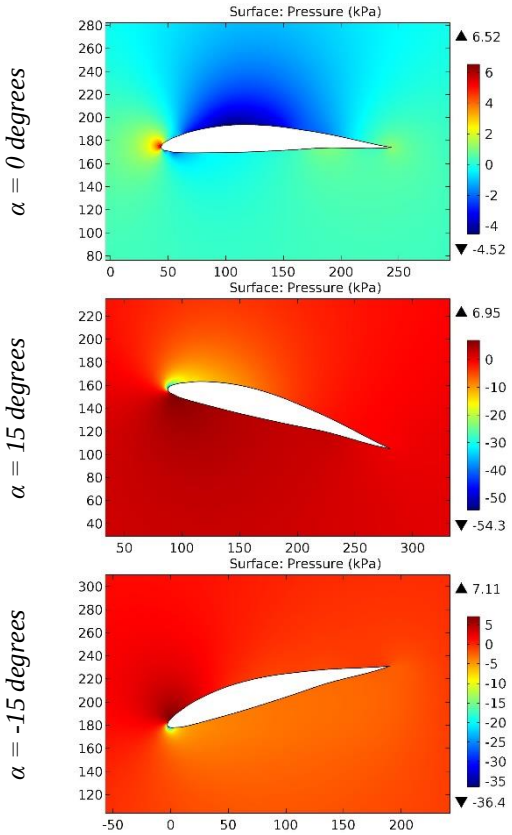

Figure 8. The pressure contours on the surfaces of the NACA BR 63-55-12 airfoil.

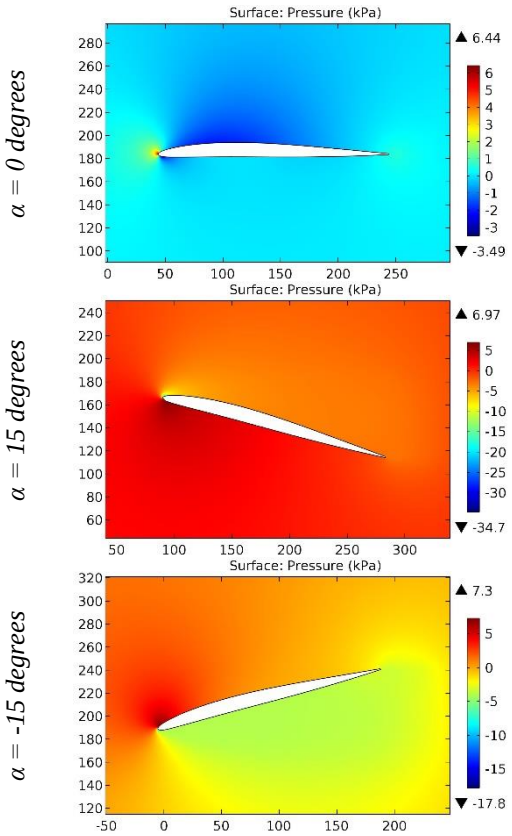

Figure 9. The pressure contours on the surfaces of the NACA M10 airfoil.

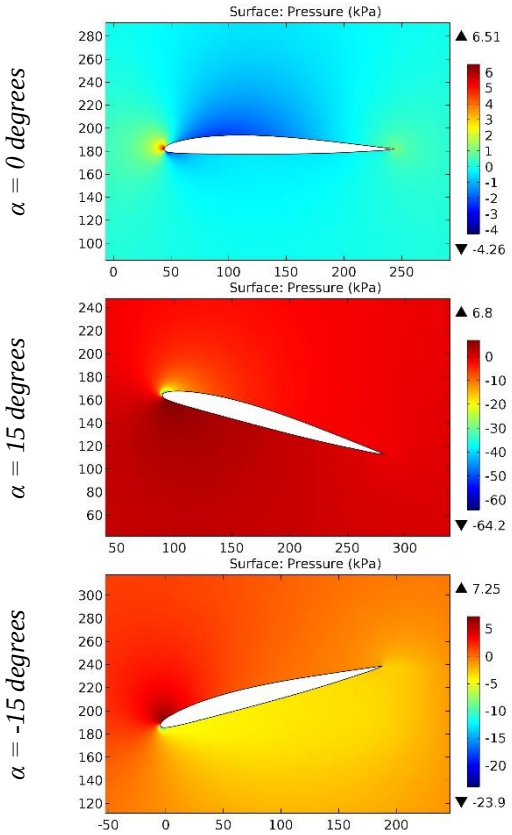

Figure 10. The pressure contours on the surfaces of the NACA M11 airfoil.

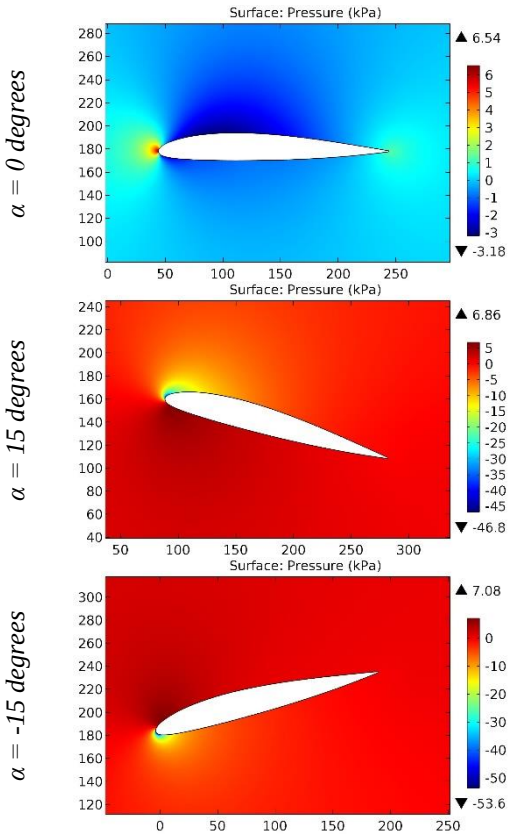

Figure 11. The pressure contours on the surfaces of the NACA M12 airfoil.

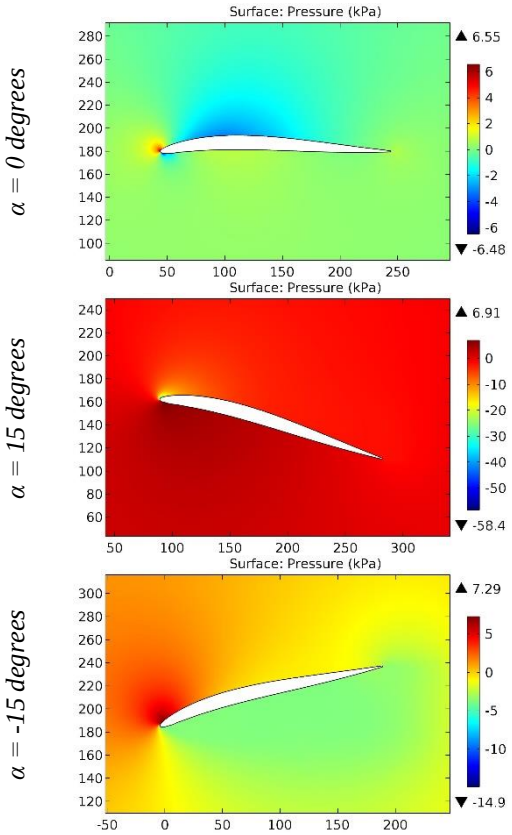

Figure 12. The pressure contours on the surfaces of the NACA M13 airfoil.

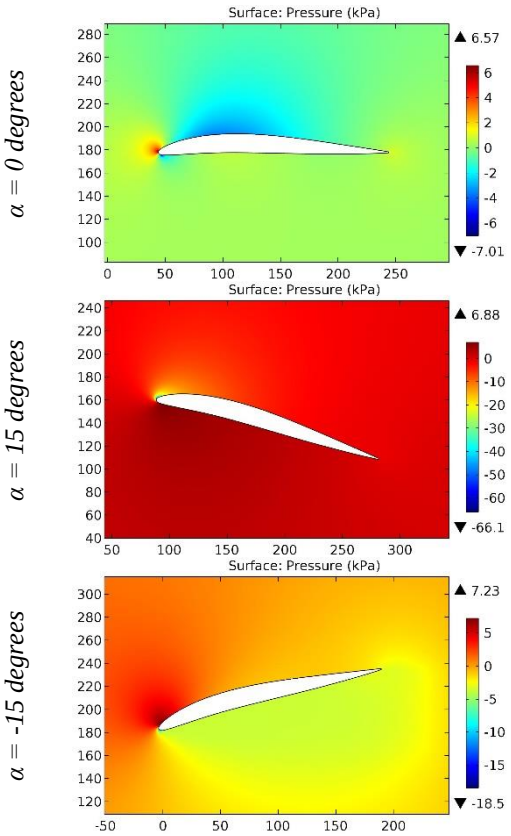

Figure 13. The pressure contours on the surfaces of the NACA M14 airfoil.

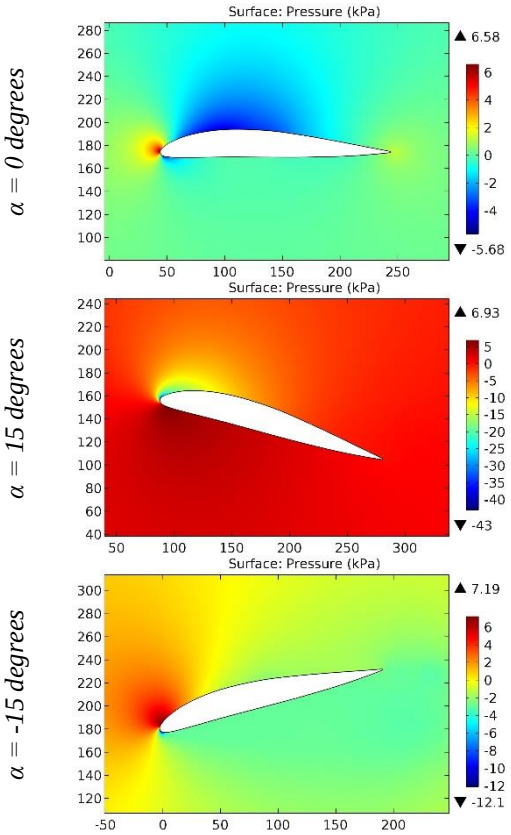

Figure 14. The pressure contours on the surfaces of the NACA M15 airfoil.

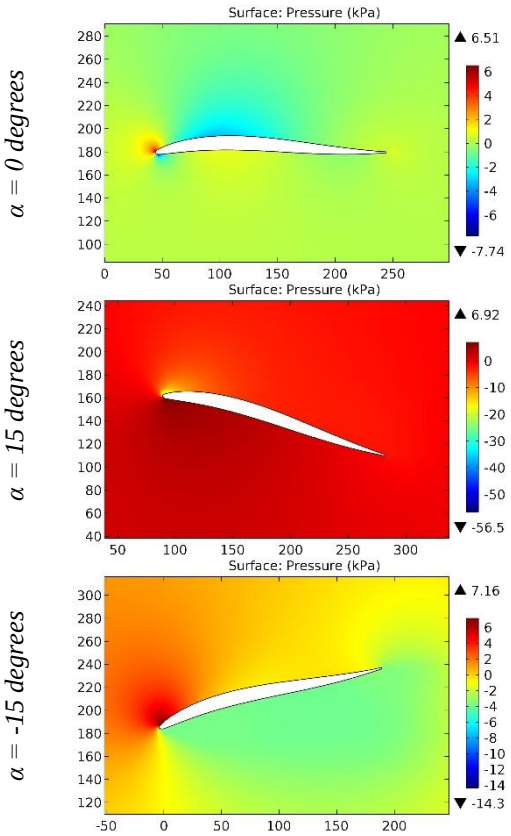

Figure 15. The pressure contours on the surfaces of the NACA M16 airfoil.

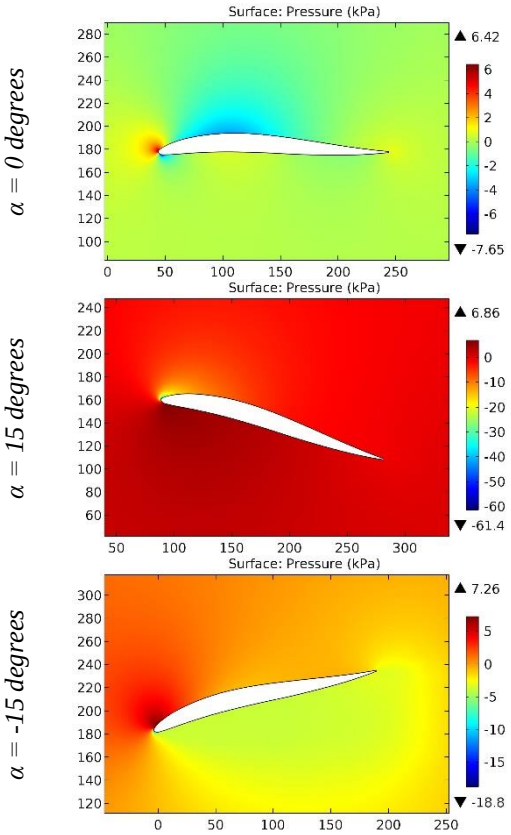

Figure 16. The pressure contours on the surfaces of the NACA M17 airfoil.

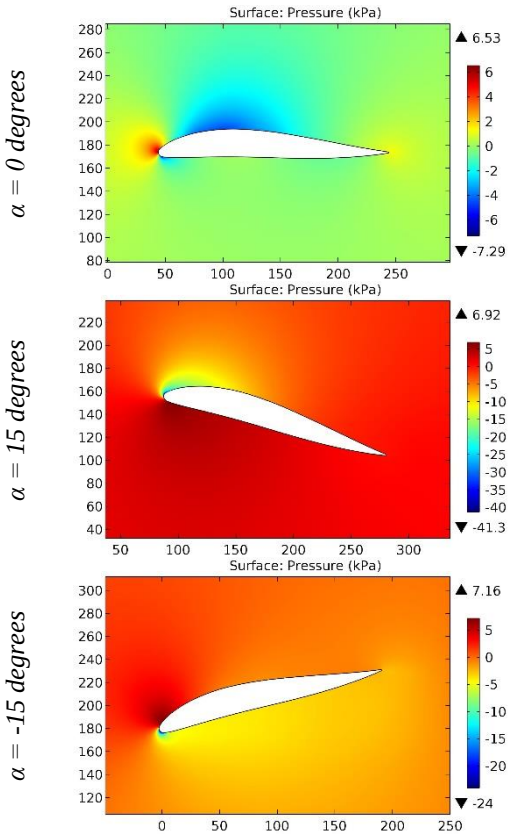

Figure 17. The pressure contours on the surfaces of the NACA M18 airfoil.

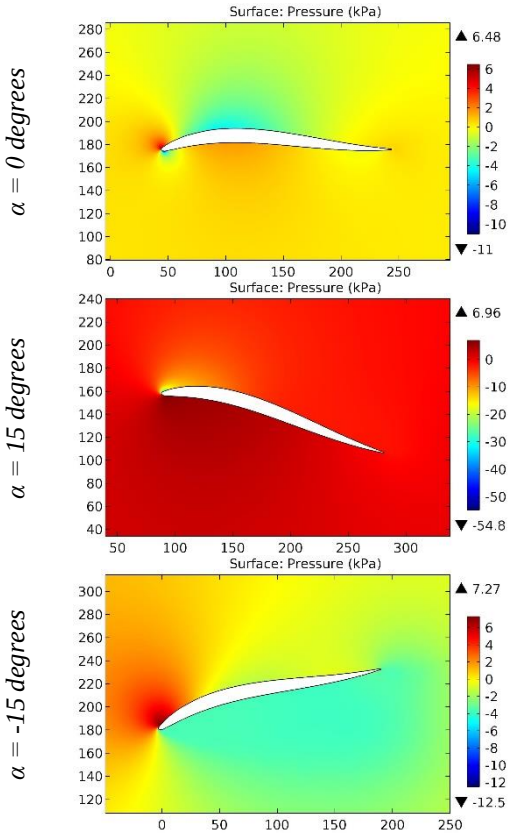

Figure 18. The pressure contours on the surfaces of the NACA M19 airfoil.

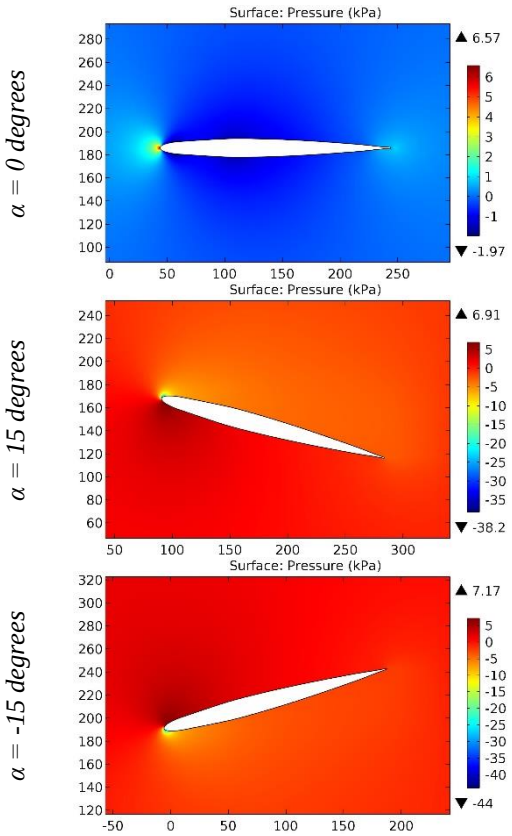

Figure 19. The pressure contours on the surfaces of the NACA M2 airfoil.

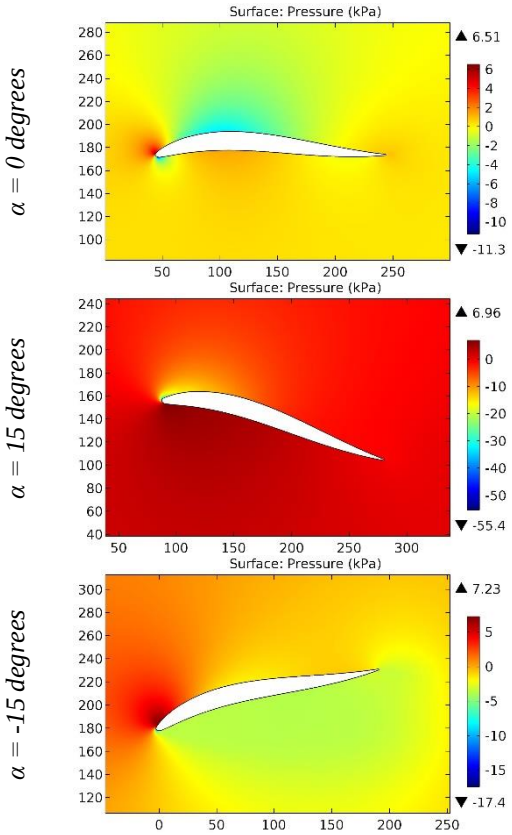

Figure 20. The pressure contours on the surfaces of the NACA M20 airfoil.

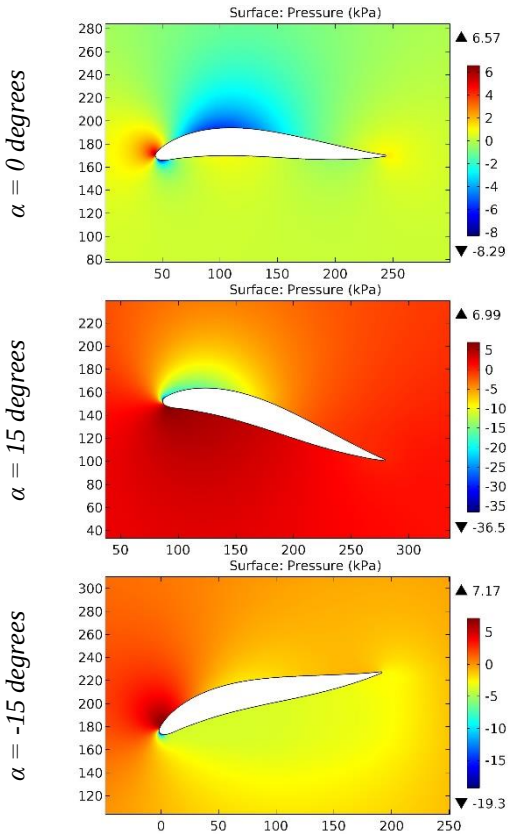

Figure 21. The pressure contours on the surfaces of the NACA M21 airfoil.

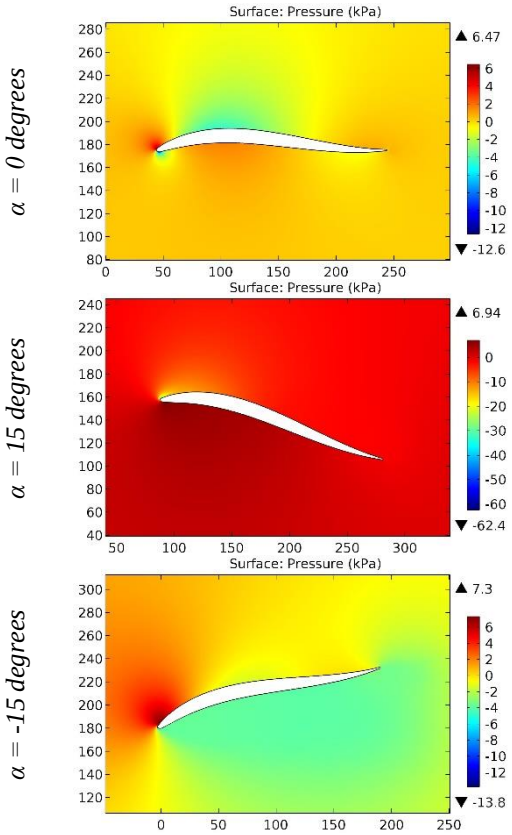

Figure 22. The pressure contours on the surfaces of the NACA M22 airfoil.

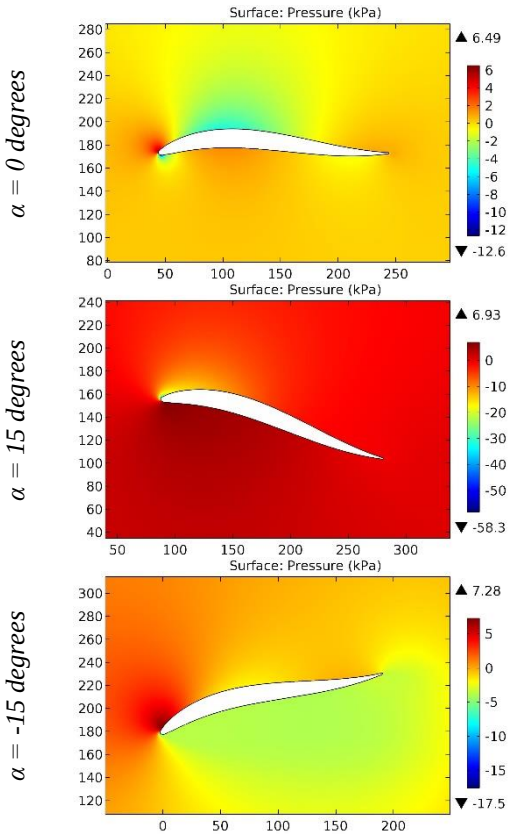

Figure 23. The pressure contours on the surfaces of the NACA M23 airfoil.

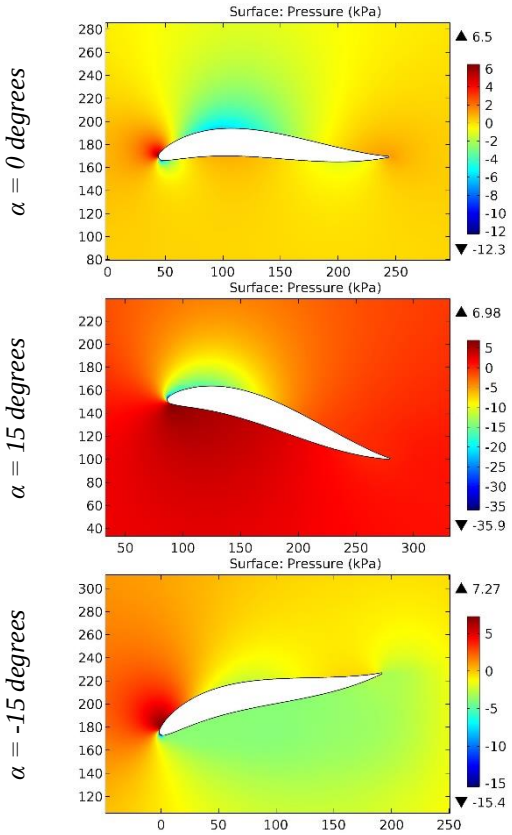

Figure 24. The pressure contours on the surfaces of the NACA M24 airfoil.

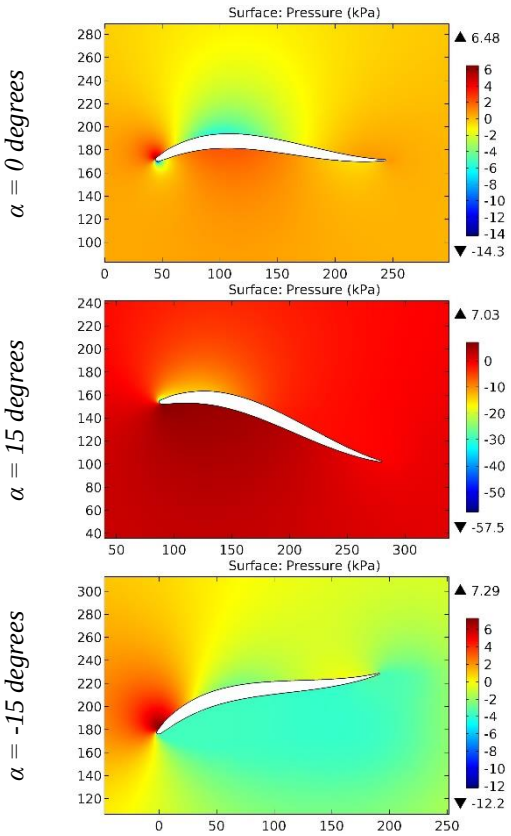

Figure 25. The pressure contours on the surfaces of the NACA M25 airfoil.

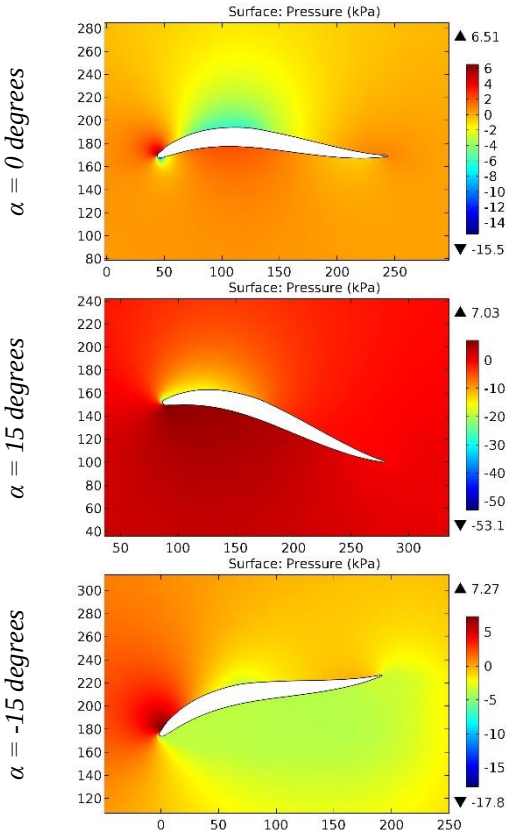

Figure 26. The pressure contours on the surfaces of the NACA M26 airfoil.

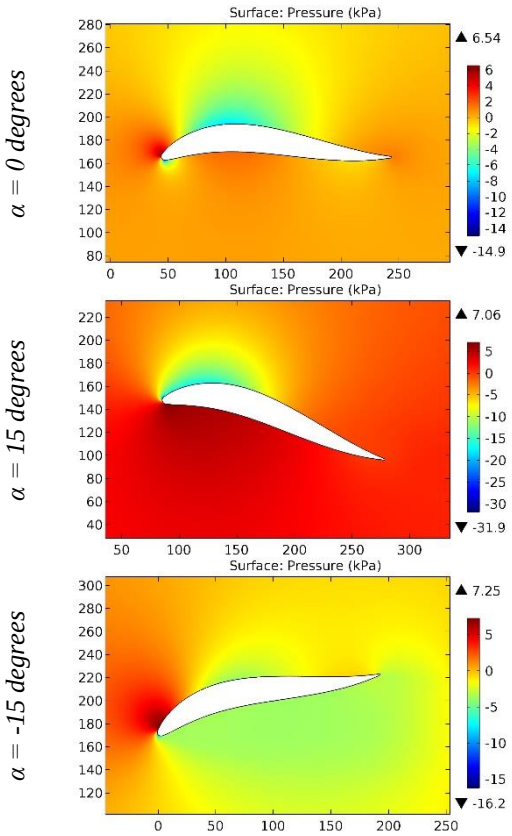

Figure 27. The pressure contours on the surfaces of the NACA M27 airfoil.

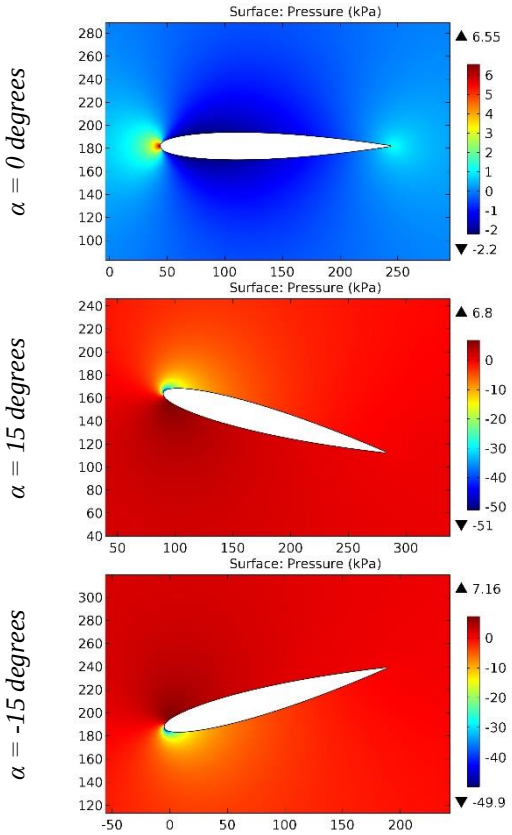

Figure 28. The pressure contours on the surfaces of the NACA M3 airfoil.

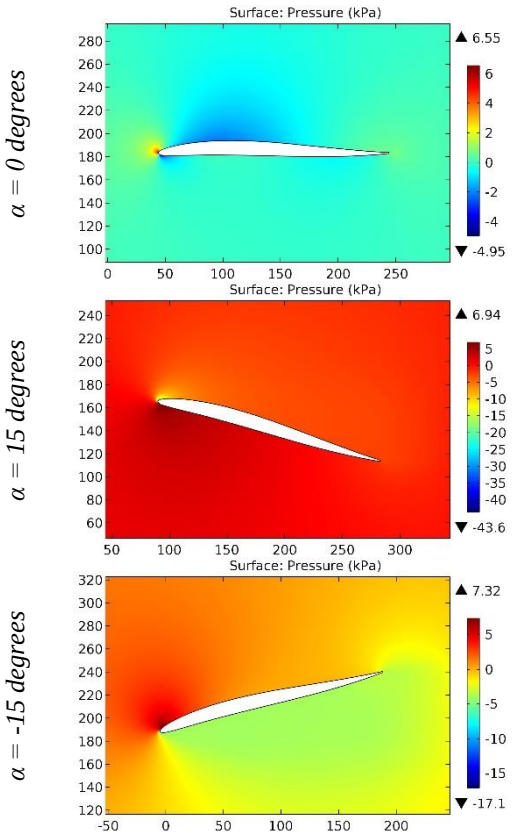

Figure 29. The pressure contours on the surfaces of the NACA M4 airfoil.

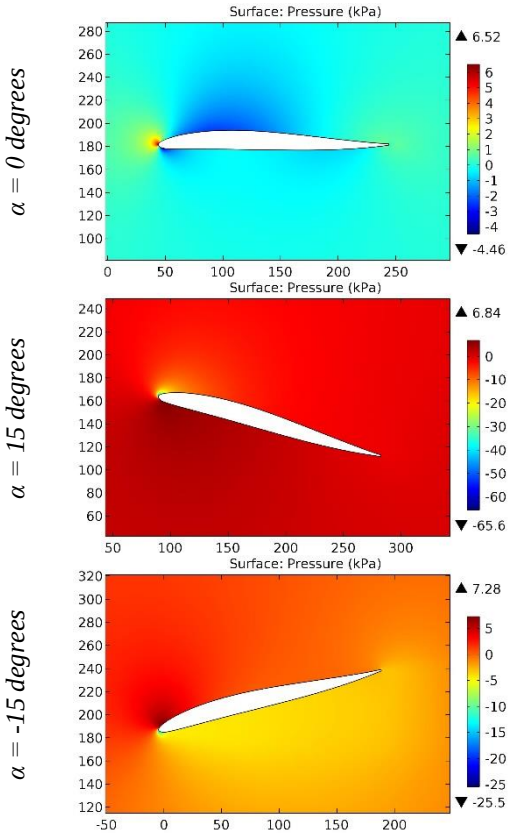

Figure 30. The pressure contours on the surfaces of the NACA M5 airfoil.

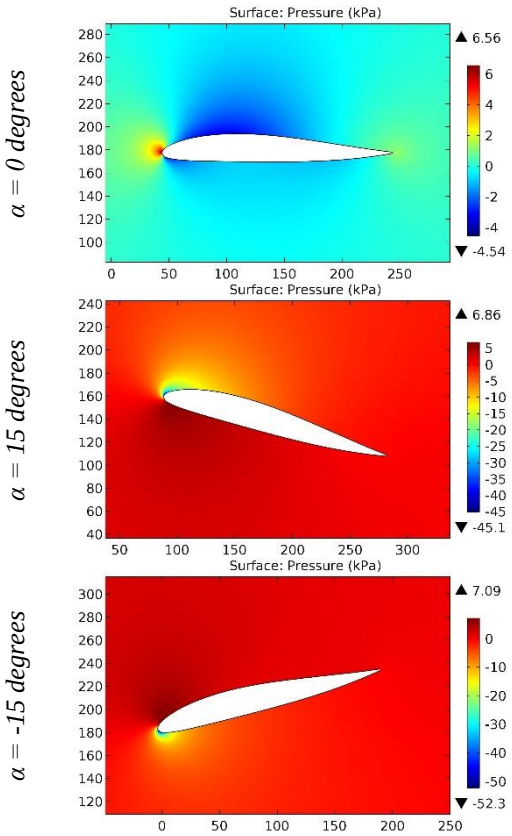

Figure 31. The pressure contours on the surfaces of the NACA M6 airfoil.

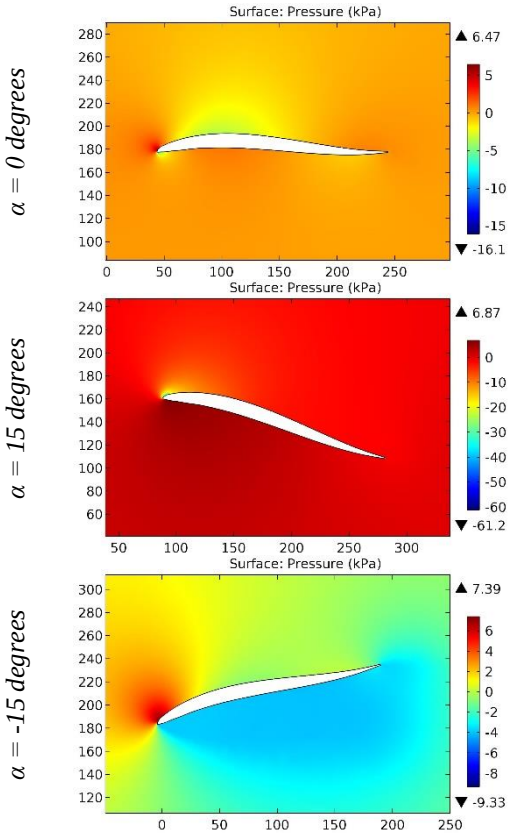

Figure 32. The pressure contours on the surfaces of the NACA M7 airfoil.

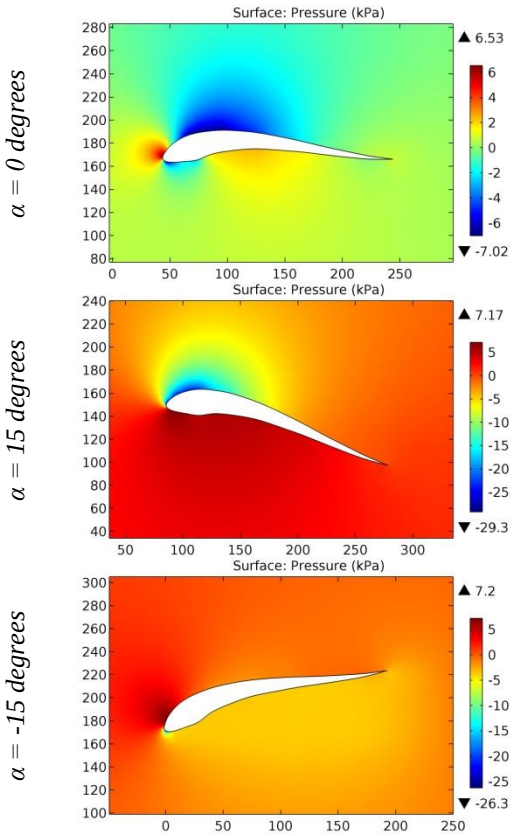

Figure 33. The pressure contours on the surfaces of the NACA M8 airfoil.

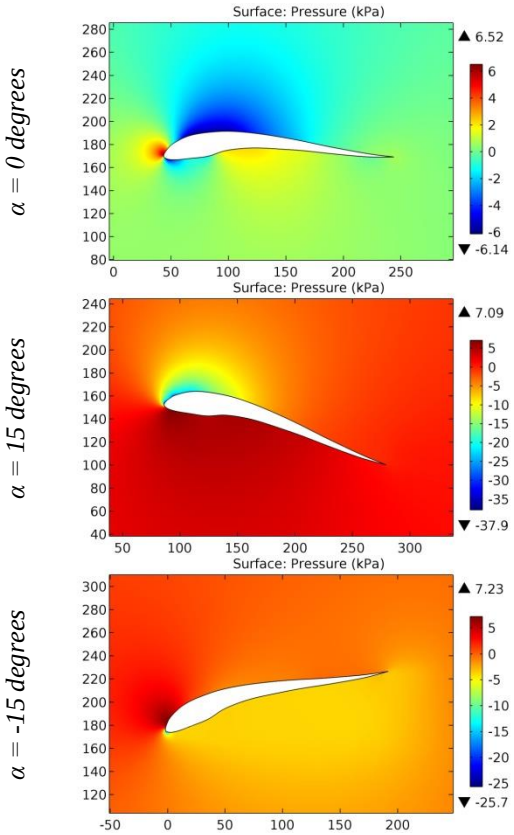

Figure 34. The pressure contours on the surfaces of the NACA M9 airfoil.

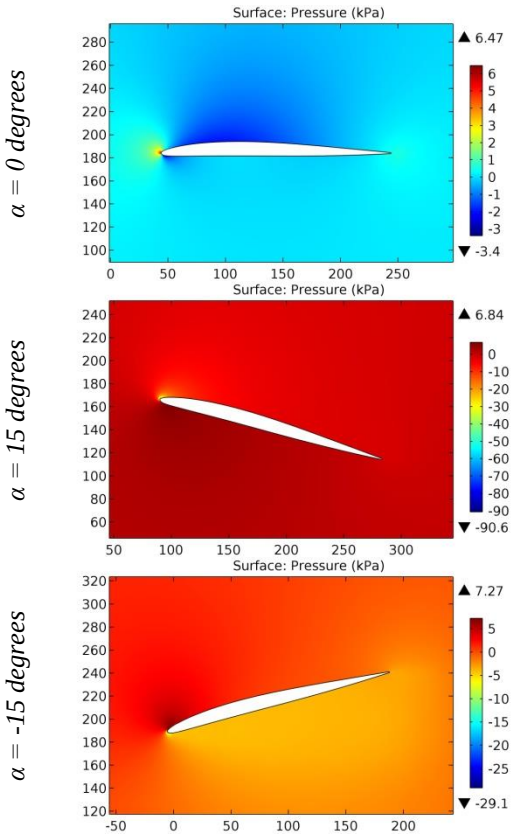

Figure 35. The pressure contours on the surfaces of the NACA/Munk M-10 airfoil.

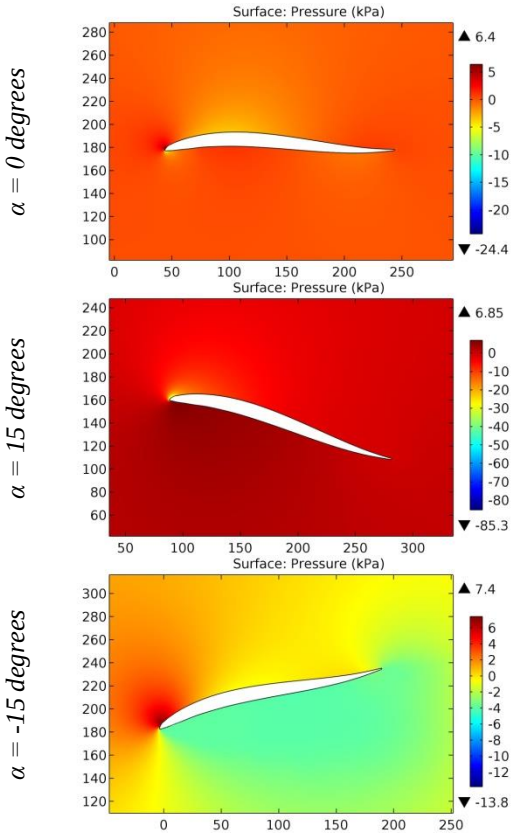

Figure 36. The pressure contours on the surfaces of the NACA/Munk M-7 airfoil.

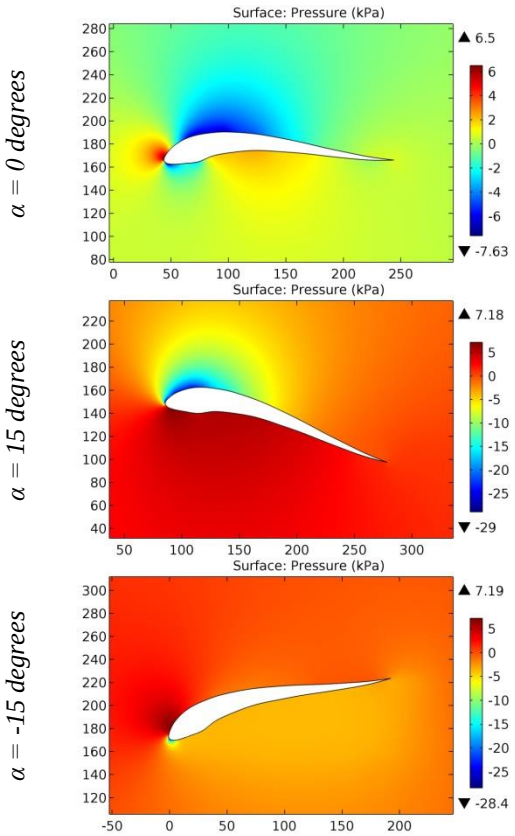

Figure 37. The pressure contours on the surfaces of the NACA/Munk M-8 airfoil.

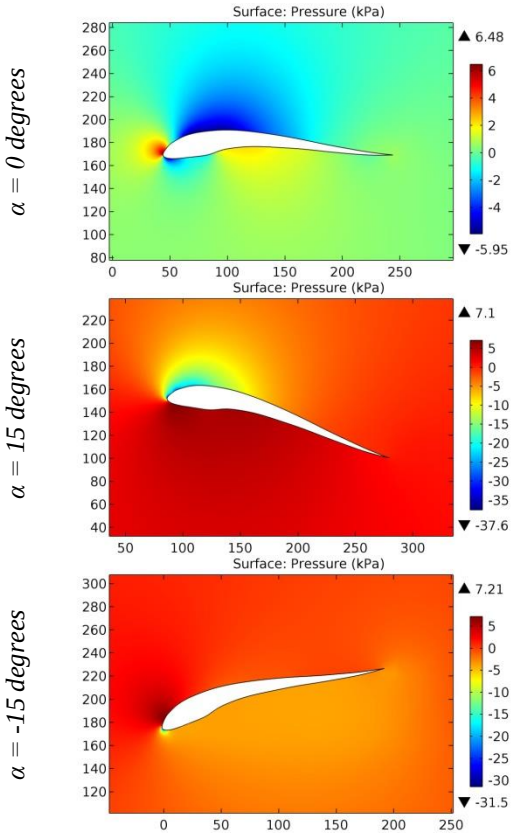

Figure 38. The pressure contours on the surfaces of the NACA/Munk M-9 airfoil.

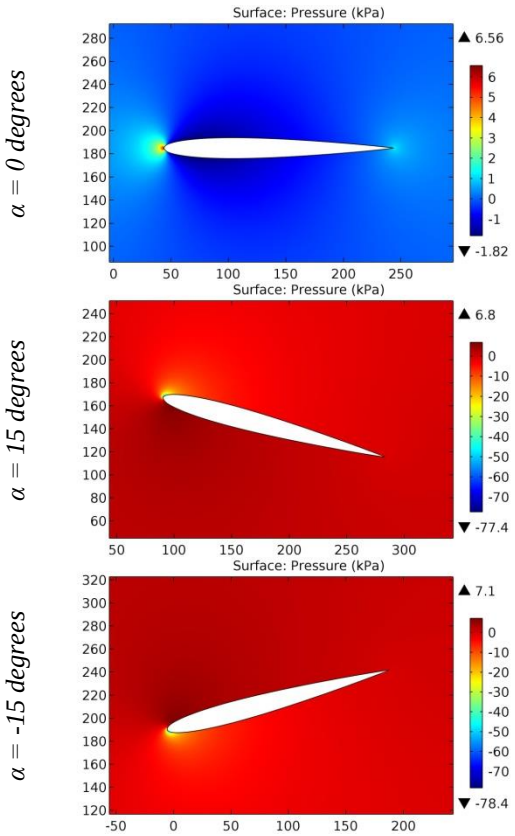

Figure 39. The pressure contours on the surfaces of the NACA0009 airfoil.

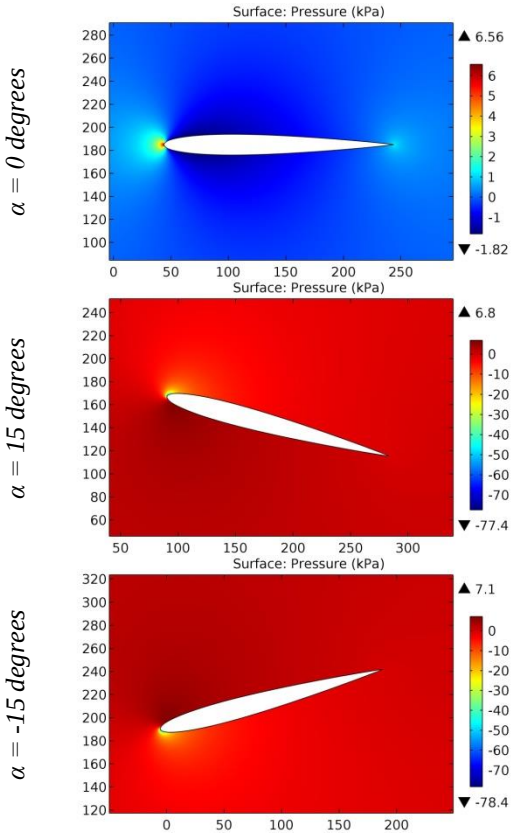

Figure 40. The pressure contours on the surfaces of the NACA-0009 9,0% smoothed airfoil.

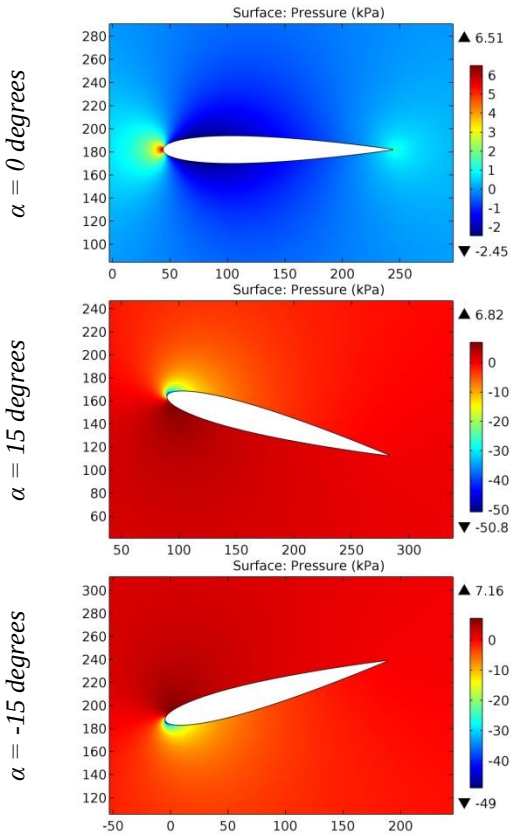

Figure 41. The pressure contours on the surfaces of the NACA0012 airfoil.

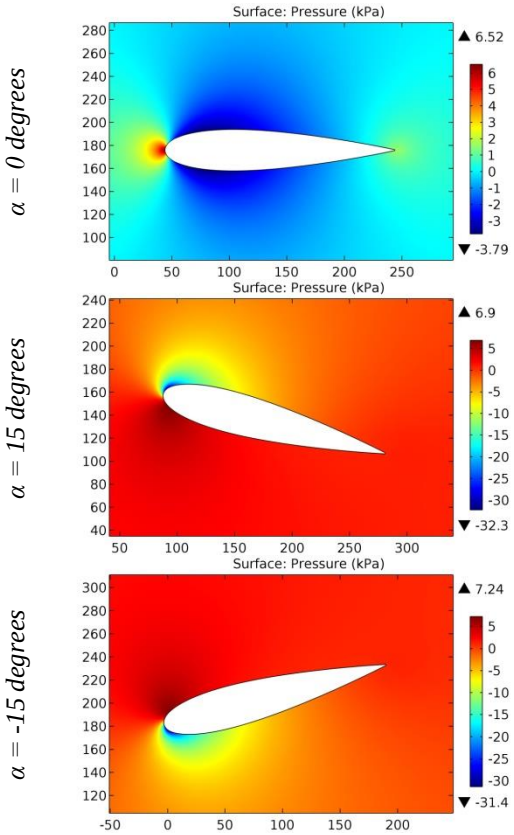

Figure 42. The pressure contours on the surfaces of the NACA0018 airfoil.

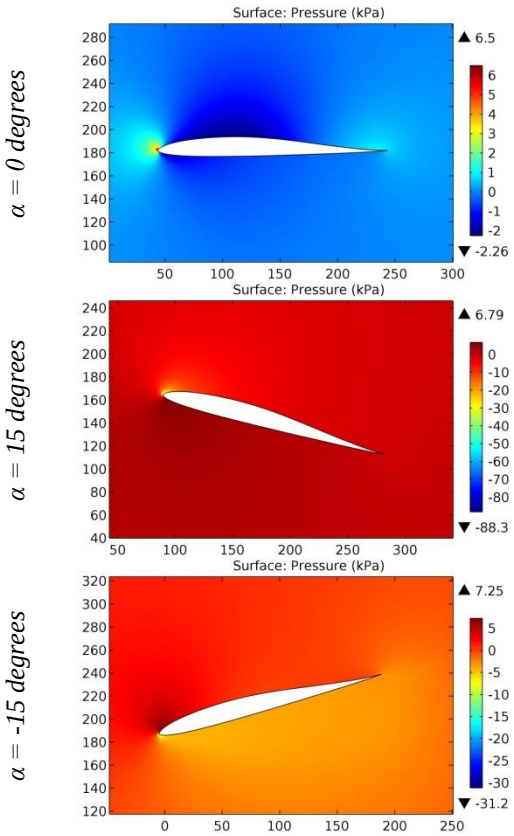

Figure 43. The pressure contours on the surfaces of the NACA1408 airfoil.

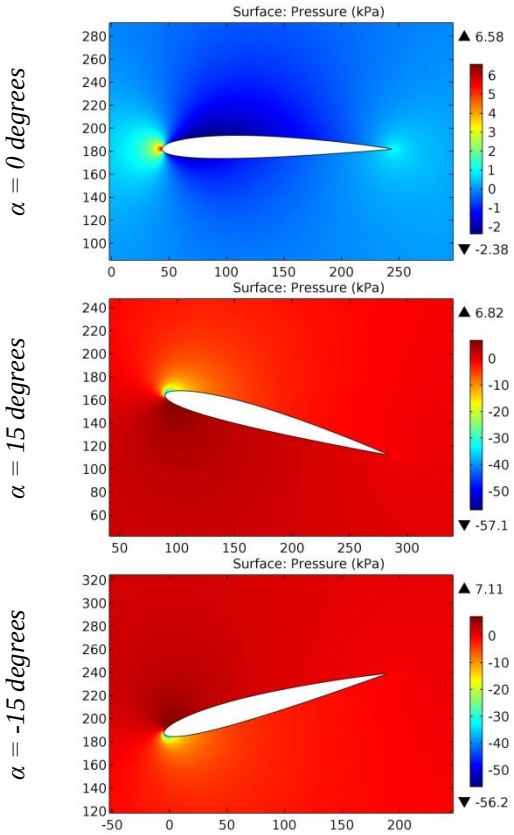

Figure 44. The pressure contours on the surfaces of the NACA1410 airfoil.

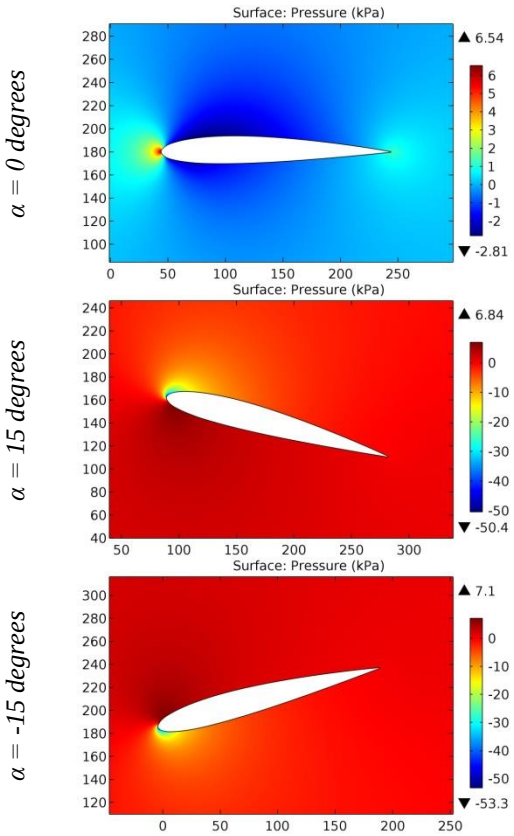

Figure 45. The pressure contours on the surfaces of the NACA1412 airfoil.

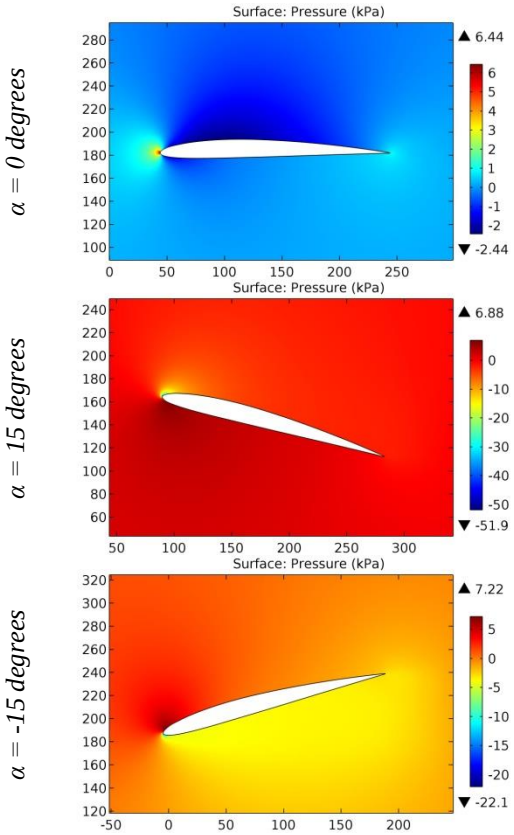

Figure 46. The pressure contours on the surfaces of the NACA2408 airfoil.

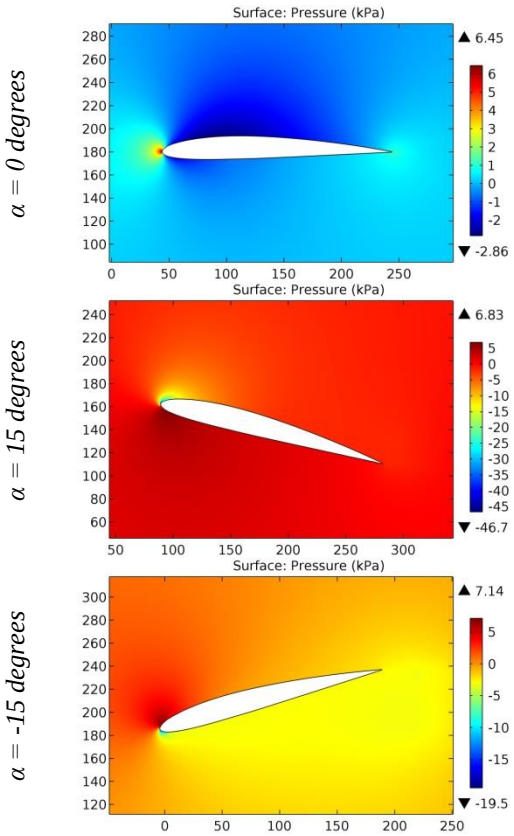

Figure 47. The pressure contours on the surfaces of the NACA2410 airfoil.

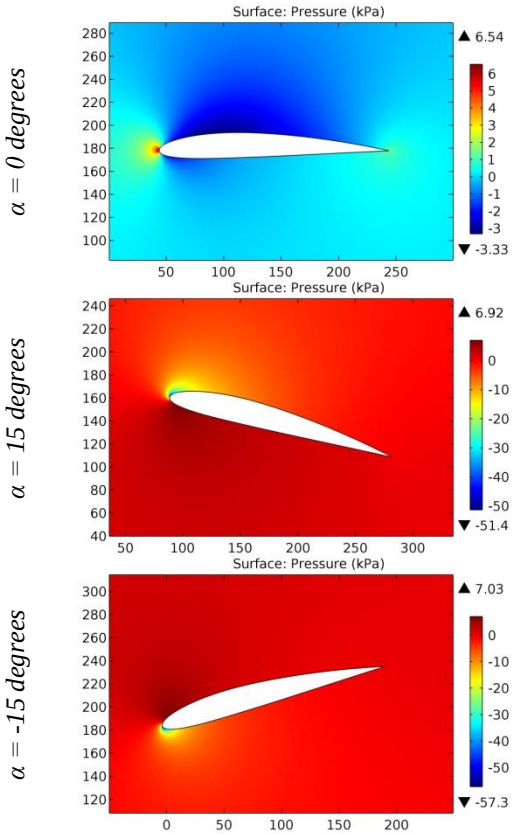

Figure 48. The pressure contours on the surfaces of the NACA2411 airfoil.

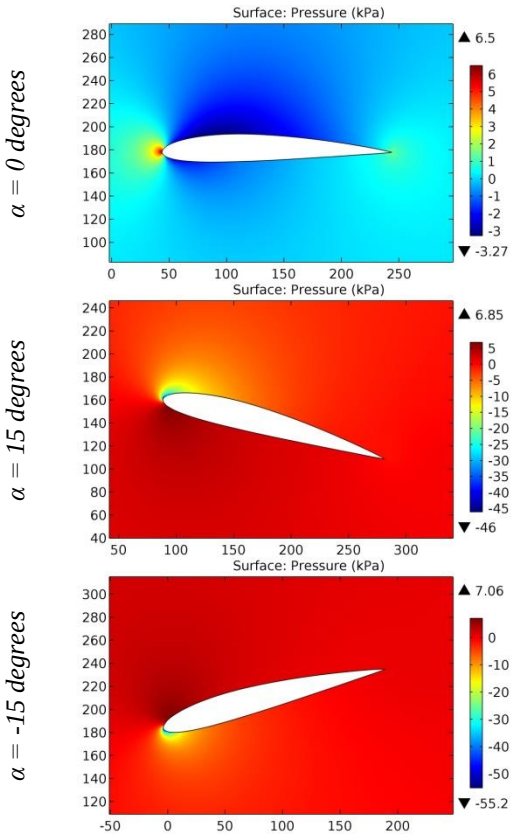

Figure 49. The pressure contours on the surfaces of the NACA2412 airfoil.

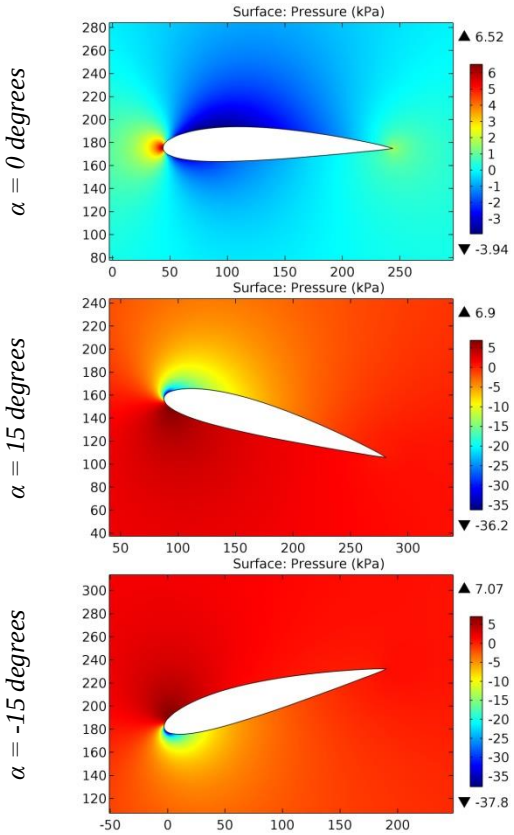

Figure 50. The pressure contours on the surfaces of the NACA2415 airfoil.

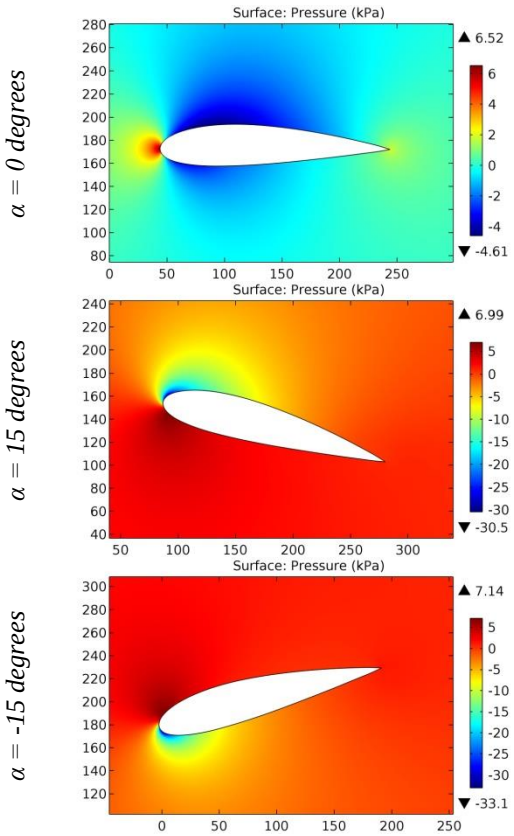

Figure 51. The pressure contours on the surfaces of the NACA2418 airfoil.

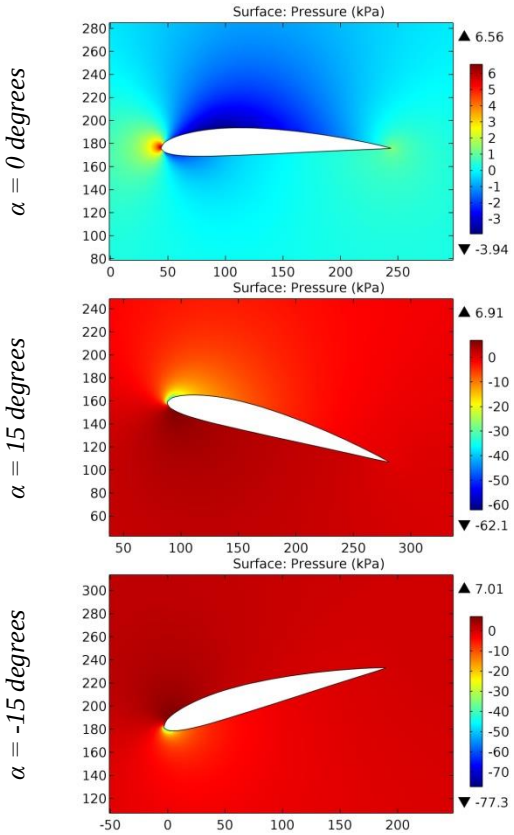

Figure 52. The pressure contours on the surfaces of the NACA3412 airfoil.

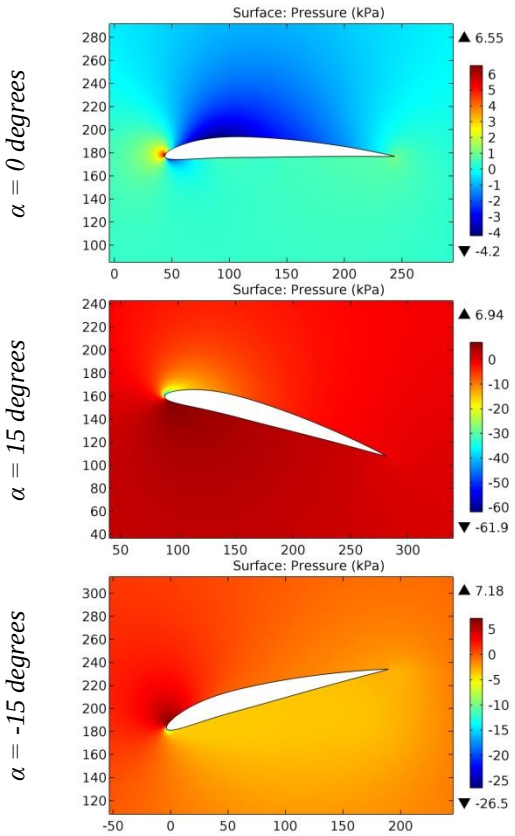

Figure 53. The pressure contours on the surfaces of the NACA4309 airfoil.

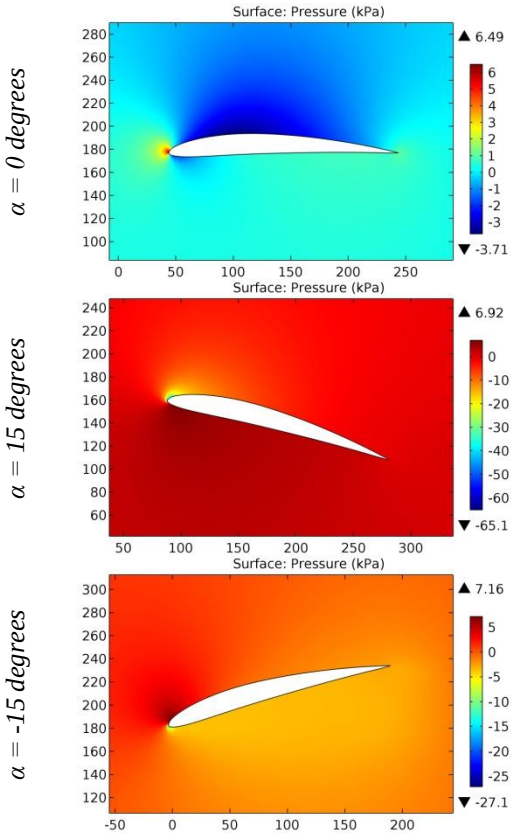

Figure 54. The pressure contours on the surfaces of the NACA4409 airfoil.

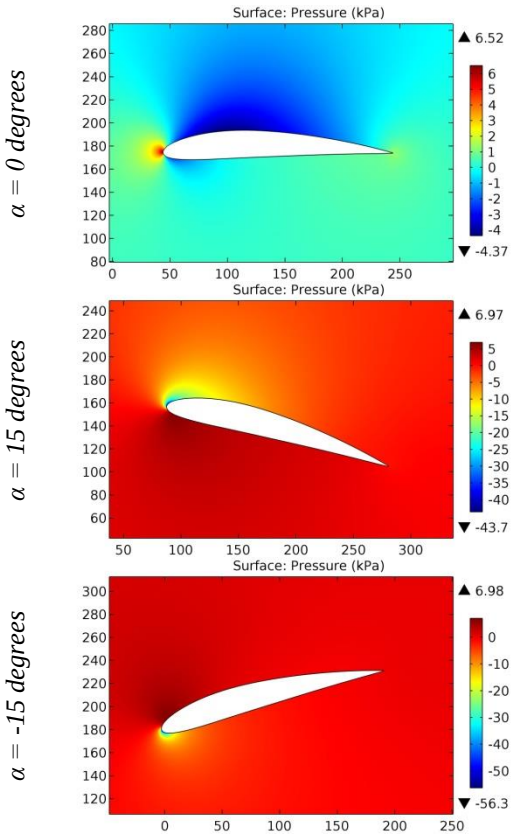

Figure 55. The pressure contours on the surfaces of the NACA4412 airfoil.

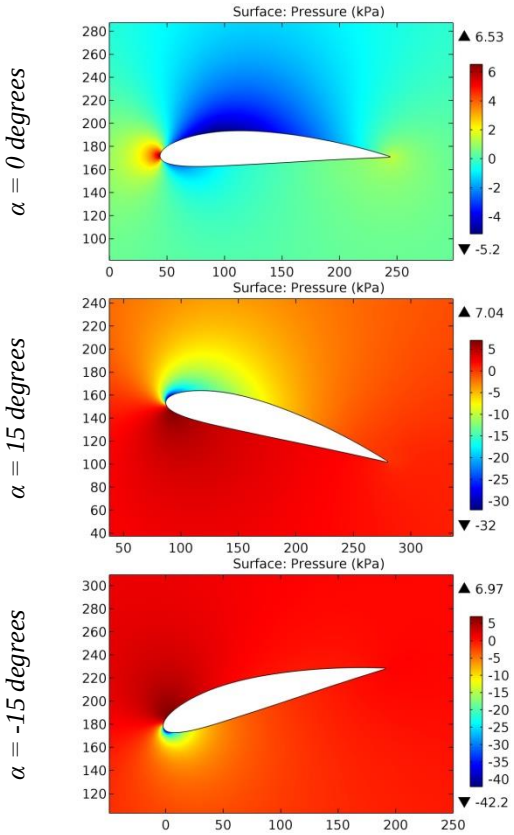

Figure 56. The pressure contours on the surfaces of the NACA4415 airfoil.

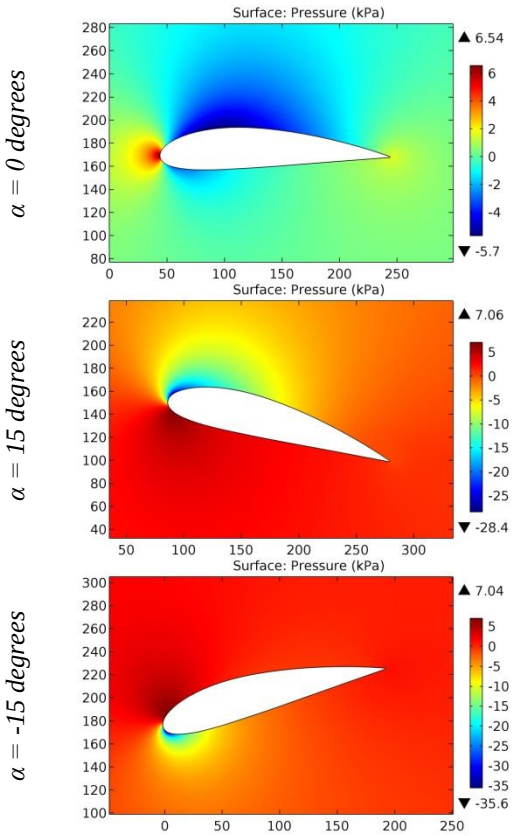

Figure 57. The pressure contours on the surfaces of the NACA4418 airfoil.

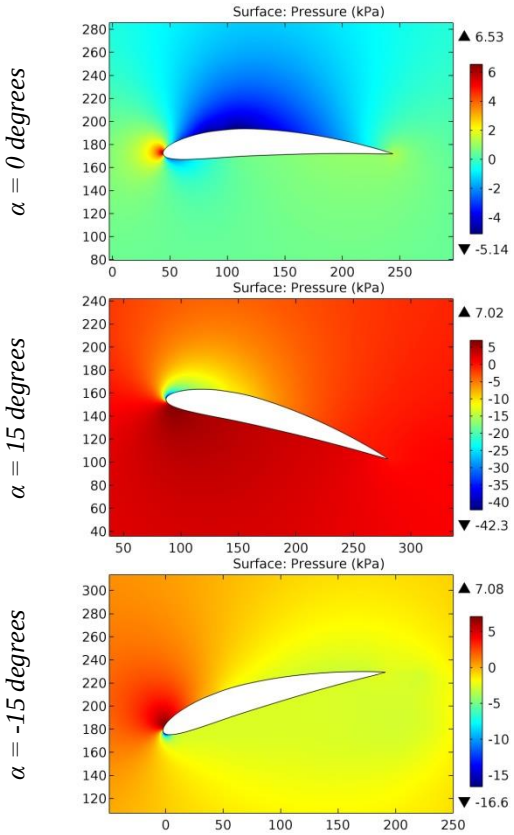

Figure 58. The pressure contours on the surfaces of the NACA5412 airfoil.

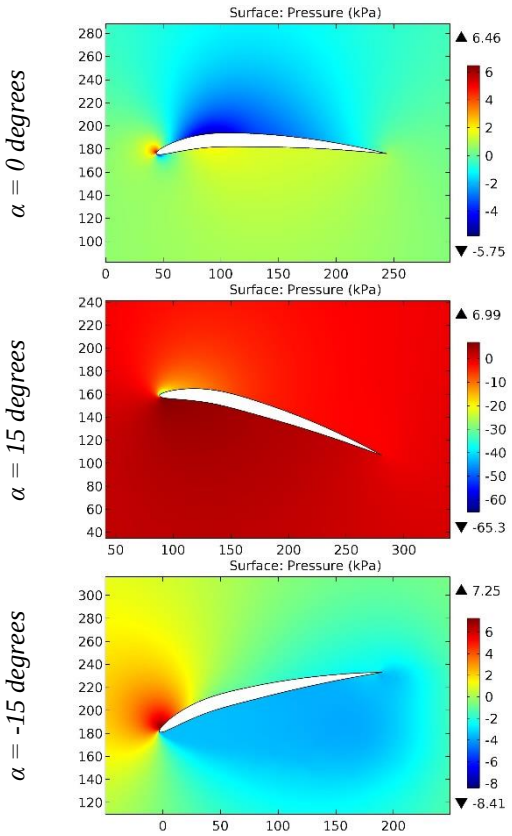

Figure 59. The pressure contours on the surfaces of the NACA6306 airfoil.

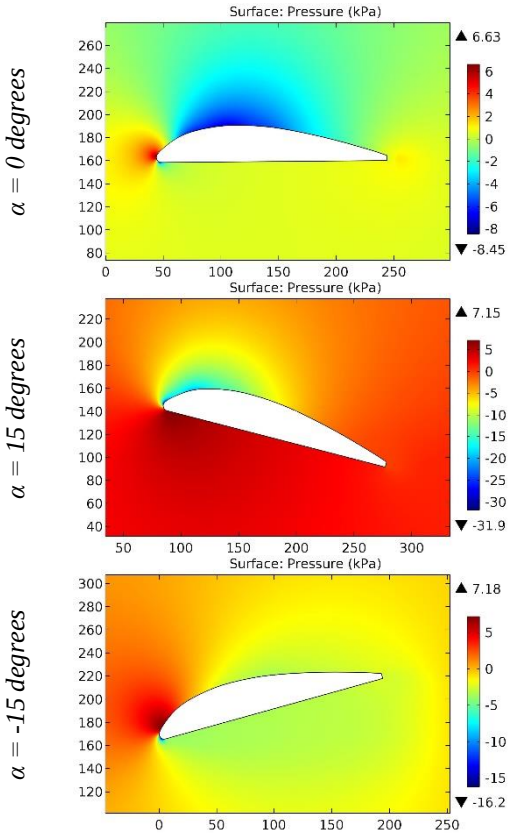

Figure 60. The pressure contours on the surfaces of the NACA-64 airfoil.

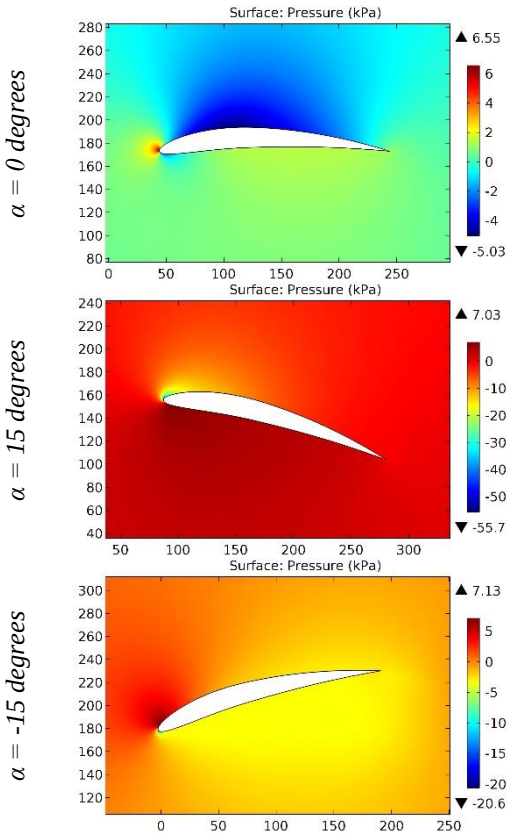

Figure 61. The pressure contours on the surfaces of the NACA6409 airfoil.

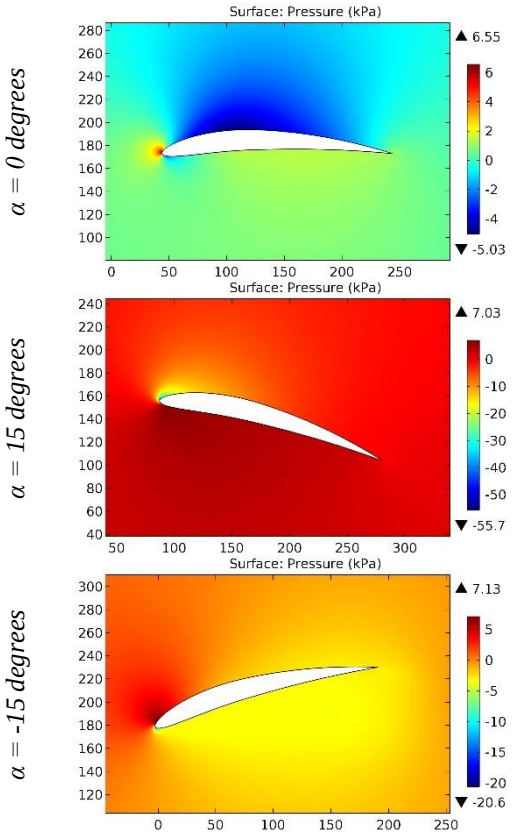

Figure 62. The pressure contours on the surfaces of the NACA6409 9% airfoil.

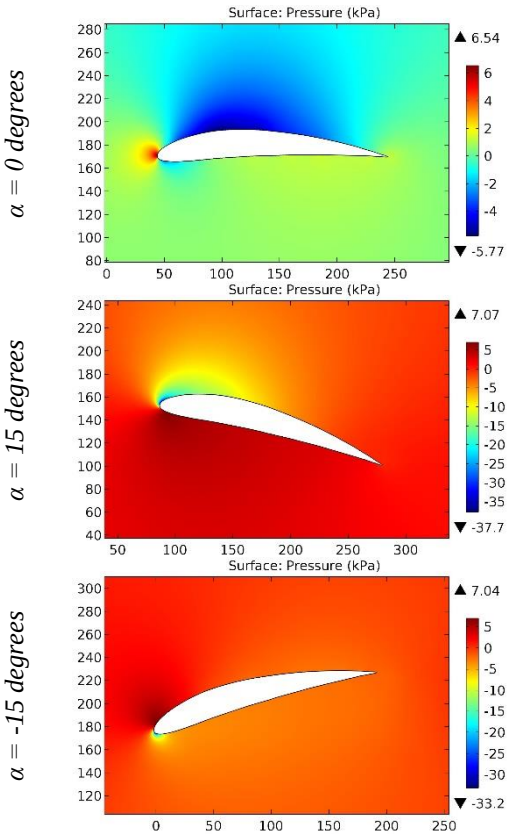

Figure 63. The pressure contours on the surfaces of the NACA6412 airfoil.

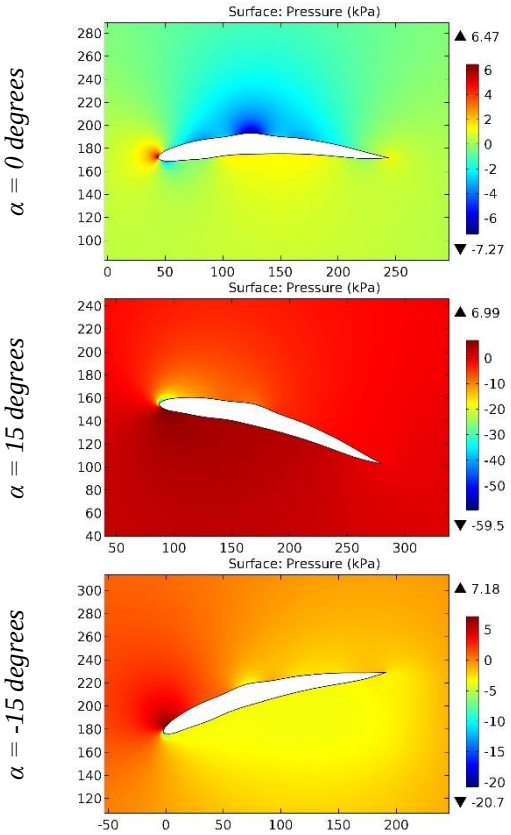

Figure 64. The pressure contours on the surfaces of the NACA6509 airfoil.

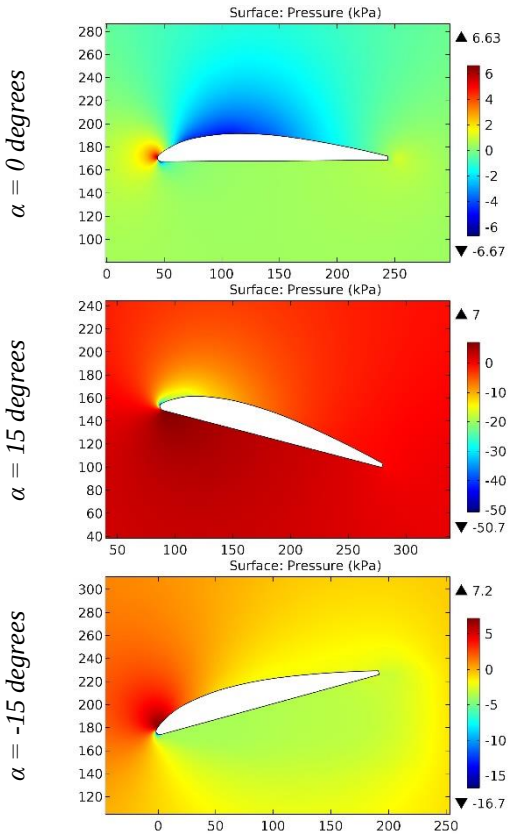

Figure 65. The pressure contours on the surfaces of the NACA-66 airfoil.

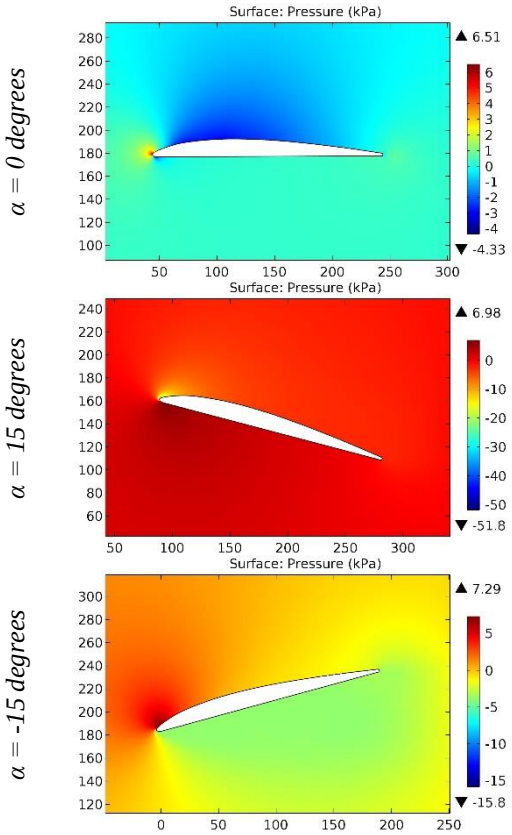

Figure 66. The pressure contours on the surfaces of the NACA-69 airfoil.

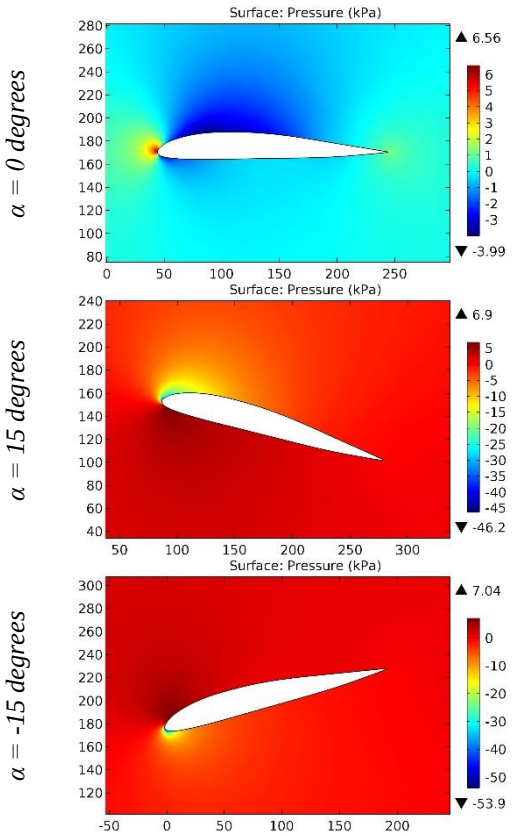

Figure 67. The pressure contours on the surfaces of the NACA-CYH airfoil.

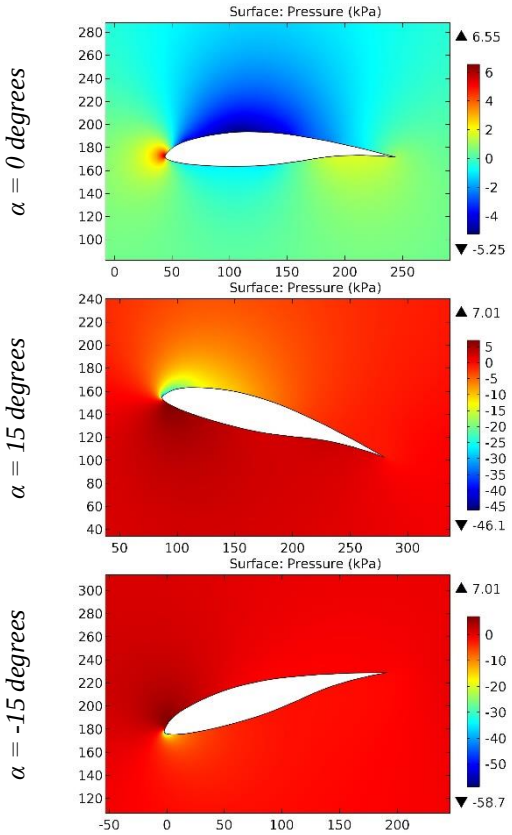

Figure 68. The pressure contours on the surfaces of the NACA-K6E airfoil.

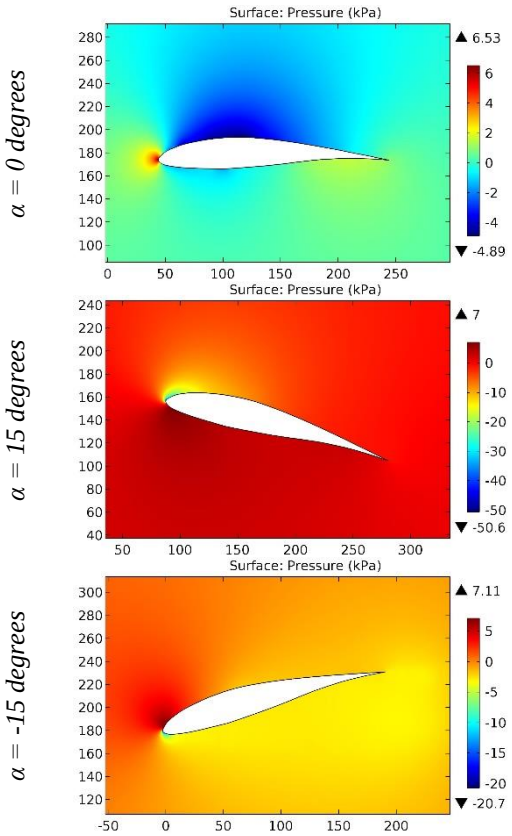

Figure 69. The pressure contours on the surfaces of the NACA-K6M airfoil.

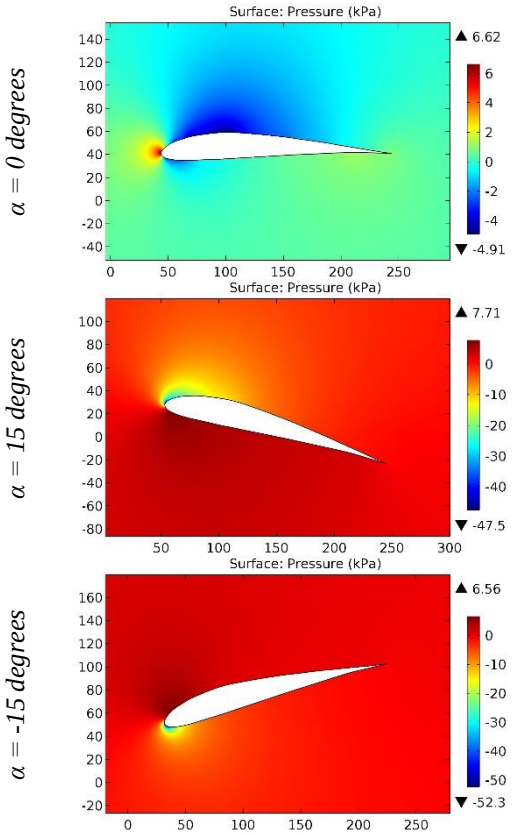

Figure 70. The pressure contours on the surfaces of the NACA-K6S airfoil.

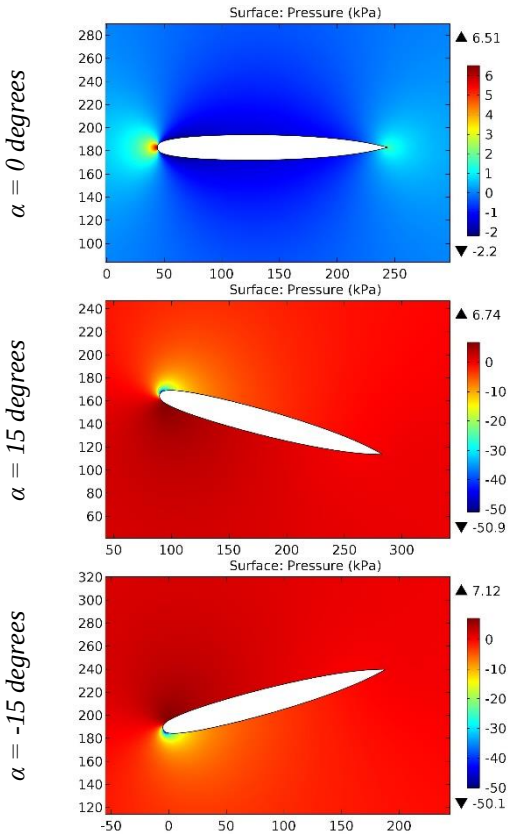

Figure 71. The pressure contours on the surfaces of the NACA-LANGLEY SYMMETRICAL, SUPERCRITICAL airfoil.

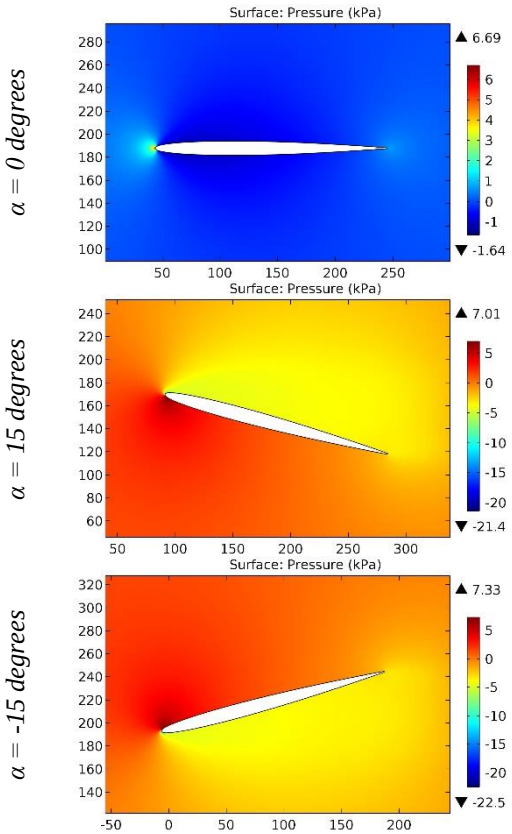

Figure 72. The pressure contours on the surfaces of the NACA-M1 airfoil.

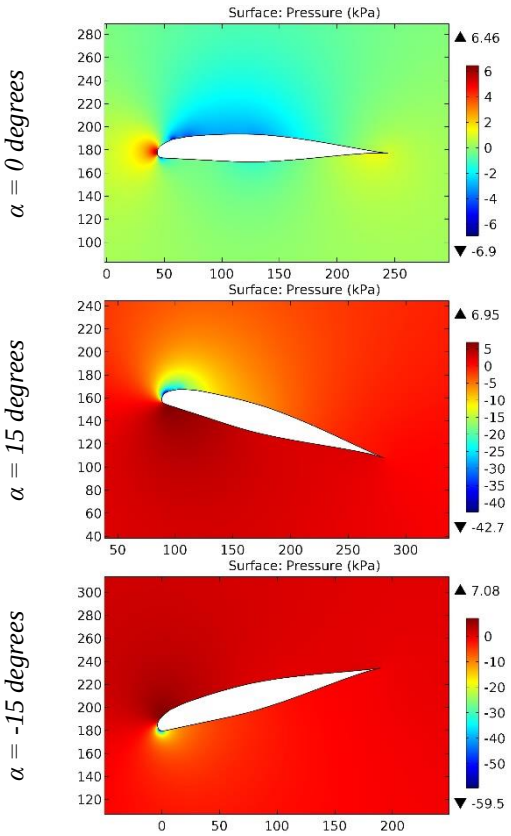

Figure 73. The pressure contours on the surfaces of the NACA-NASA/AMES/Hicks 63(1)-212 MOD A airfoil.

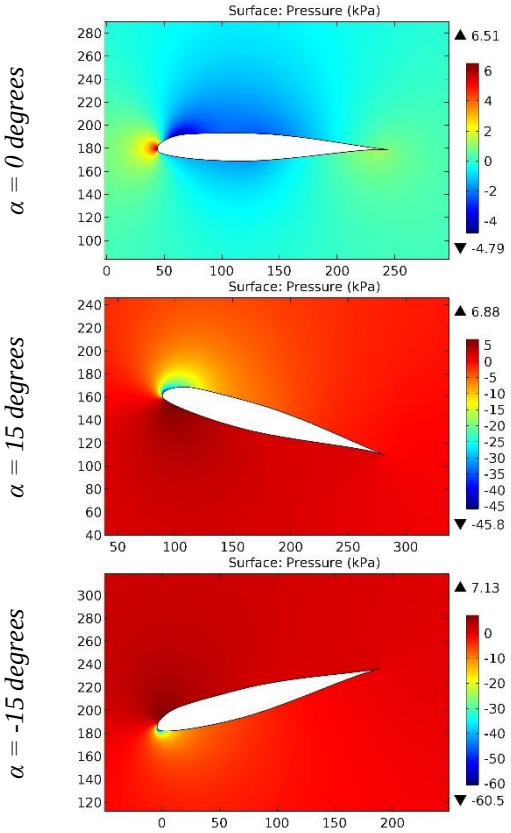

Figure 74. The pressure contours on the surfaces of the NACA-NASA/AMES/Hicks 63(1)-212 MOD B airfoil.

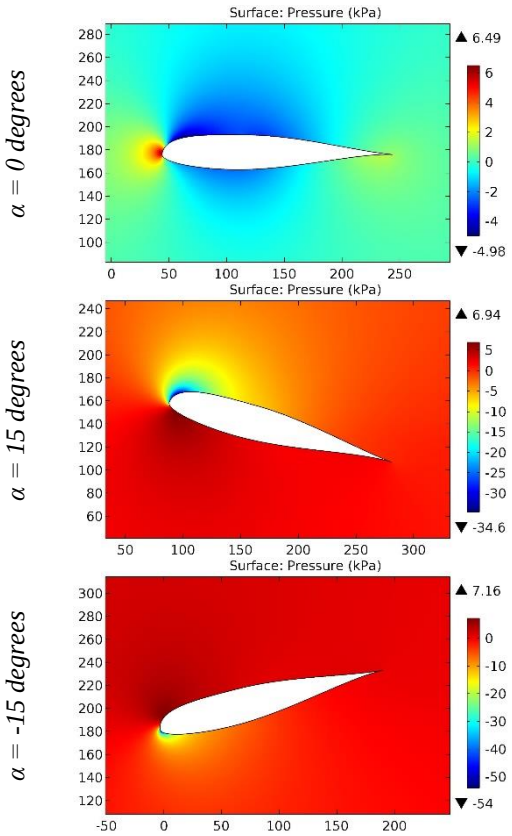

Figure 75. The pressure contours on the surfaces of the NACA-NASA/AMES/Hicks 63(2)-215 MOD B airfoil.

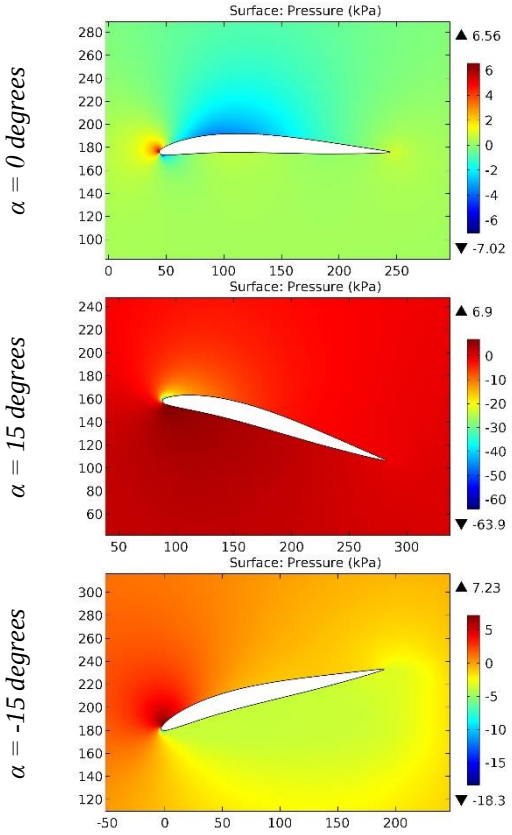

Figure 76. The pressure contours on the surfaces of the NACM14 airfoil.

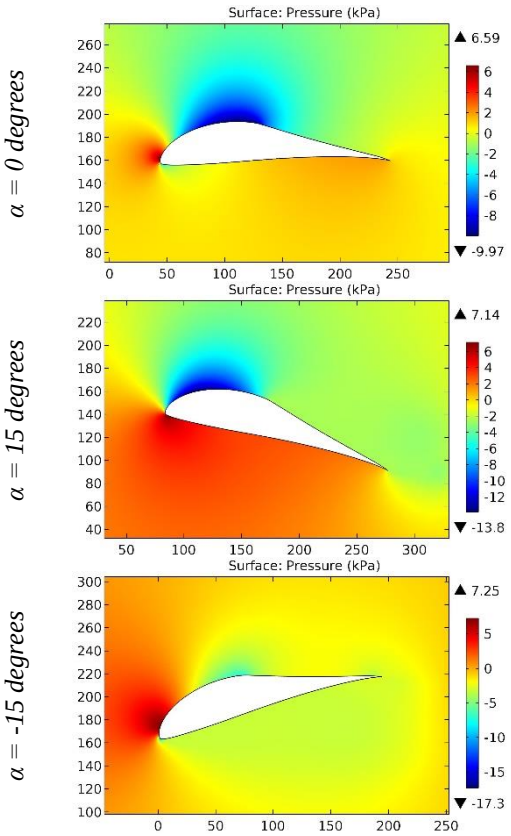

Figure 77. The pressure contours on the surfaces of the Narramore JN153 airfoil.

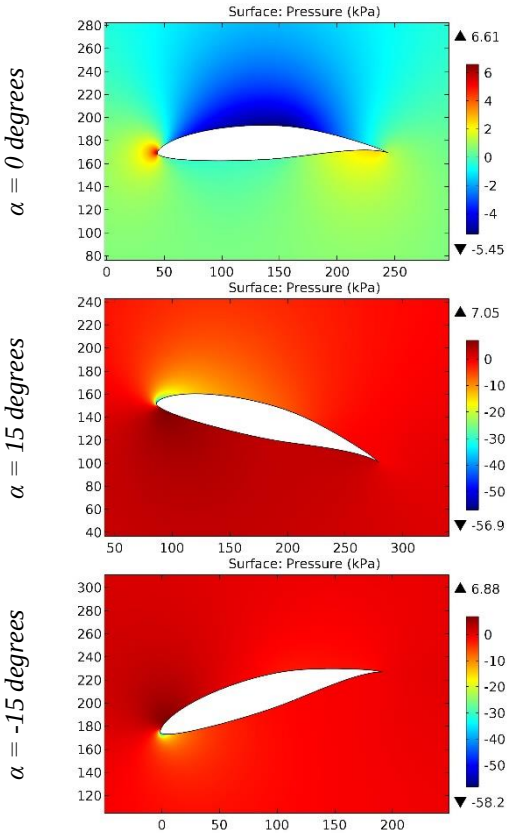

Figure 78. The pressure contours on the surfaces of the NASA NLF1015 airfoil.

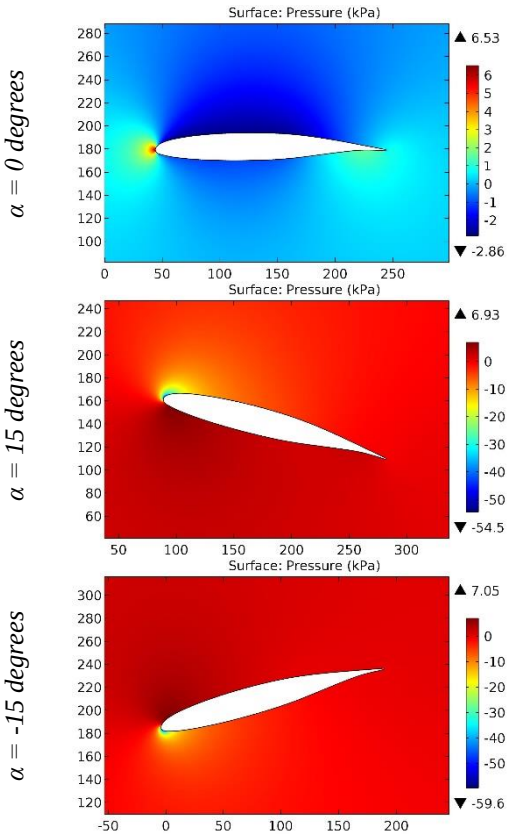

Figure 79. The pressure contours on the surfaces of the NASA GA [W] 1-12 17 airfoil.

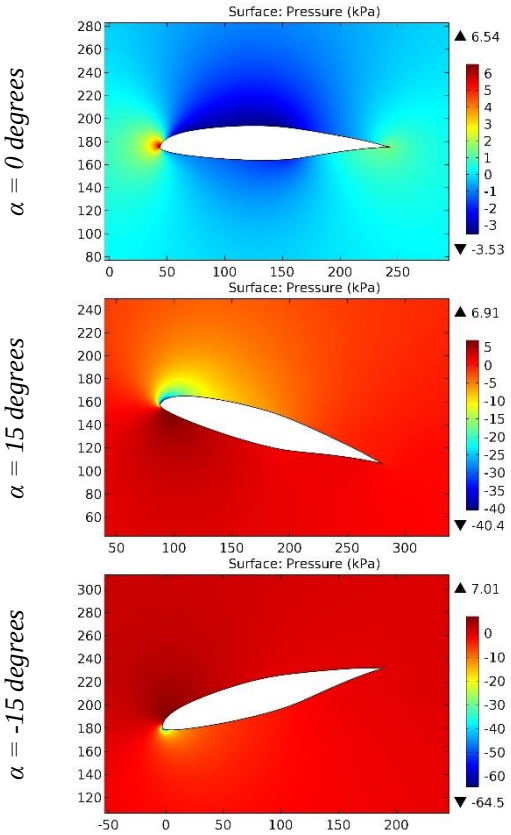

Figure 80. The pressure contours on the surfaces of the NASA NLF(1)-0115 airfoil.

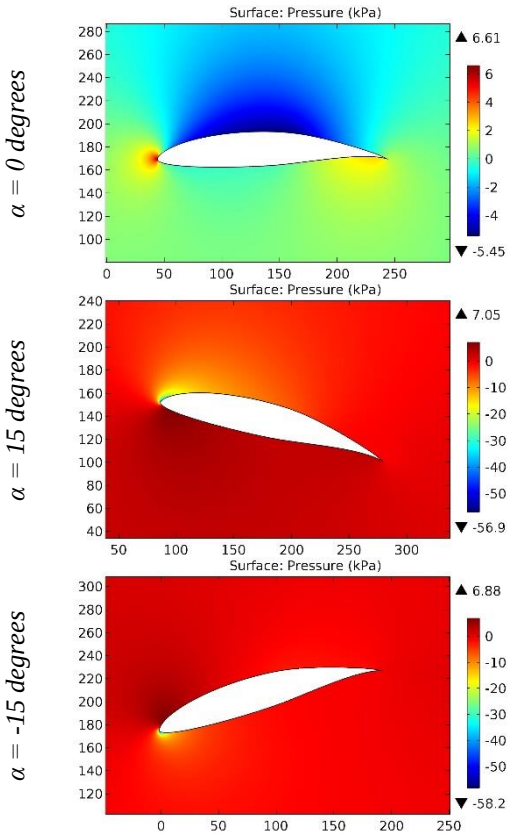

Figure 81. The pressure contours on the surfaces of the NASA NLF(1)-1015 airfoil.

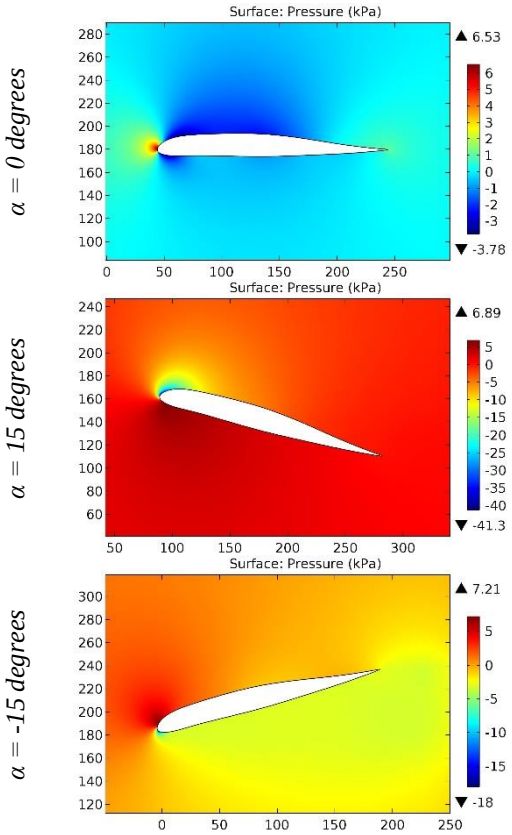

Figure 82. The pressure contours on the surfaces of the NASA RC(4)-10 airfoil.

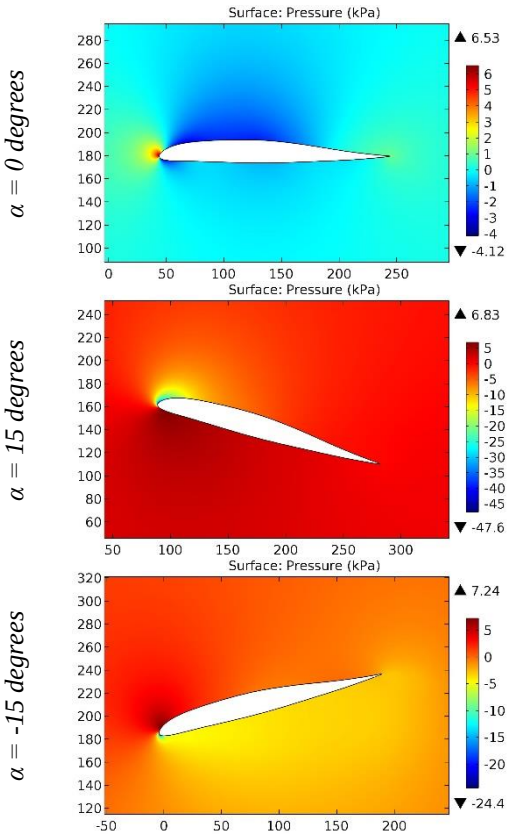

Figure 83. The pressure contours on the surfaces of the NASA RC(5)-10 airfoil.

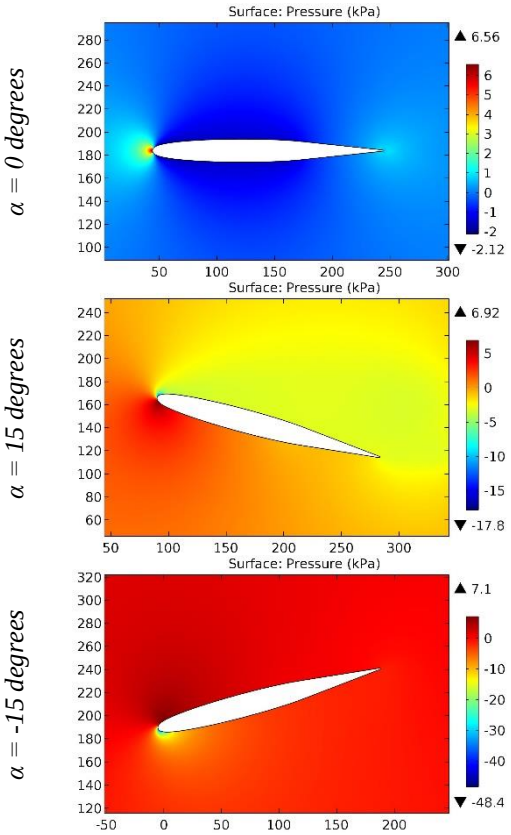

Figure 84. The pressure contours on the surfaces of the NASA SC(2)-0010 airfoil.

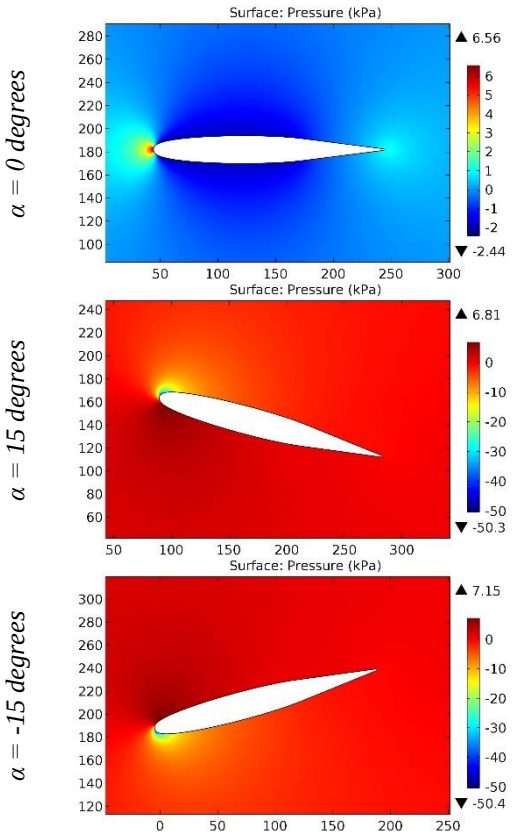

Figure 85. The pressure contours on the surfaces of the NASA SC(2)-0012 airfoil.

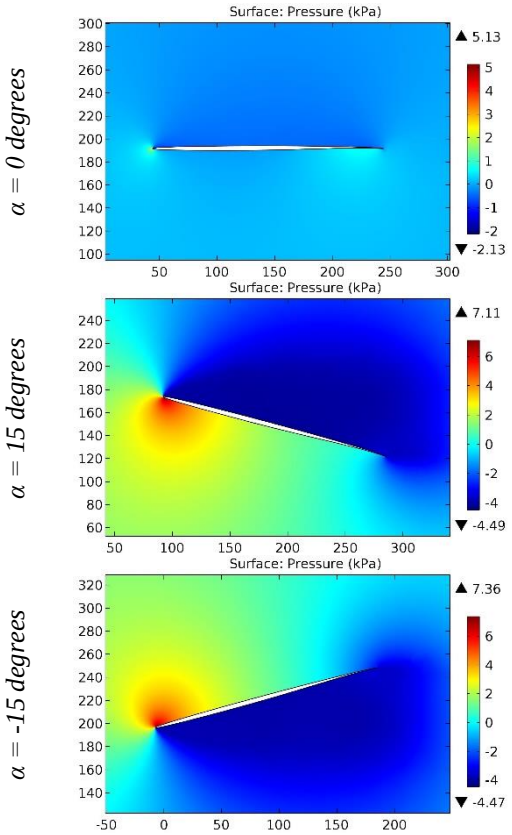

Figure 86. The pressure contours on the surfaces of the NASA SC(2)-0402 airfoil.

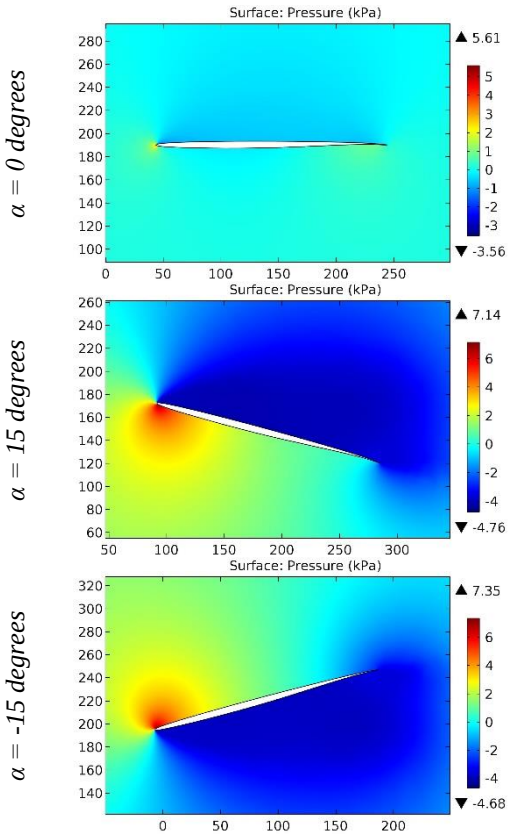

Figure 87. The pressure contours on the surfaces of the NASA SC(2)-0403 airfoil.

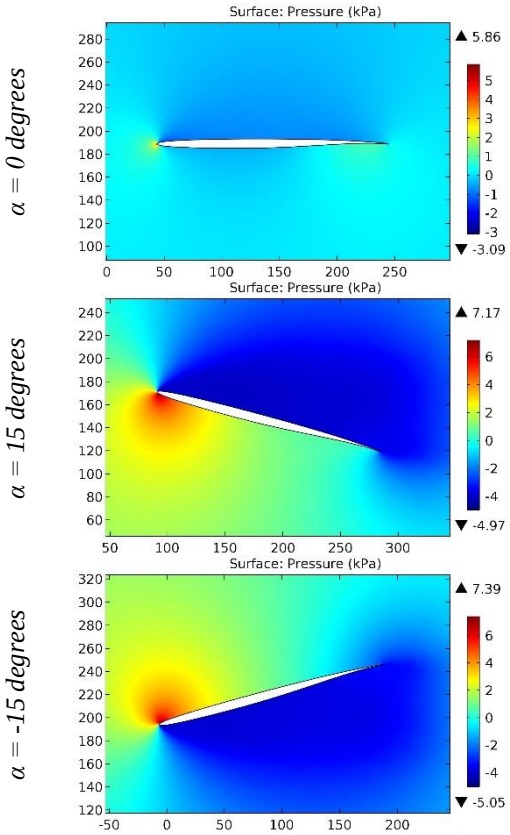

Figure 88. The pressure contours on the surfaces of the NASA SC(2)-0404 airfoil.

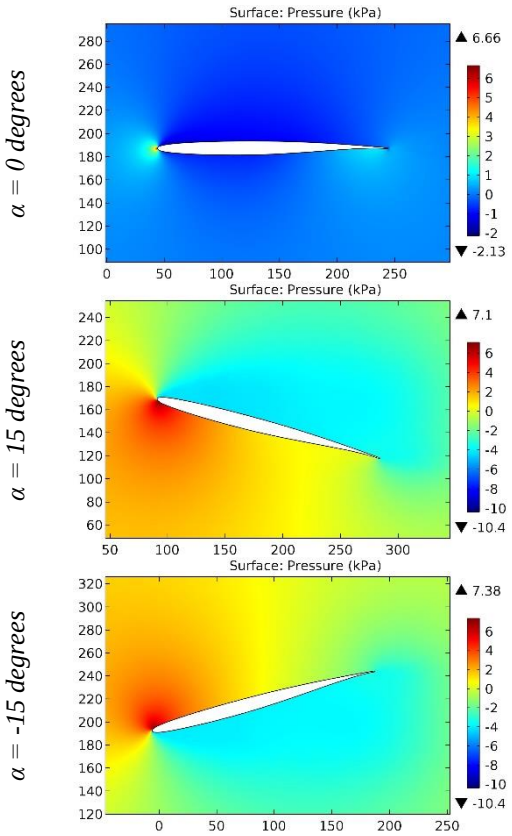

Figure 89. The pressure contours on the surfaces of the NASA SC(2)-0406 airfoil.

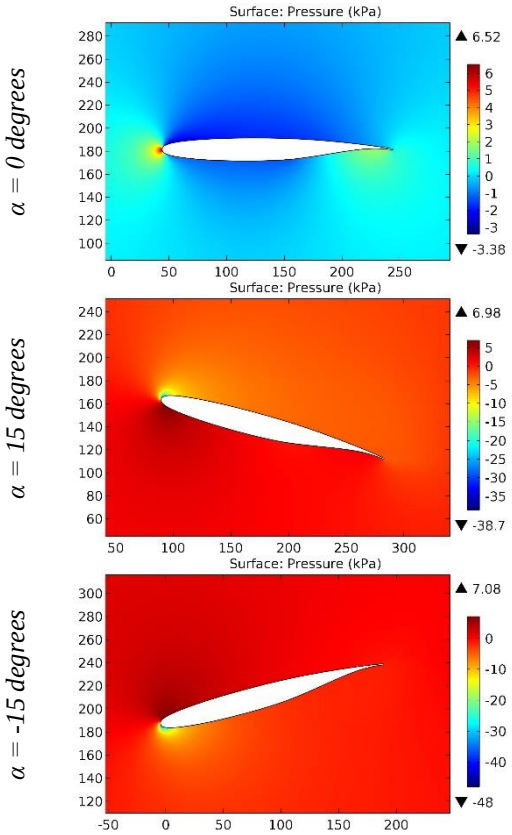

Figure 90. The pressure contours on the surfaces of the NASA SC(2)-0410 airfoil.

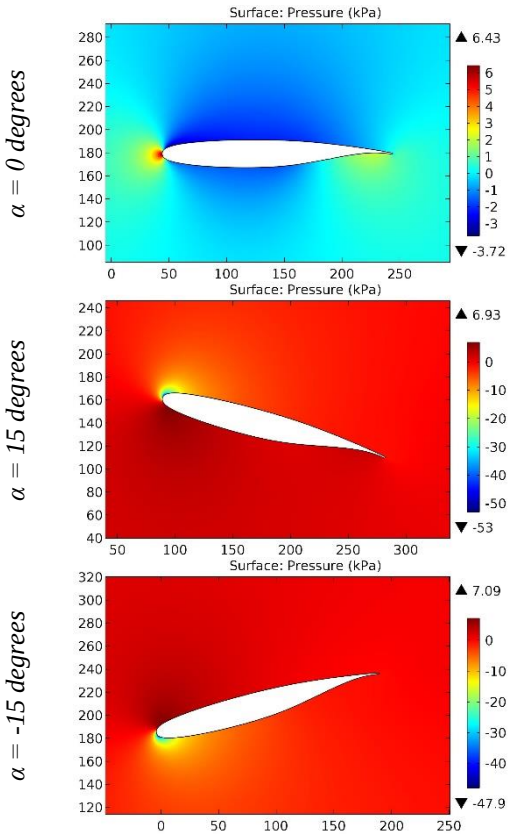

Figure 91. The pressure contours on the surfaces of the NASA SC(2)-0412 airfoil.

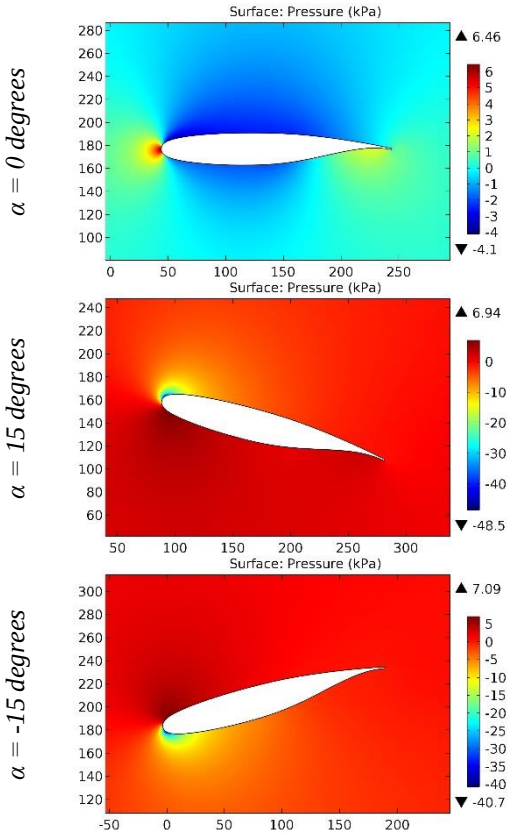

Figure 92. The pressure contours on the surfaces of the NASA SC(2)-0414 airfoil.

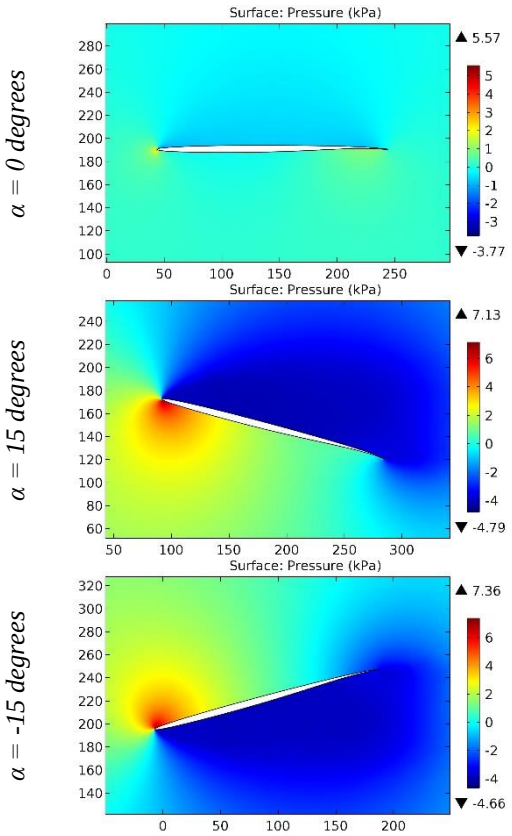

Figure 93. The pressure contours on the surfaces of the NASA SC(2)-0503 airfoil.

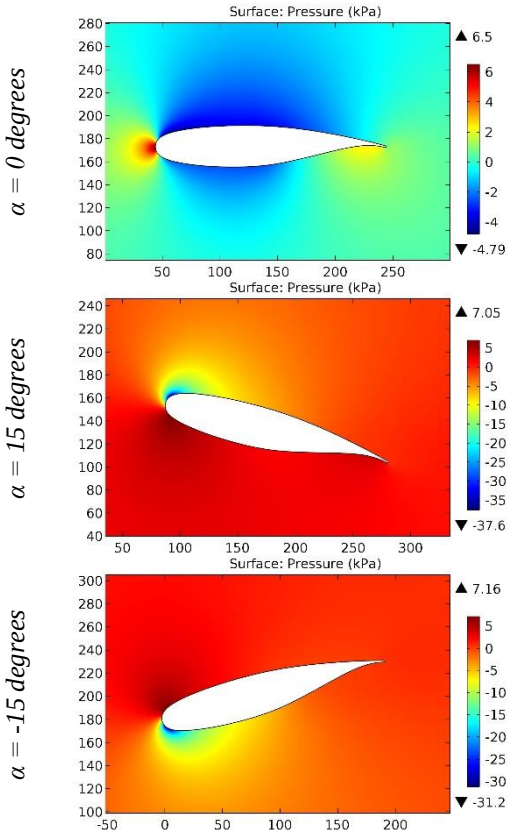

Figure 94. The pressure contours on the surfaces of the NASA SC(2)-0518 airfoil.

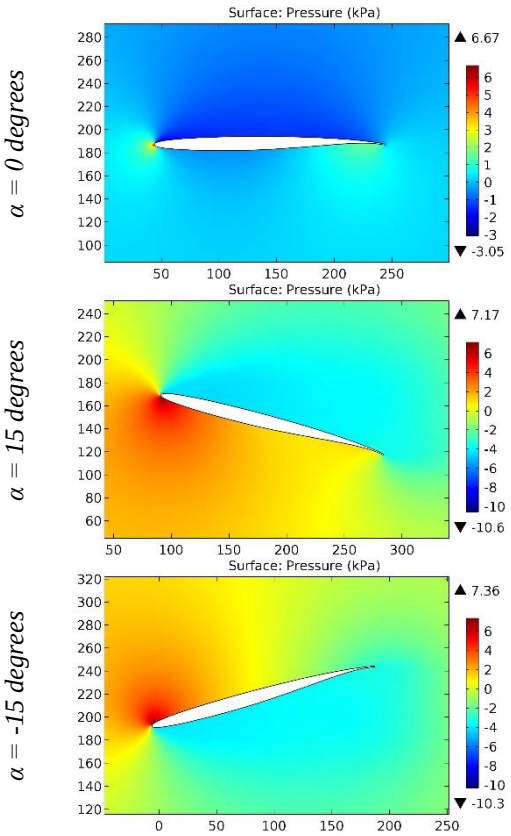

Figure 95. The pressure contours on the surfaces of the NASA SC(2)-0606 airfoil.

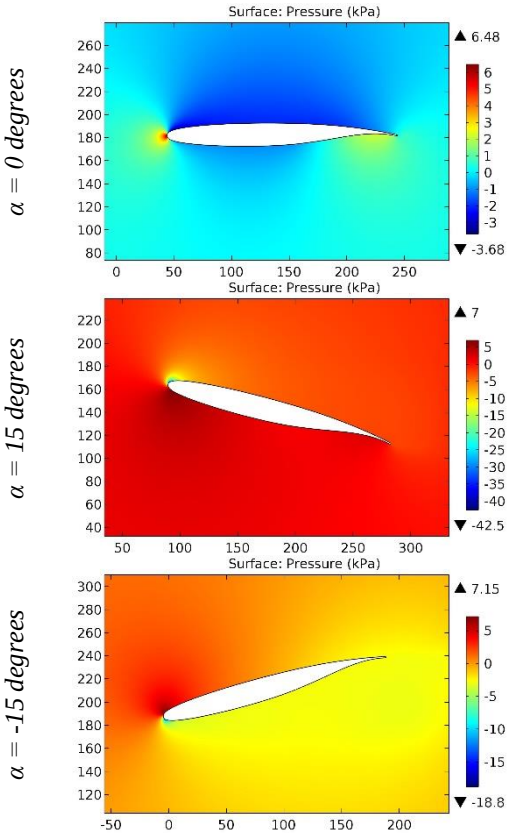

Figure 96. The pressure contours on the surfaces of the NASA SC(2)-0610 airfoil.

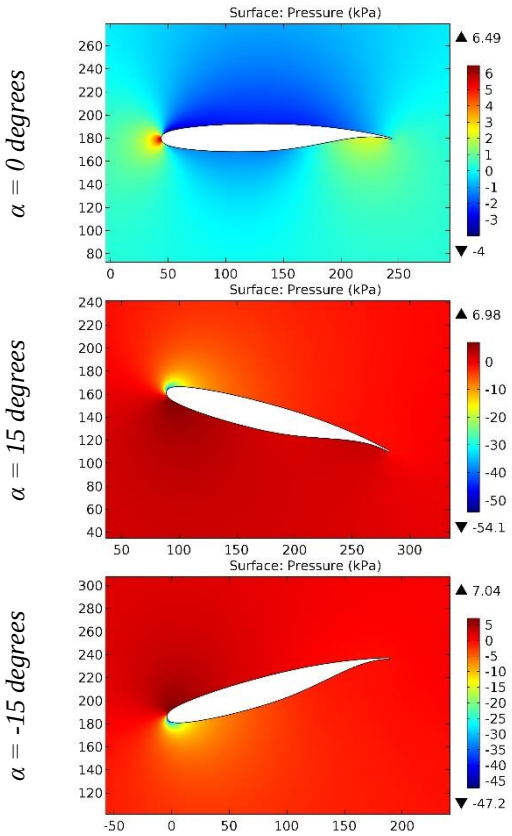

Figure 97. The pressure contours on the surfaces of the NASA SC(2)-0612 airfoil.

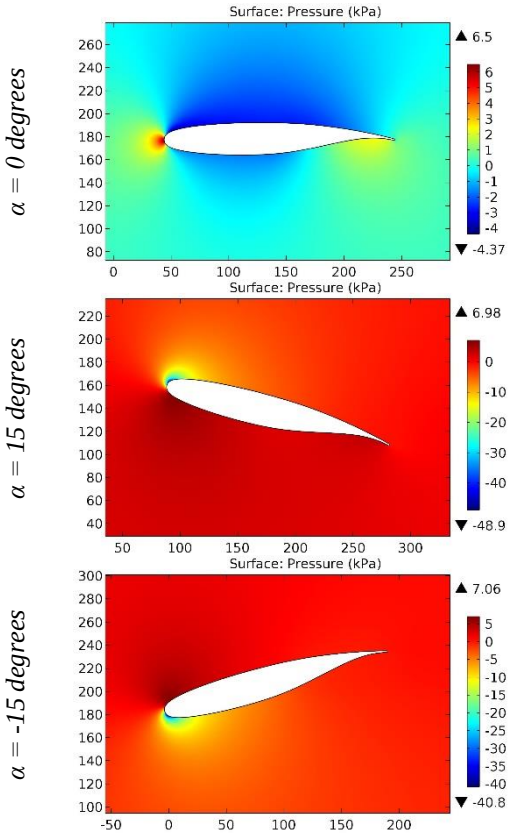

Figure 98. The pressure contours on the surfaces of the NASA SC(2)-0614 airfoil.

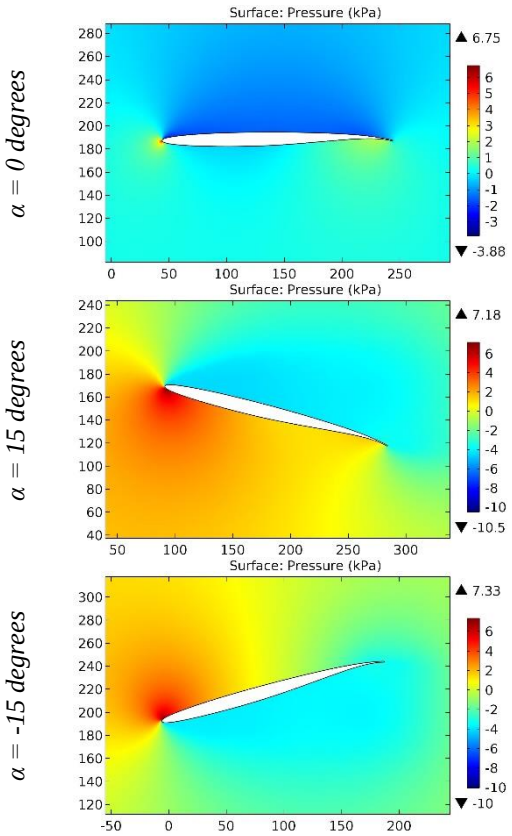

Figure 99. The pressure contours on the surfaces of the NASA SC(2)-0706 airfoil.

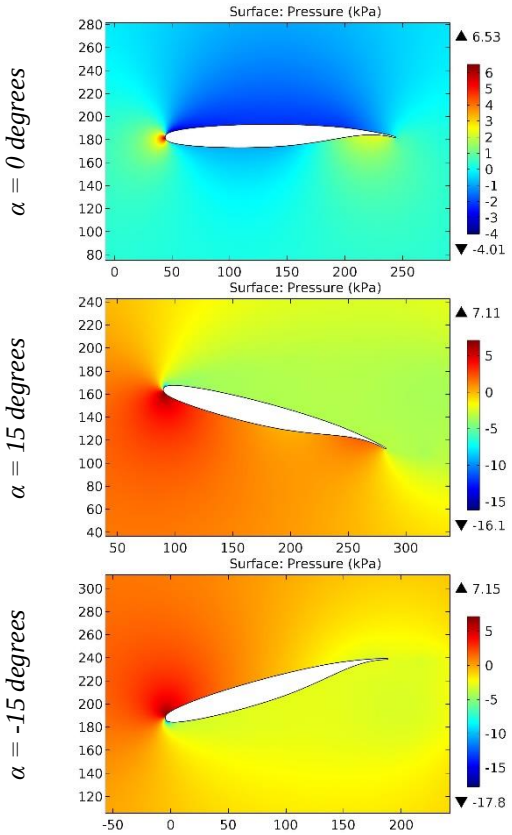

Figure 100. The pressure contours on the surfaces of the NASA SC(2)-0710 airfoil.

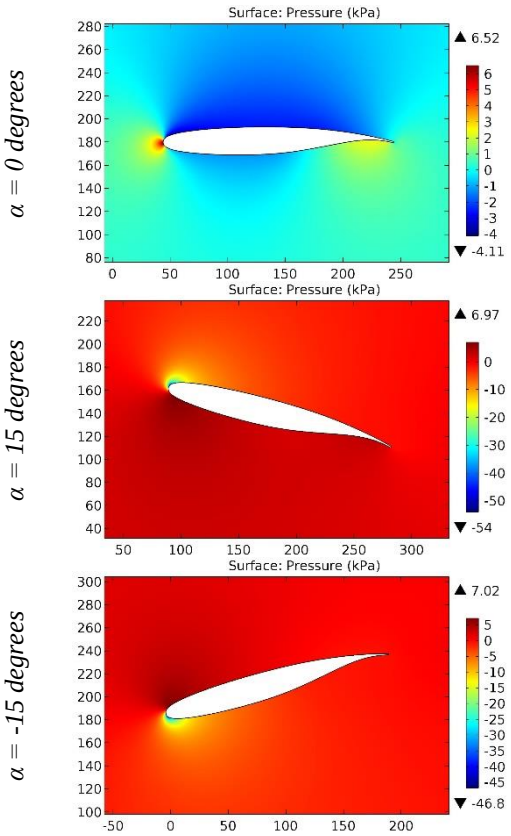

Figure 101. The pressure contours on the surfaces of the NASA SC(2)-0712 airfoil.

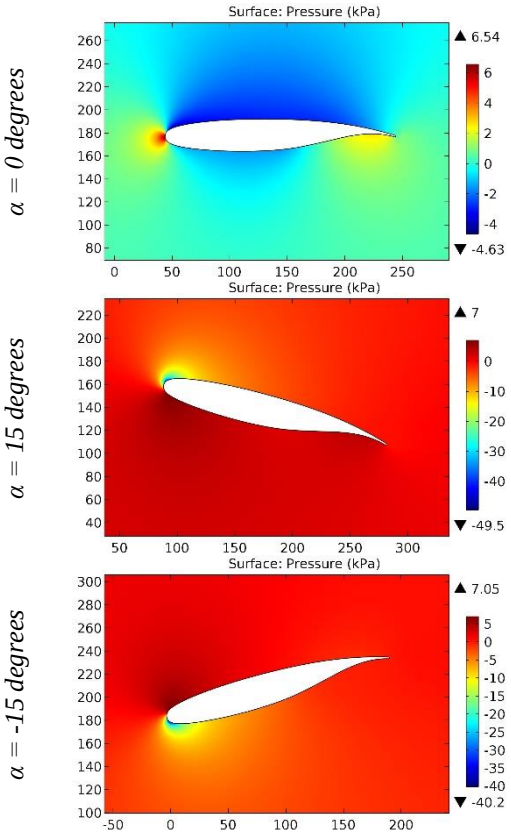

Figure 102. The pressure contours on the surfaces of the NASA SC(2)-0714 airfoil.

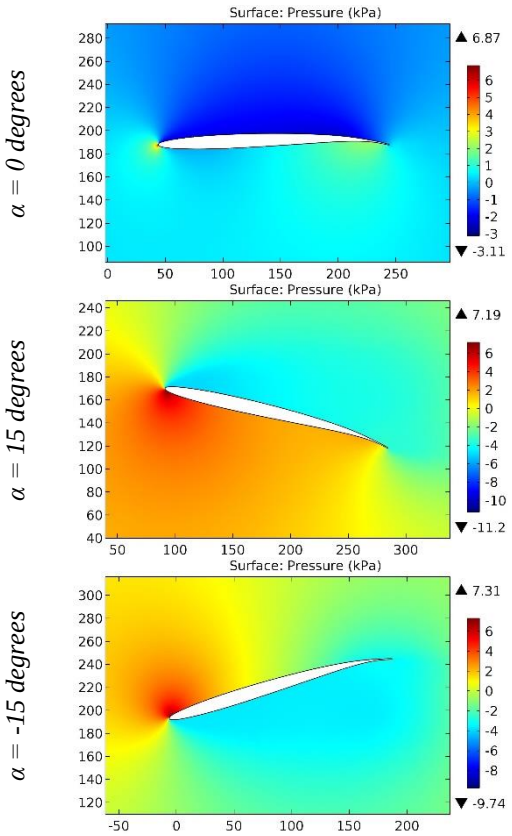

Figure 103. The pressure contours on the surfaces of the NASA SC(2)-1006 airfoil.

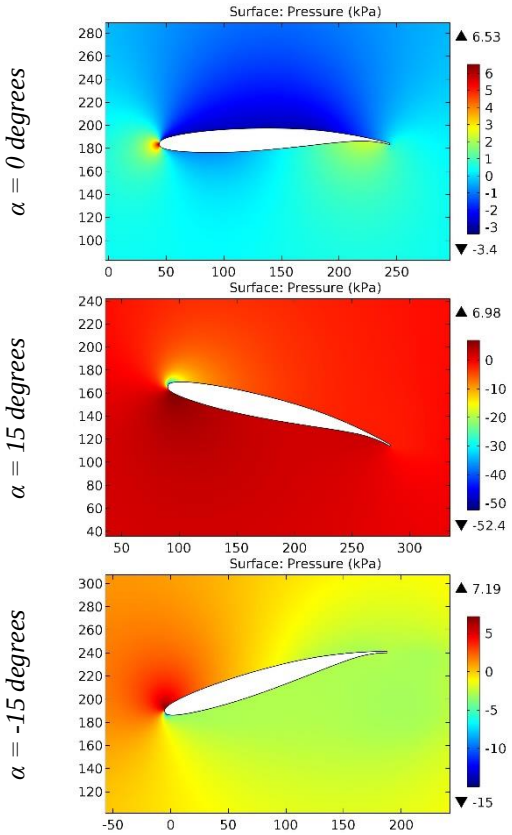

Figure 104. The pressure contours on the surfaces of the NASA SC(2)-1010 airfoil.

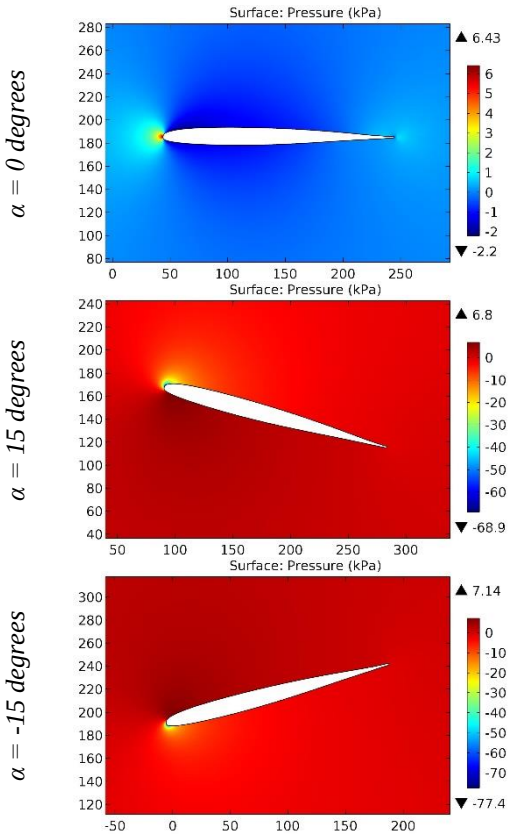

Figure 105. The pressure contours on the surfaces of the NASA/AMES airfoil.

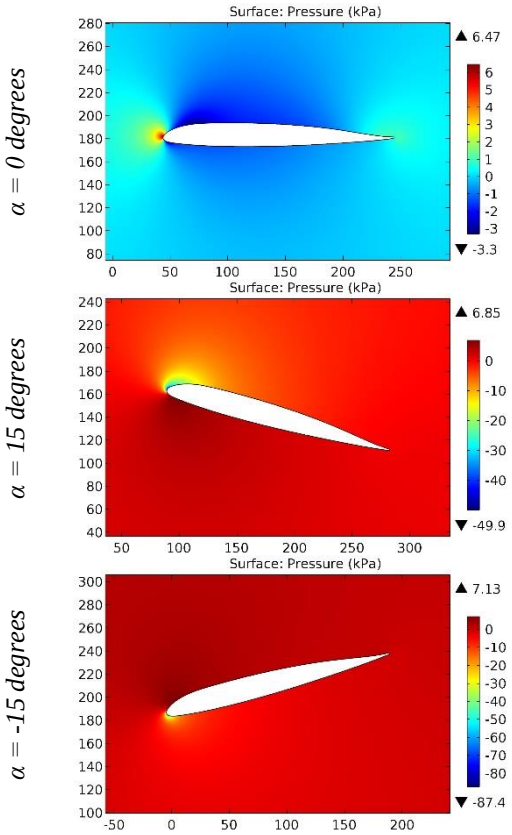

Figure 106. The pressure contours on the surfaces of the NASA/AMES/Hicks A-01 airfoil.

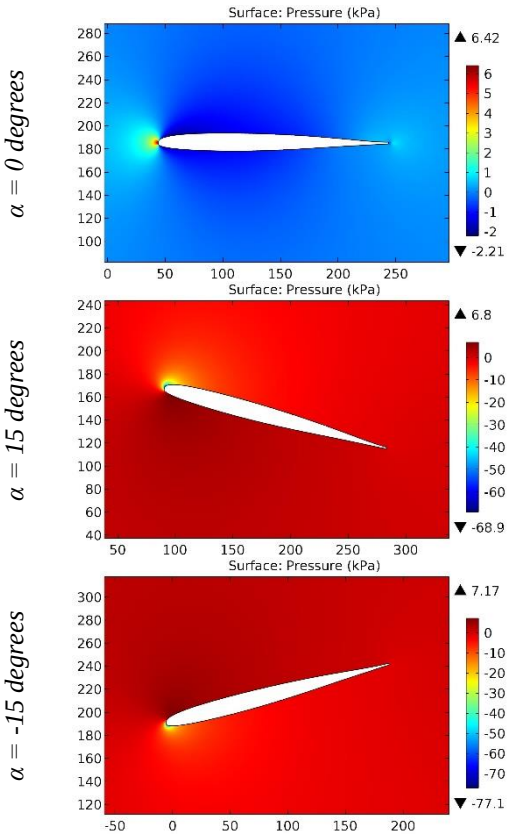

Figure 107. The pressure contours on the surfaces of the NASA/AMES/Hicks A-02 airfoil.

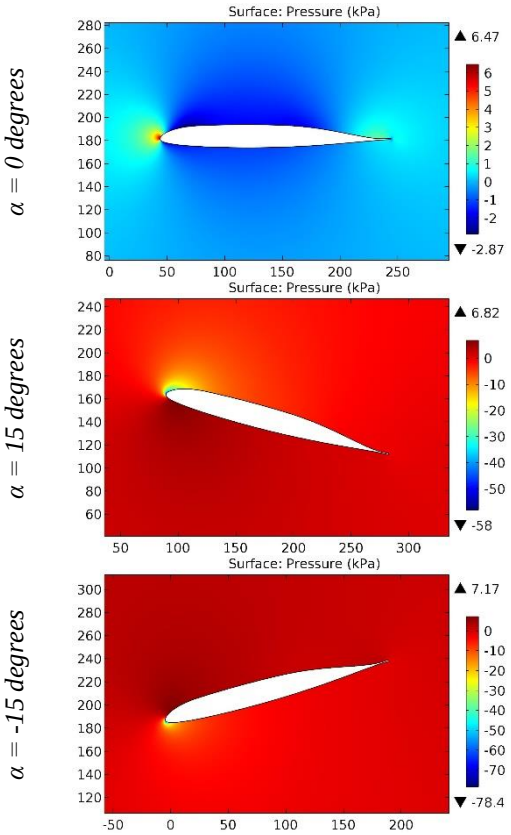

Figure 108. The pressure contours on the surfaces of the NASA/AMES/Kennelly A-03 airfoil.

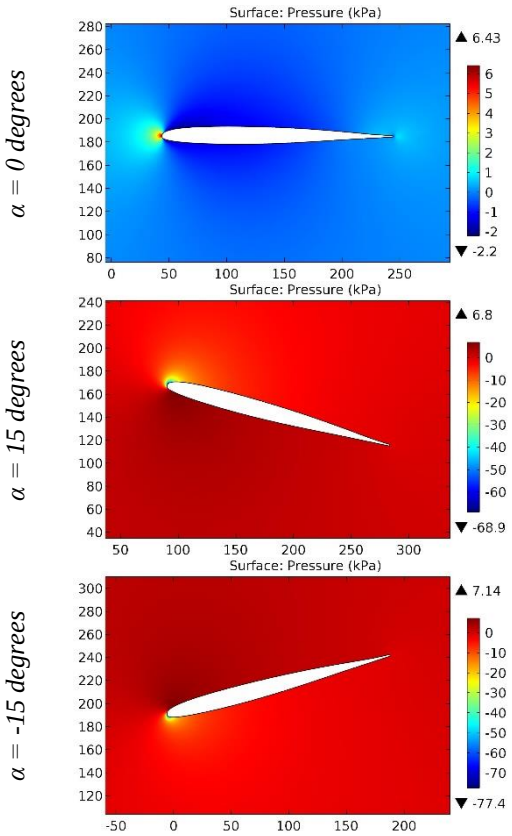

Figure 109. The pressure contours on the surfaces of the NASA-AMES 63A108 MOD C airfoil.

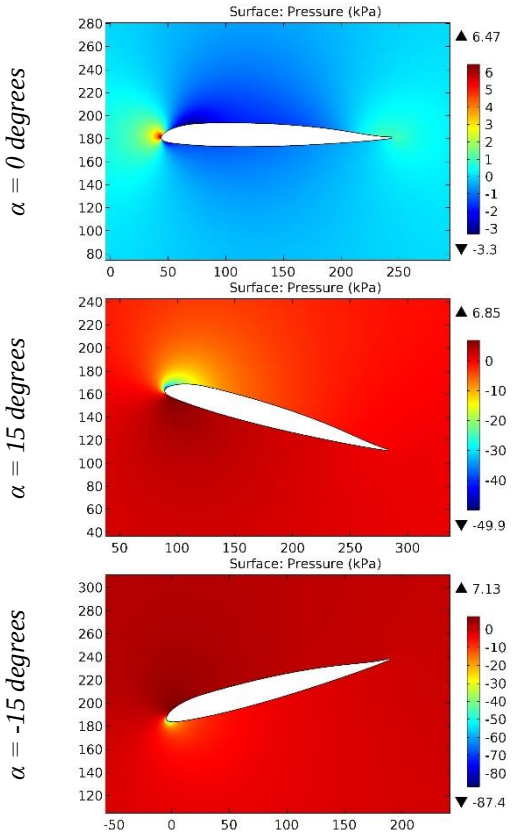

Figure 110. The pressure contours on the surfaces of the NASA-AMES A-01 airfoil.

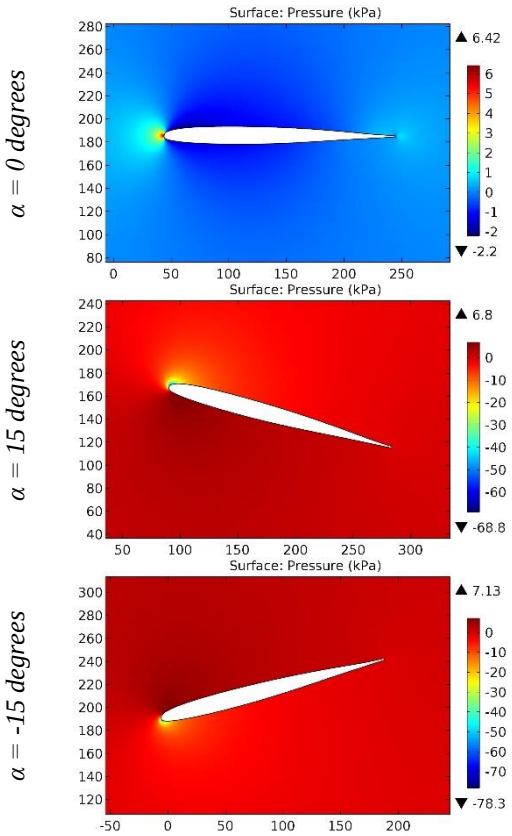

Figure 111. The pressure contours on the surfaces of the NASA-AMES A-02 airfoil.

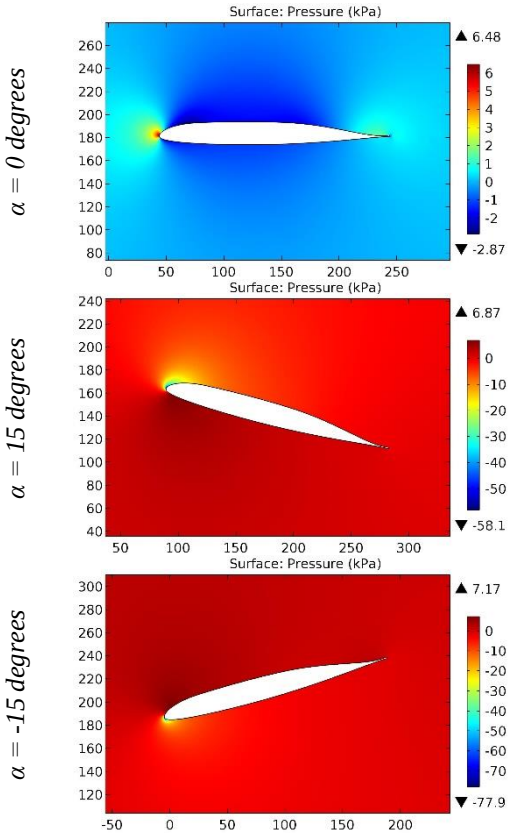

Figure 112. The pressure contours on the surfaces of the NASA-AMES A-03 airfoil.

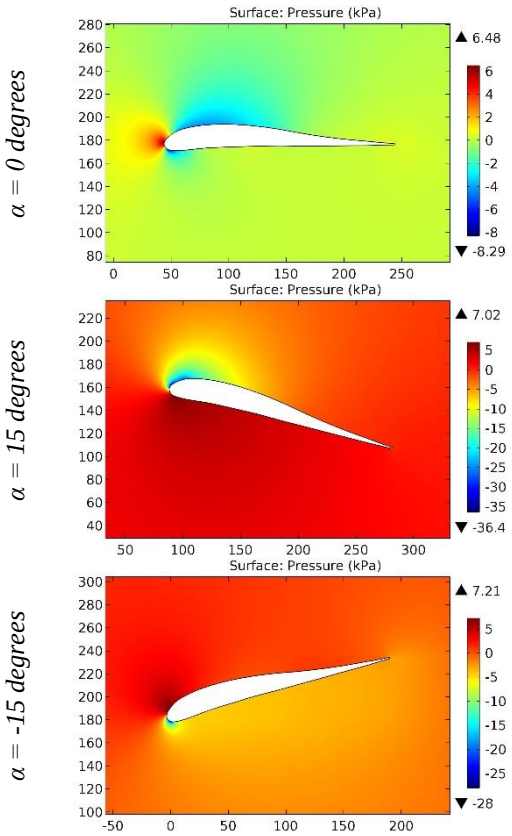

Figure 113. The pressure contours on the surfaces of the NASA F G8 airfoil.

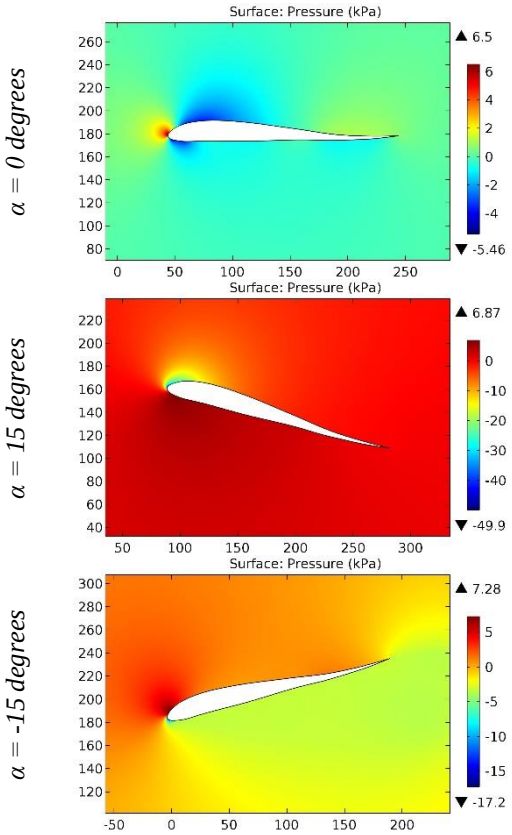

Figure 114. The pressure contours on the surfaces of the NASA F PG 7 airfoil.

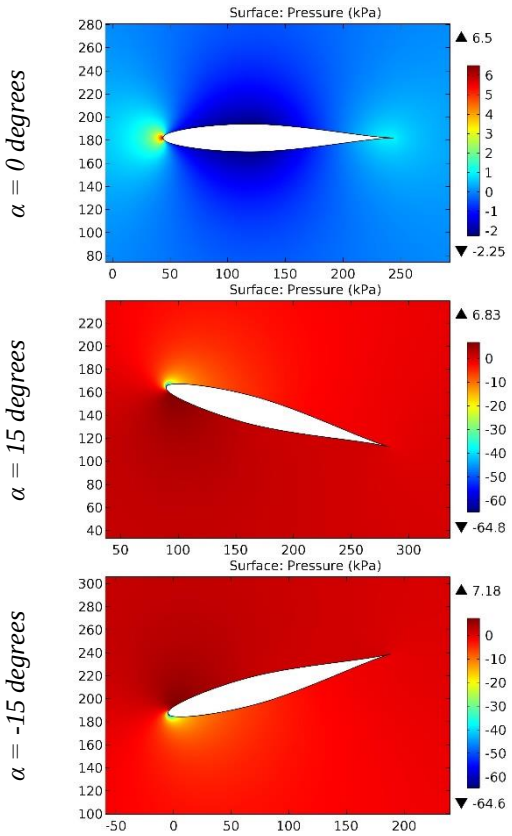

Figure 115. The pressure contours on the surfaces of the NASA-LANGLEY 64-012 airfoil.

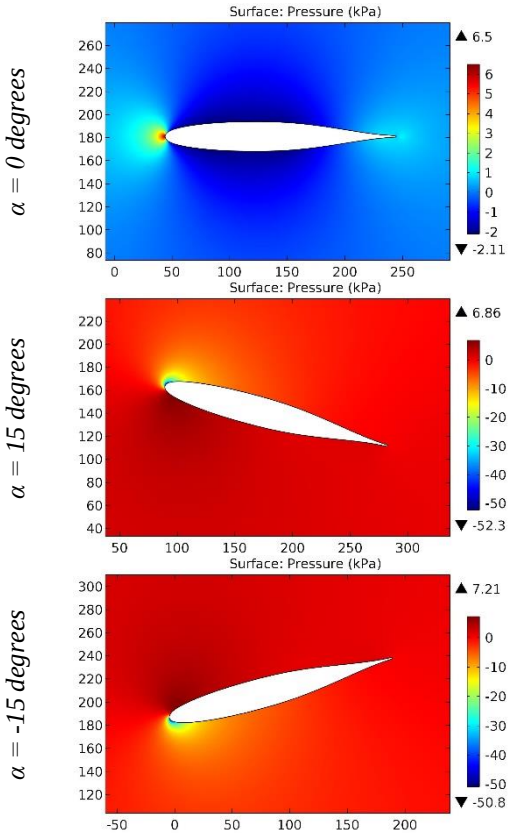

Figure 116. The pressure contours on the surfaces of the NASA-LANGLEY LS(1)-0013 airfoil.

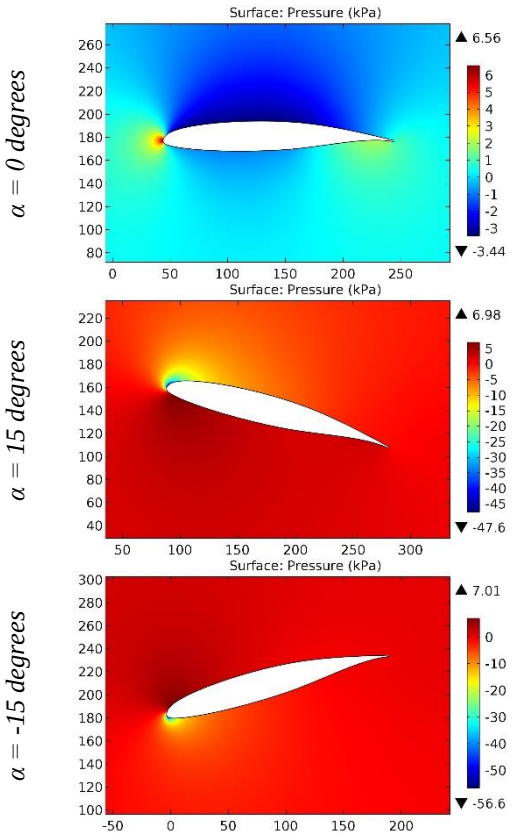

Figure 117. The pressure contours on the surfaces of the NASA-LANGLEY LS(1)-0413 (GA(W)-2) airfoil.

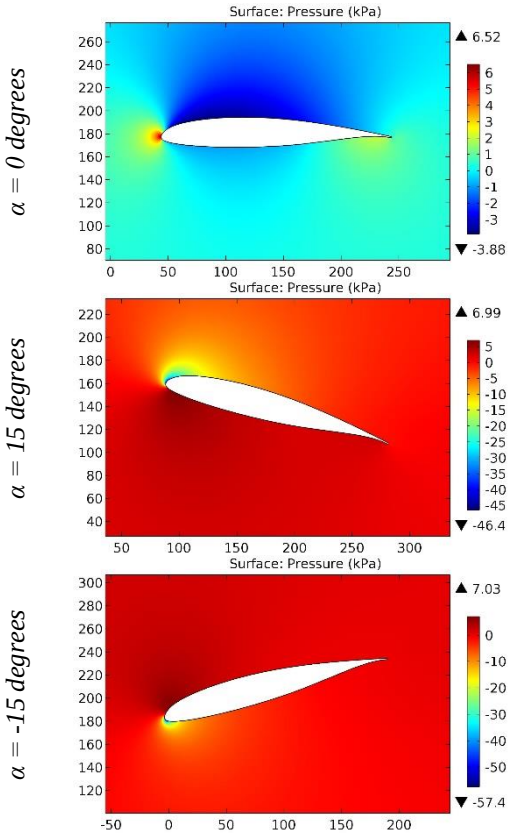

Figure 118. The pressure contours on the surfaces of the NASA-LANGLEY LS(1)-0413MOD airfoil.

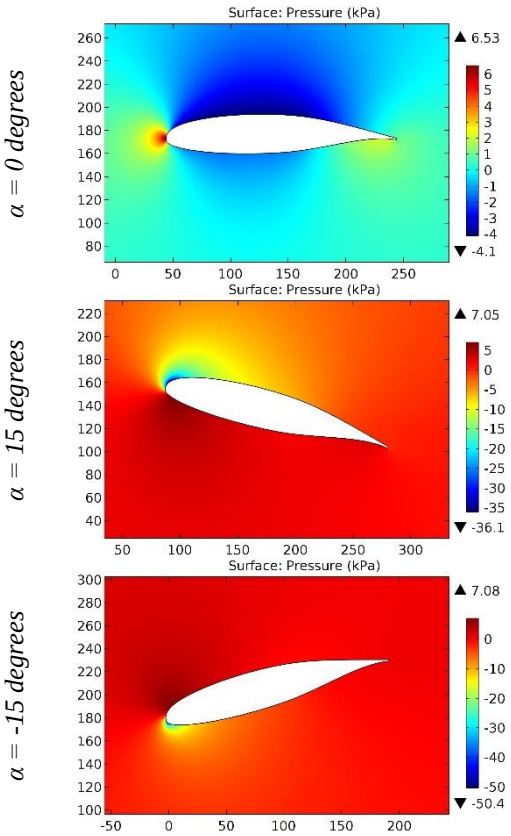

Figure 119. The pressure contours on the surfaces of the NASA-LANGLEY LS(1)-0417 (GA(W)-1) airfoil.

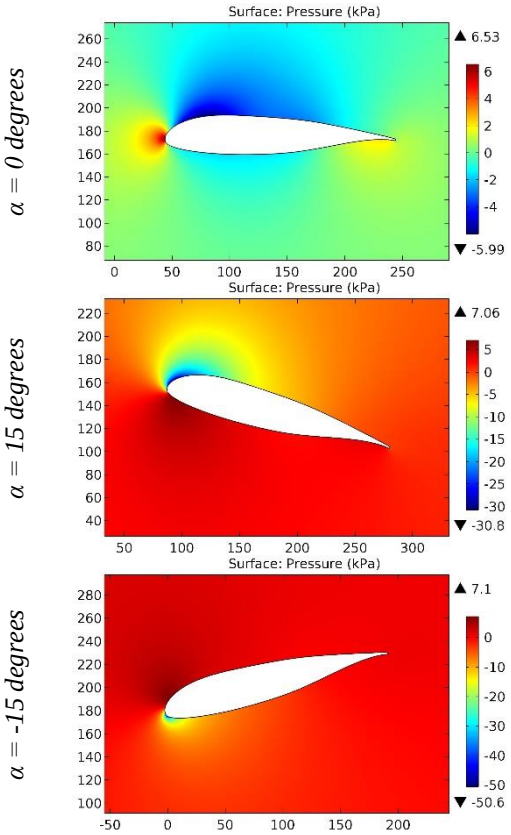

Figure 120. The pressure contours on the surfaces of the NASA-LANGLEY LS(1)-0417MOD airfoil.

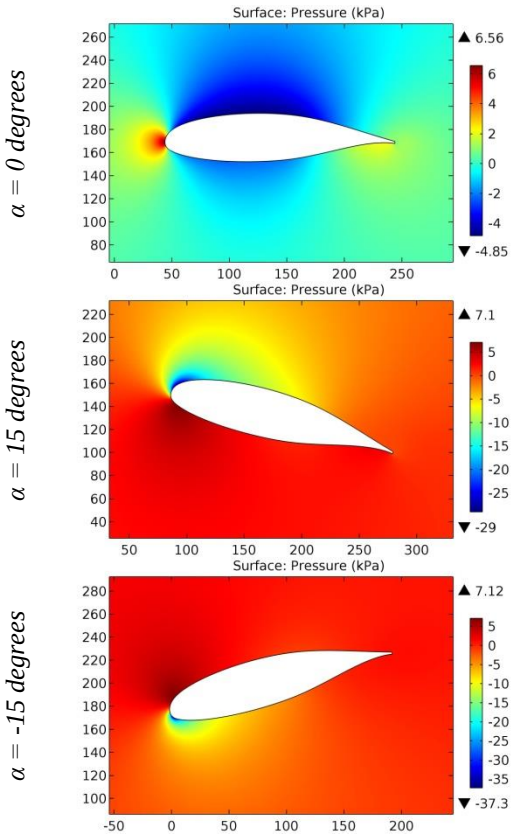

Figure 121. The pressure contours on the surfaces of the NASA-LANGLEY LS(1)-0421 airfoil.

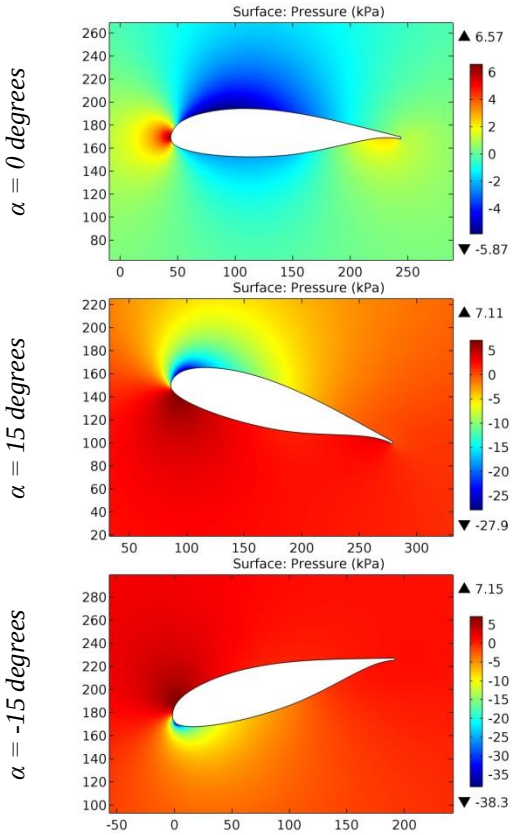

Figure 122. The pressure contours on the surfaces of the NASA-LANGLEY LS(1)-0421MOD airfoil.

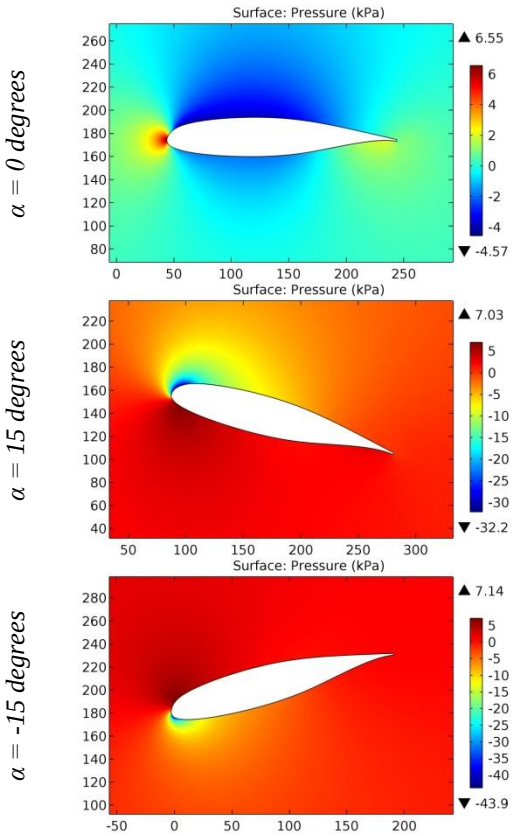

Figure 123. The pressure contours on the surfaces of the NASA-LANGLEY MS(1)-0317 airfoil.

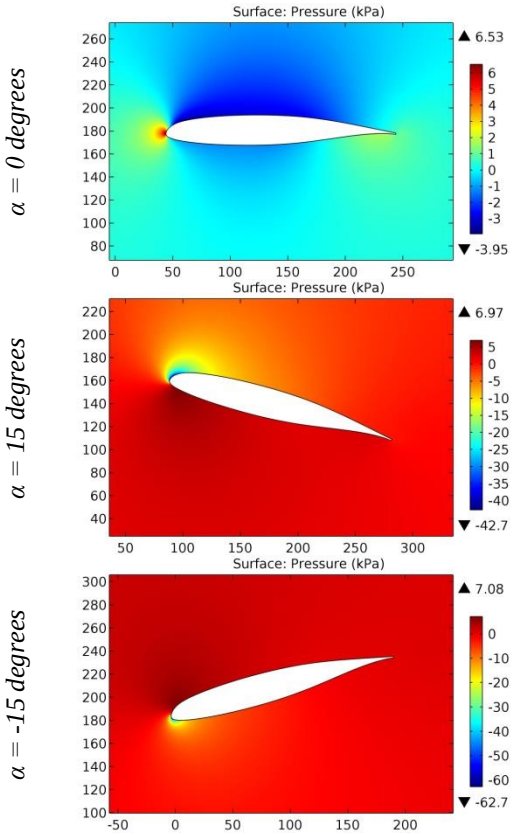

Figure 124. The pressure contours on the surfaces of the NASA-LANGLEY MS(1)-0413 airfoil.

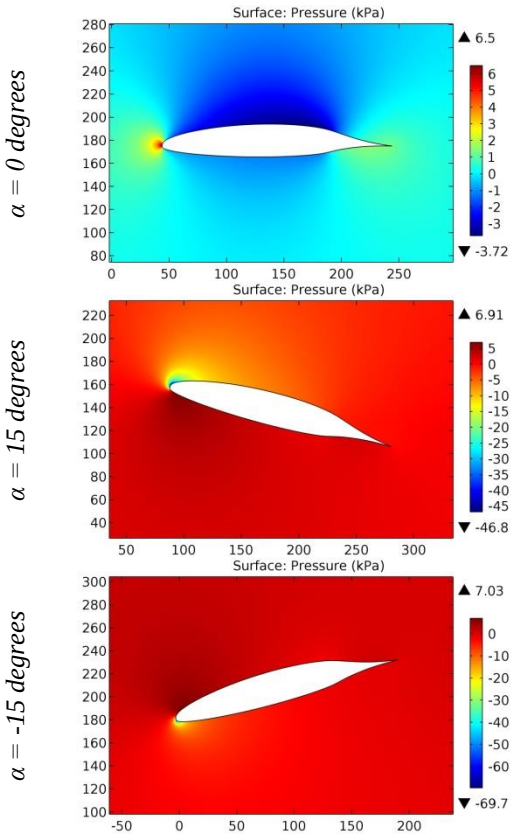

Figure 125. The pressure contours on the surfaces of the NASA-LANGLEY NLF 0414F airfoil.

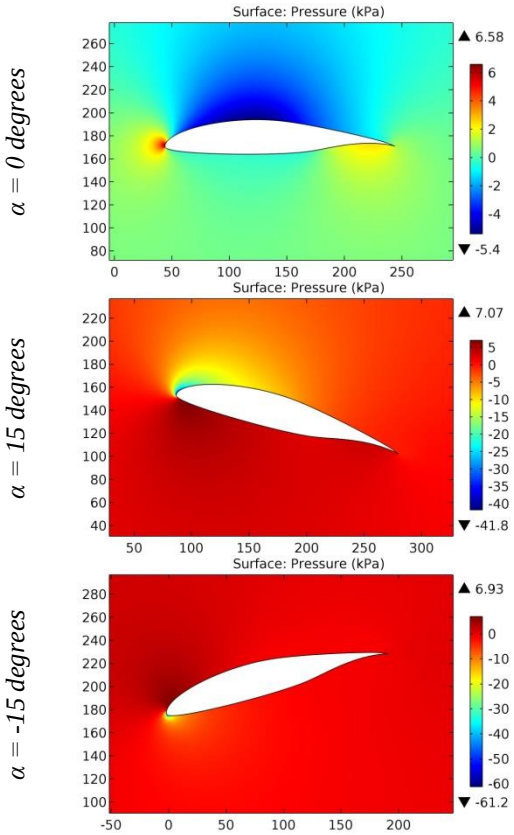

Figure 126. The pressure contours on the surfaces of the NASA-LANGLEY NLF(1)-0215F airfoil.

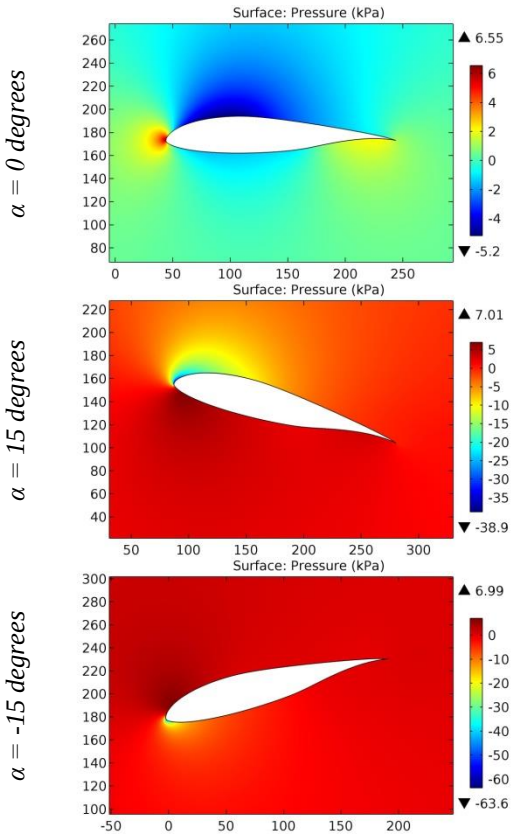

Figure 127. The pressure contours on the surfaces of the NASA-LANGLEY NLF(1)-0416 airfoil.

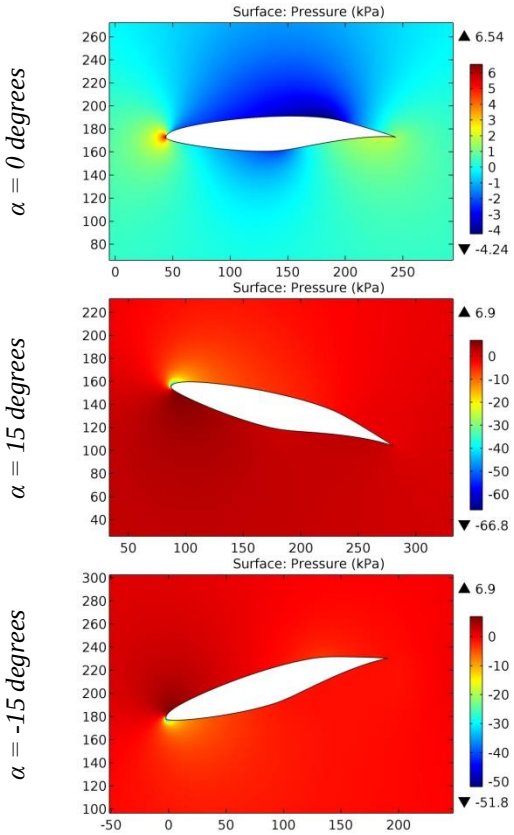

Figure 128. The pressure contours on the surfaces of the NASA-LANGLEY NLF(2)-0415 airfoil.

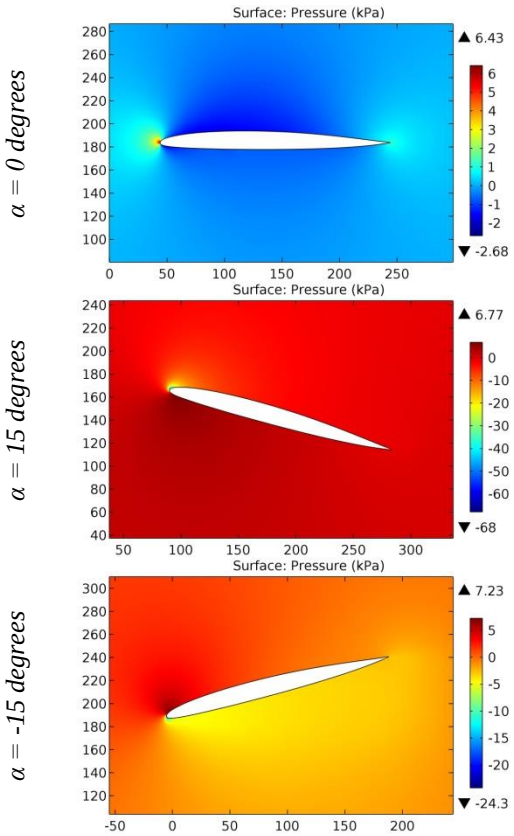

Figure 129. The pressure contours on the surfaces of the NASA-LANGLEY RC-08(B)3 airfoil.

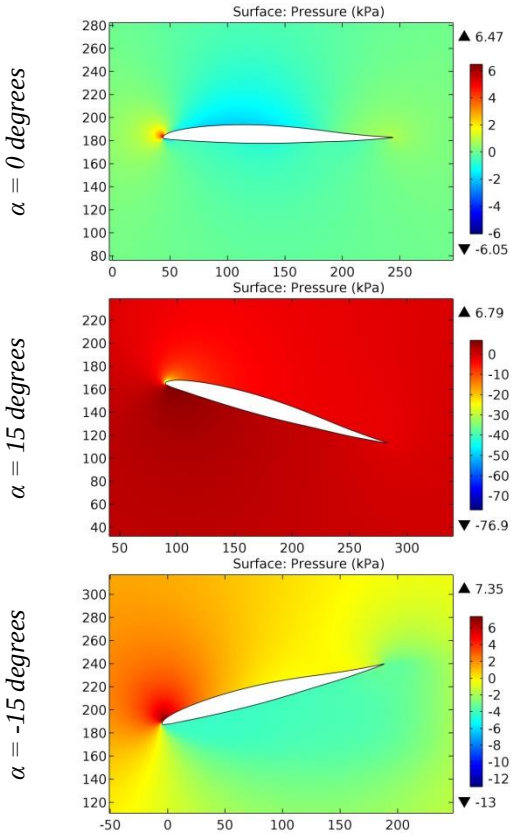

Figure 130. The pressure contours on the surfaces of the NASA-LANGLEY RC-08(N)1 airfoil.

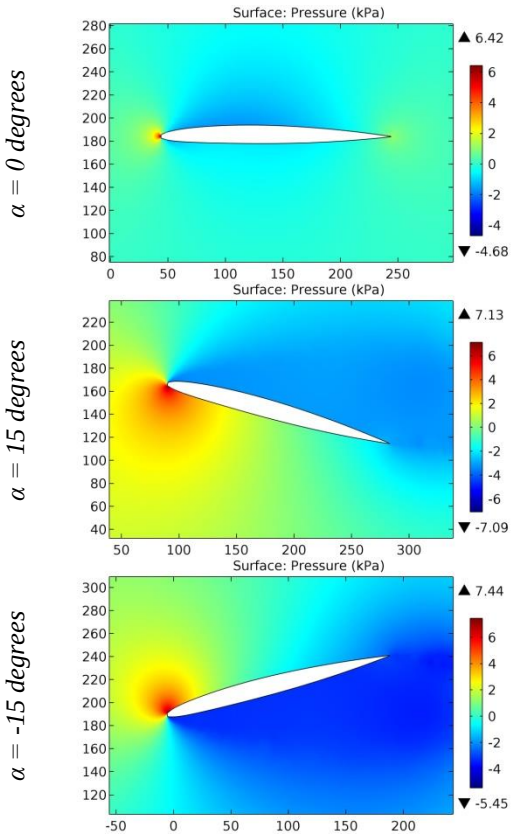

Figure 131. The pressure contours on the surfaces of the NASA-LANGLEY RC08-64C airfoil.

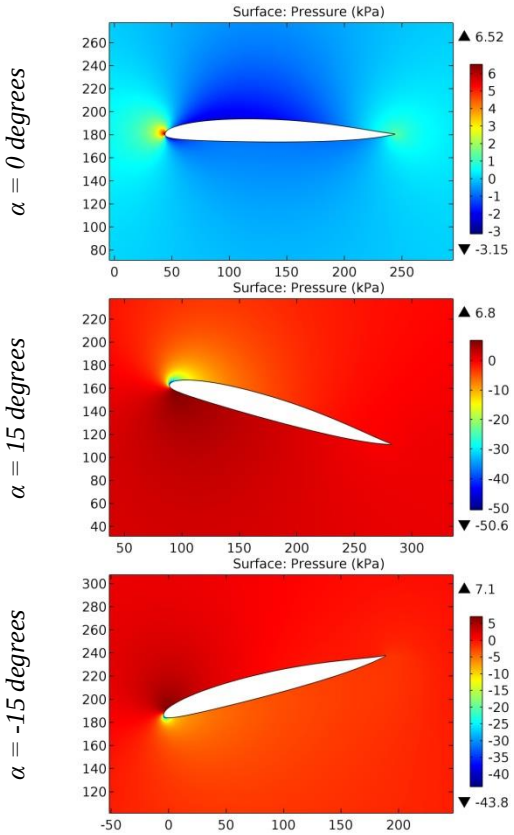

Figure 132. The pressure contours on the surfaces of the NASA-LANGLEY RC-10(B)3 airfoil.

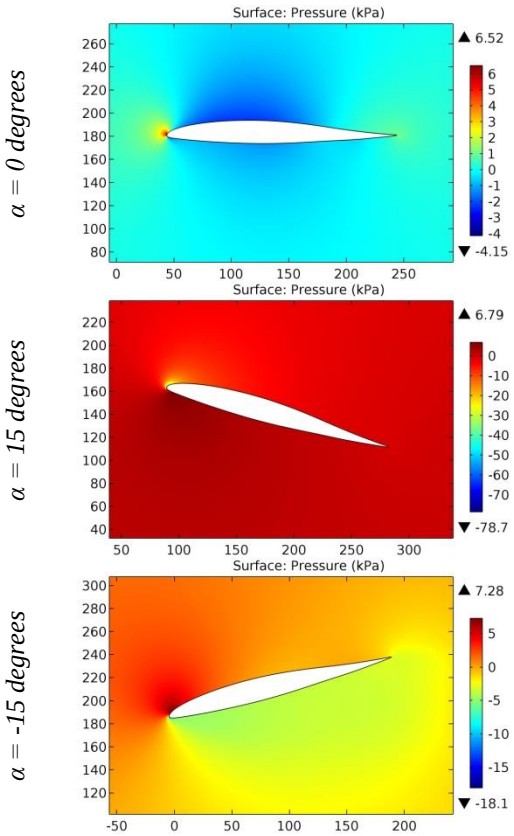

Figure 133. The pressure contours on the surfaces of the NASA-LANGLEY RC-10(N)1 airfoil.

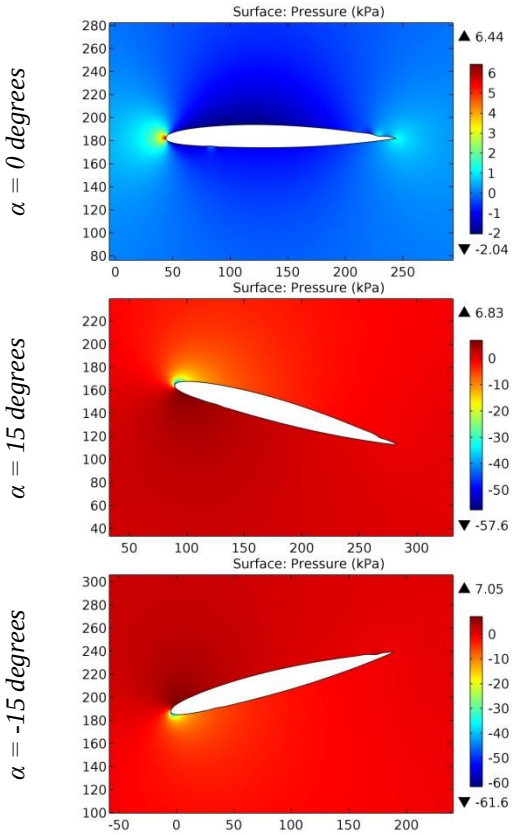

Figure 134. The pressure contours on the surfaces of the NASA-LANGLEY RC10-64C airfoil.

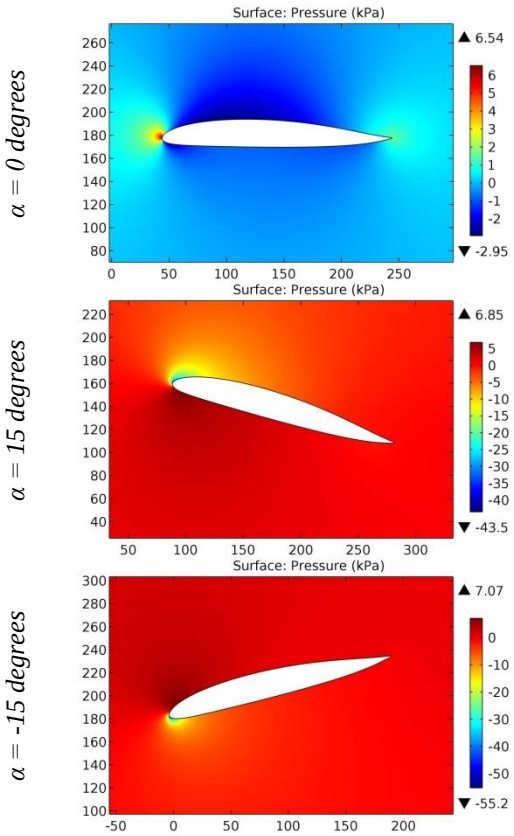

Figure 135. The pressure contours on the surfaces of the NASA-LANGLEY RC-12(B)3 airfoil.

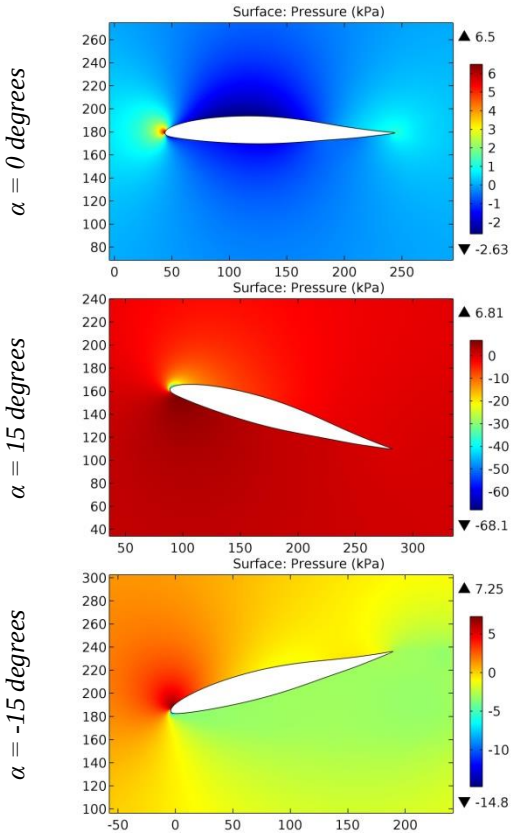

Figure 136. The pressure contours on the surfaces of the NASA-LANGLEY RC-12(N)1 airfoil.

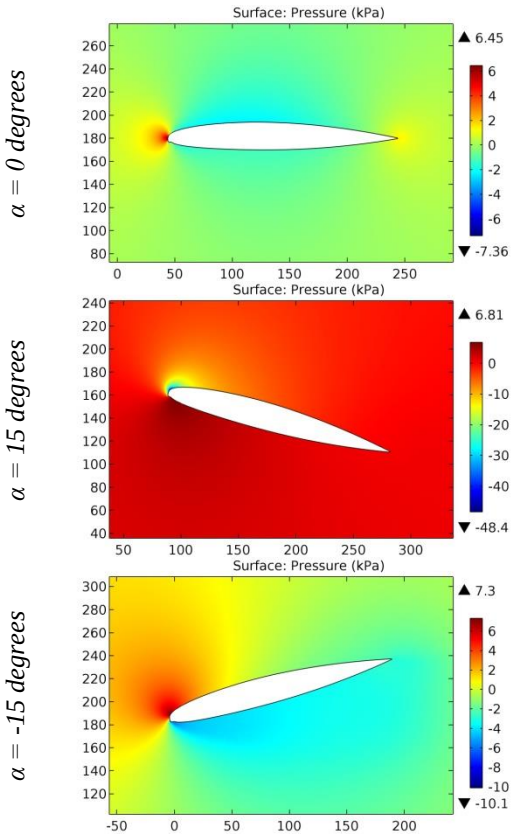

Figure 137. The pressure contours on the surfaces of the NASA-LANGLEY RC12-64C airfoil.

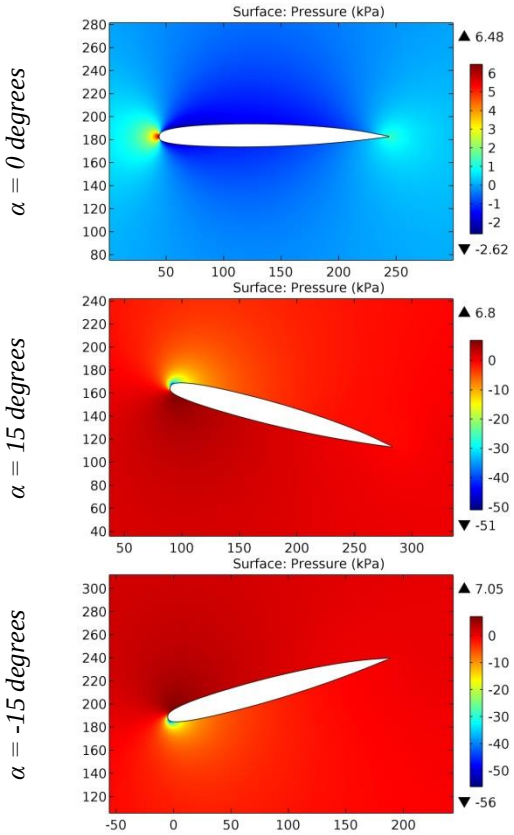

Figure 138. The pressure contours on the surfaces of the NASA-LANGLEY RC-SC2 airfoil.

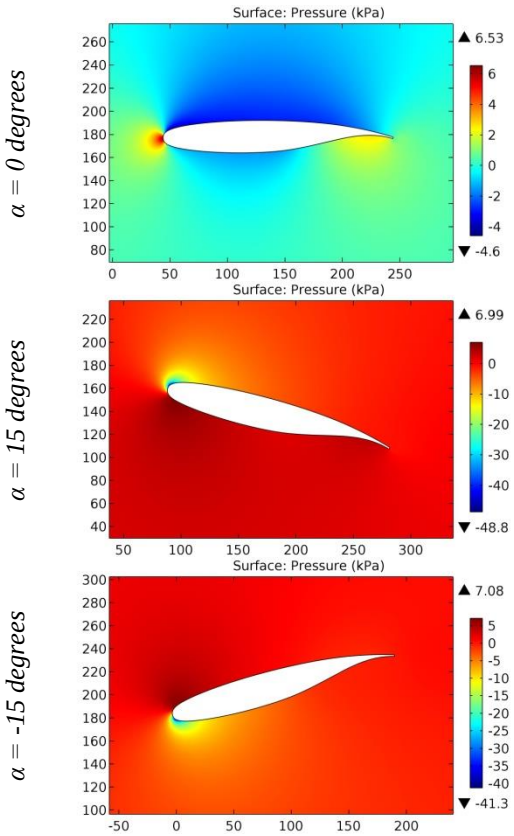

Figure 139. The pressure contours on the surfaces of the NASA-LANGLEY SC(2)-0714 SUPERCRITICAL airfoil.

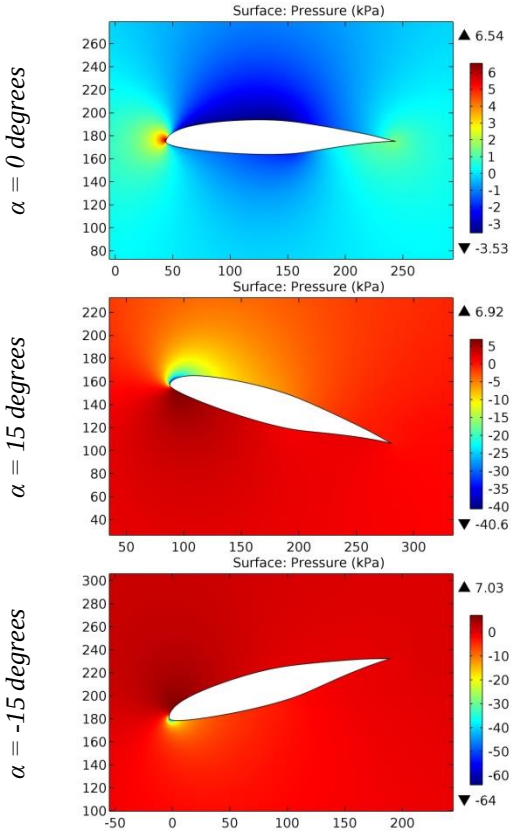

Figure 140. The pressure contours on the surfaces of the NASANLF1 airfoil.

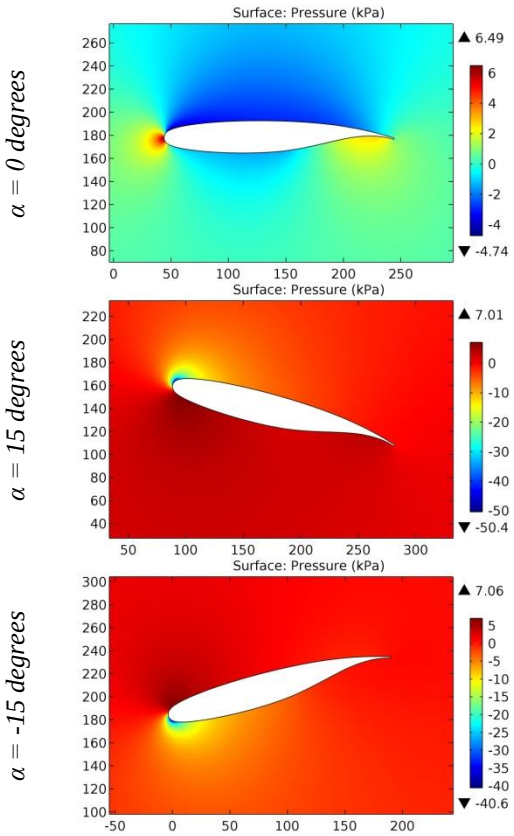

Figure 141. The pressure contours on the surfaces of the NASA-SC2 airfoil.

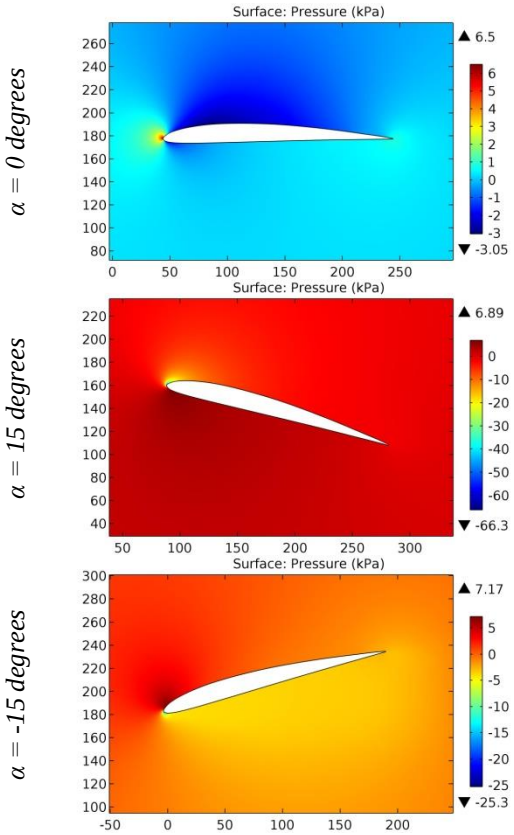

Figure 142. The pressure contours on the surfaces of the NAVY-N-9 airfoil.

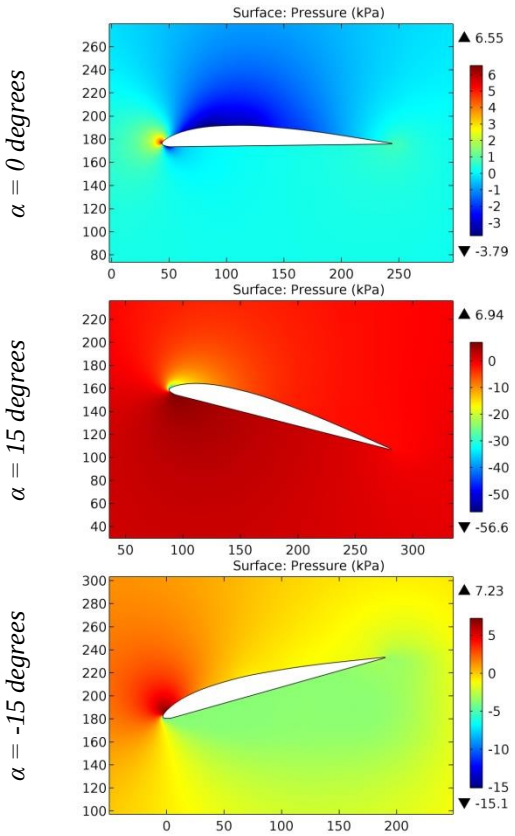

Figure 143. The pressure contours on the surfaces of the Neelmeyer airfoil.

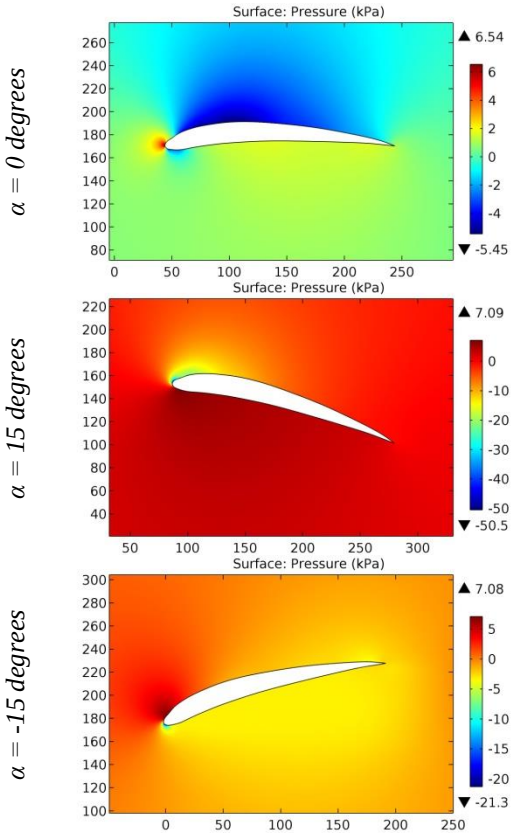

Figure 144. The pressure contours on the surfaces of the NEUMANN airfoil.

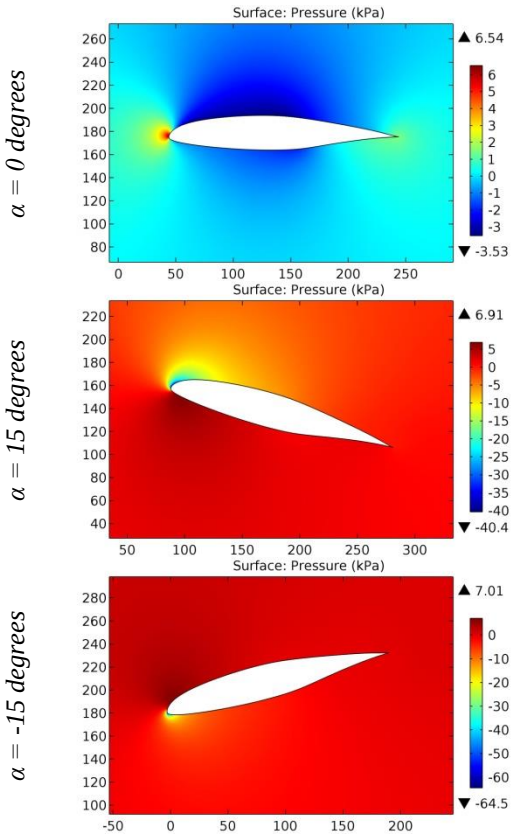

Figure 145. The pressure contours on the surfaces of the NLF(1)-0115 airfoil.

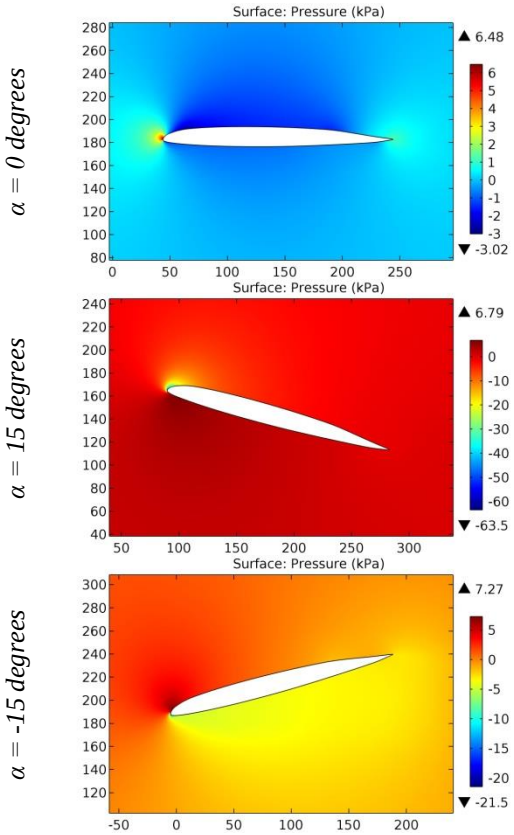

Figure 146. The pressure contours on the surfaces of the NLR-1T airfoil.

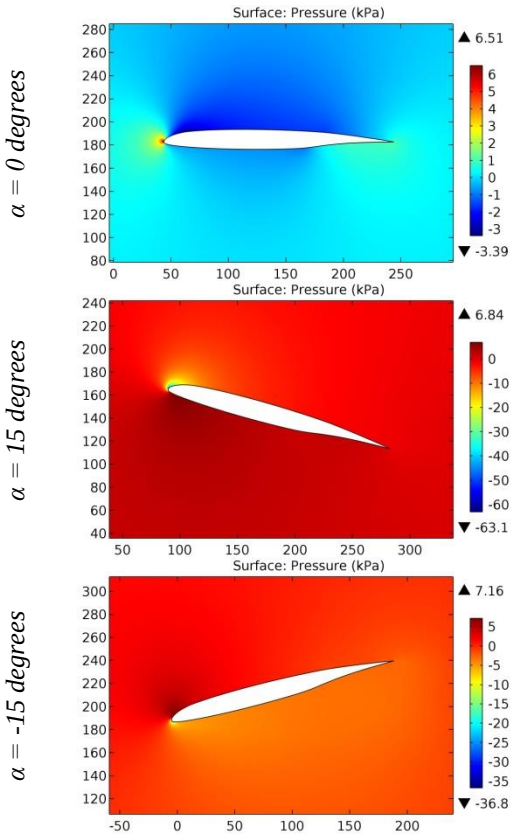

Figure 147. The pressure contours on the surfaces of the NLR-7223-43 airfoil.

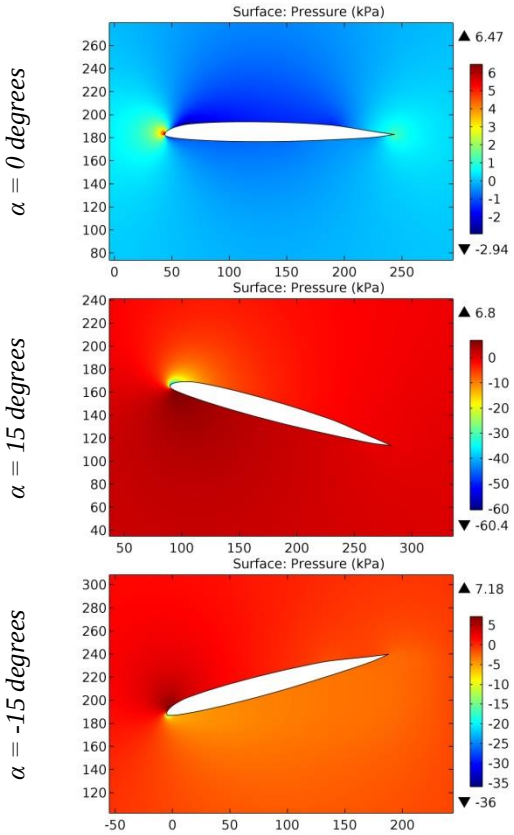

Figure 148. The pressure contours on the surfaces of the NLR-7223-62 airfoil.

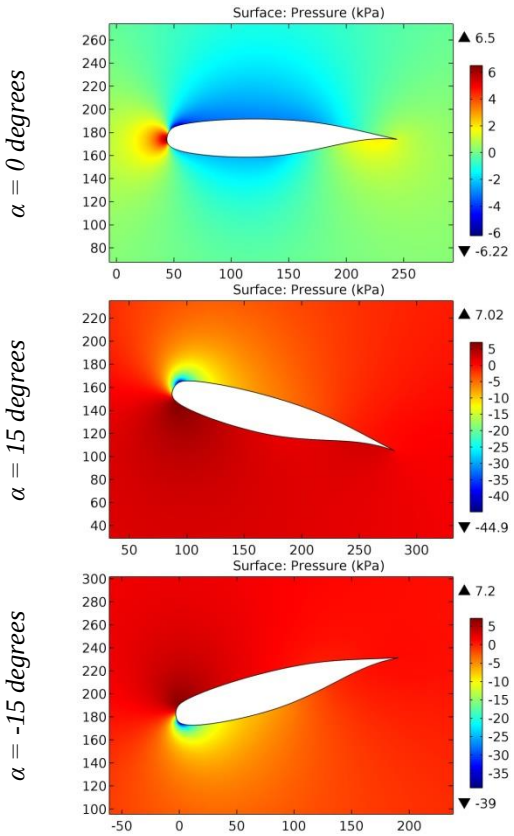

Figure 149. The pressure contours on the surfaces of the NLR-7301 airfoil.

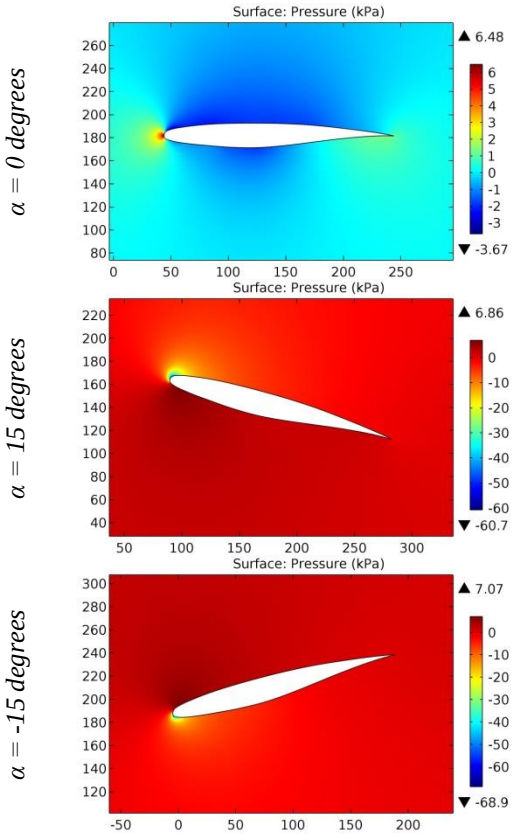

Figure 150. The pressure contours on the surfaces of the NPL airfoil.

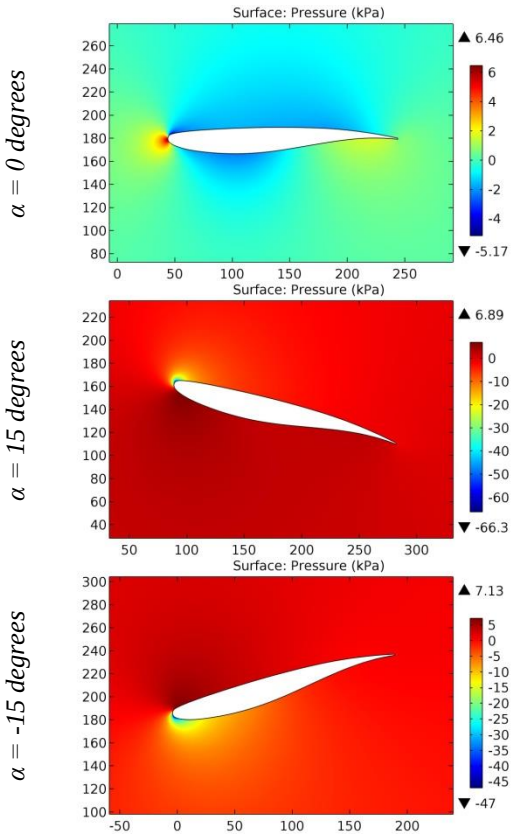

Figure 151. The pressure contours on the surfaces of the NPL 9510 airfoil.

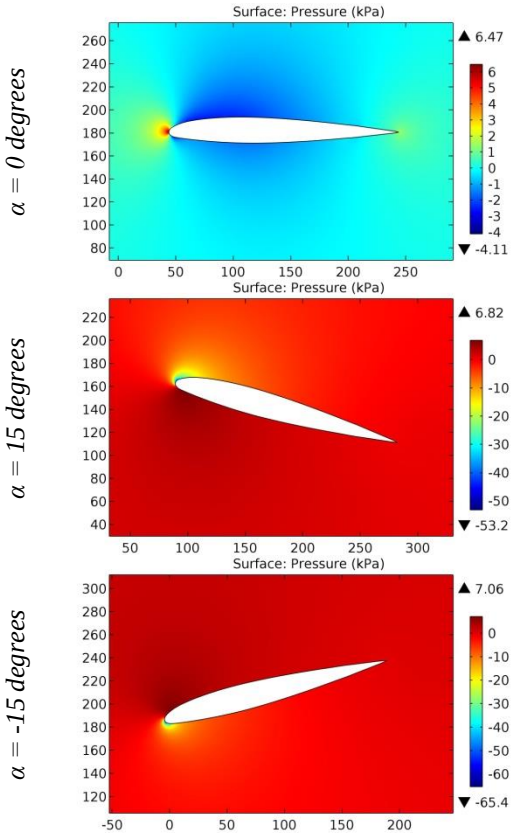

Figure 152. The pressure contours on the surfaces of the NPL 9615 airfoil.

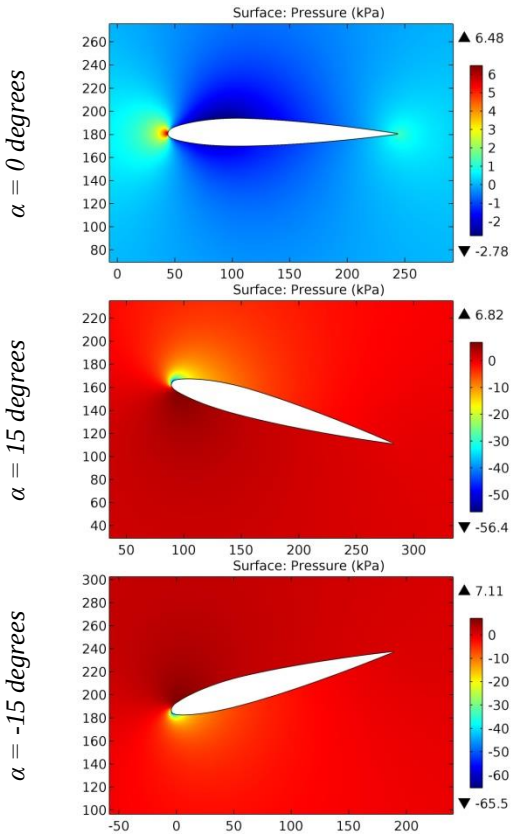

Figure 153. The pressure contours on the surfaces of the NPL 9626 airfoil.

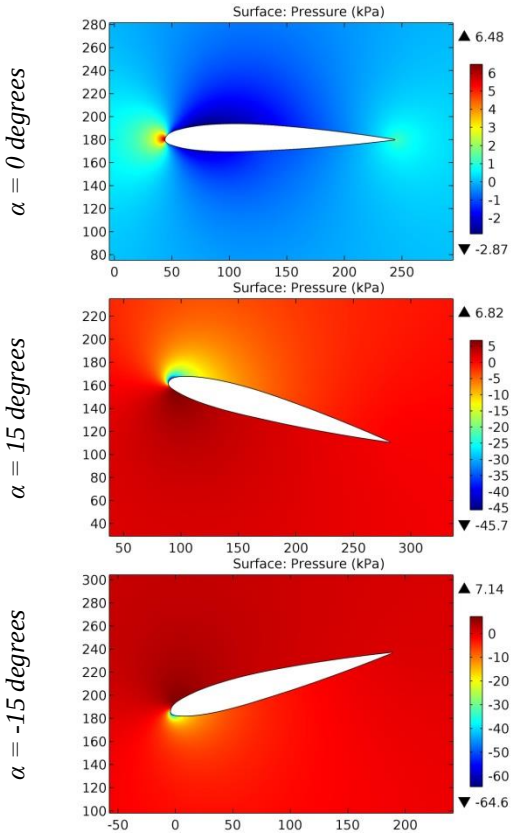

Figure 154. The pressure contours on the surfaces of the NPL 9627 airfoil.

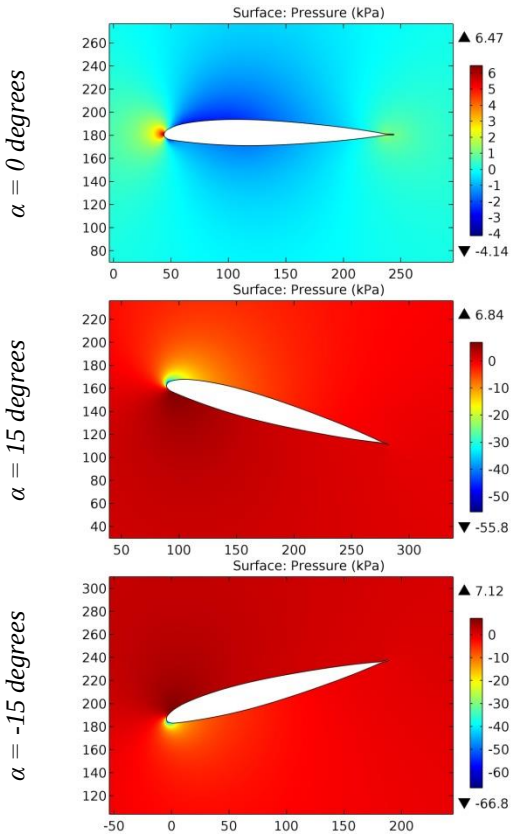

Figure 155. The pressure contours on the surfaces of the NPL 9660 airfoil.

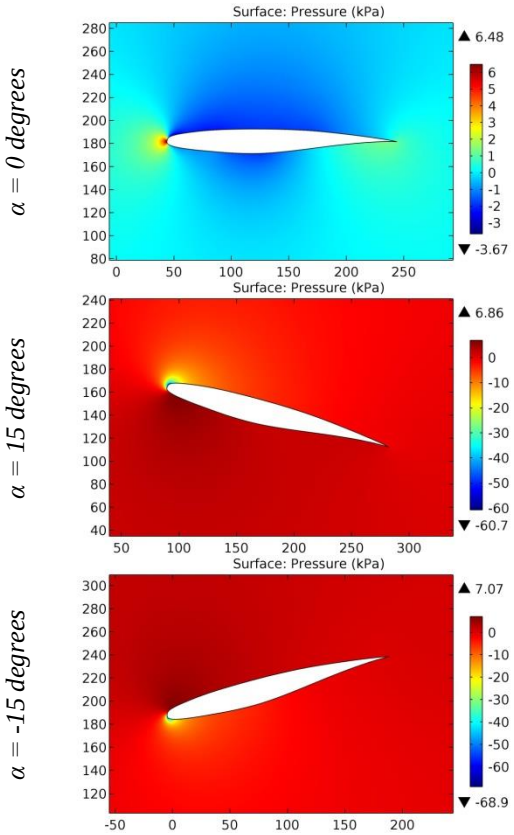

Figure 156. The pressure contours on the surfaces of the NPL transonic airfoil FROM ARC CP 1372.

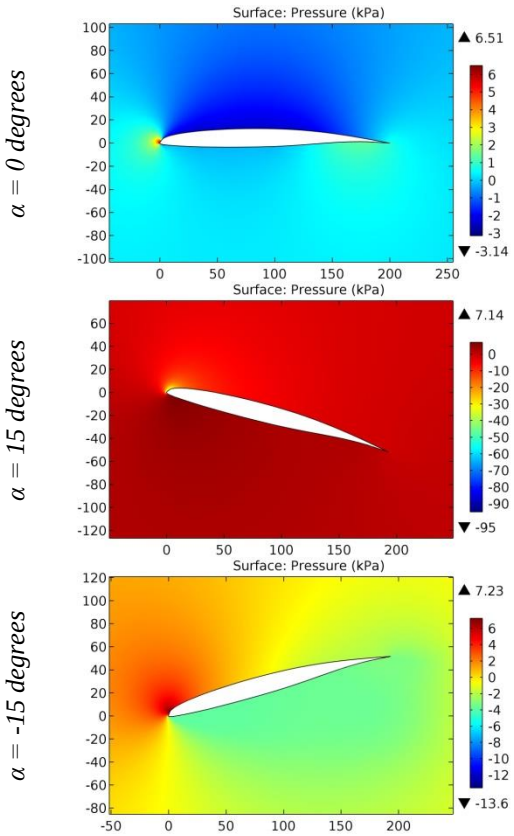

Figure 157. The pressure contours on the surfaces of the NWINGLET airfoil.

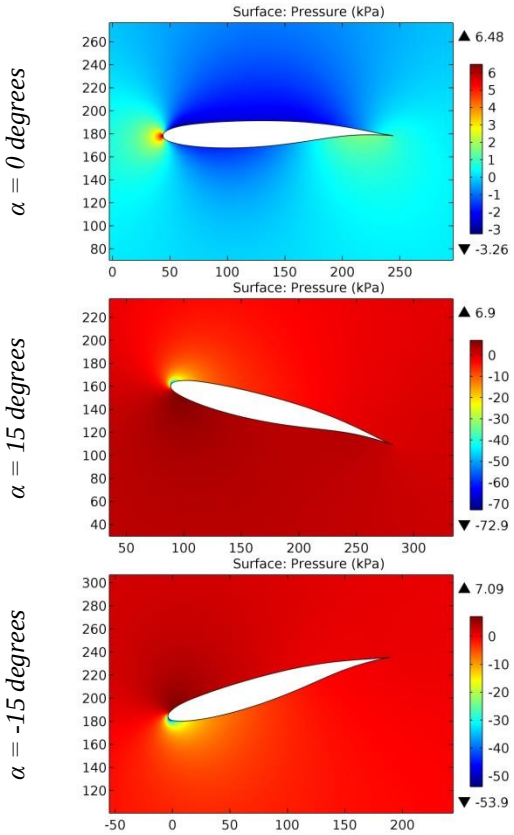

Figure 158. The pressure contours on the surfaces of the NYU-GRUMMAN K-1 airfoil.

The Neelmeyer airfoil has good aerodynamic characteristics during maneuvers and horizontal flight of the airplane: the minimum contact area of the leading edge with air ensures pressure distribution over the small area.

Maximum negative pressure occurs on the leading edge of the NWINGLET airfoil at an angle of attack of 15 degrees.

Conclusion

According to the results of computer calculations, the airfoils with the convex upper surface are subjected to variable pressures from all sides during maneuvers. Thin airfoils of the NASA type experience minimal loads during the horizontal flight of the airplane, so they are ideal for high-speed movements. The NWINGLET airfoil is subjected to significant drag during the climb maneuver of the airplane.

References:

1. Anderson, J. D. (2010). *Fundamentals of Aerodynamics.* McGraw-Hill, Fifth edition.
2. Shevell, R. S. (1989). *Fundamentals of Flight.* Prentice Hall, Second edition.
3. Houghton, E. L., & Carpenter, P. W. (2003). *Aerodynamics for Engineering Students*. Fifth edition, Elsevier.
4. Lan, E. C. T., & Roskam, J. (2003). *Airplane Aerodynamics and Performance*. DAR Corp.
5. Sadraey, M. (2009). *Aircraft Performance Analysis.* VDM Verlag Dr. Müller.
6. Anderson, J. D. (1999). *Aircraft Performance and Design*. McGraw-Hill.
7. Roskam, J. (2007). *Airplane Flight Dynamics and Automatic Flight Control*, Part I. DAR Corp.
8. Etkin, B., & Reid, L. D. (1996). *Dynamics of Flight, Stability and Control*. Third Edition, Wiley.
9. Stevens, B. L., & Lewis, F. L. (2003). *Aircraft Control and Simulation.* Second Edition, Wiley.
10. Chemezov, D., et al. (2021). Pressure distribution on the surfaces of the NACA 0012 airfoil under conditions of changing the angle of attack. *ISJ Theoretical & Applied Science, 09 (101)*, 601-606.
11. Chemezov, D., et al. (2021). Stressed state of surfaces of the NACA 0012 airfoil at high angles of attack. *ISJ Theoretical & Applied Science, 10 (102)*, 601-604.
12. Chemezov, D., et al. (2021). Reference data of pressure distribution on the surfaces of airfoils having the names beginning with the letter A (the first part). *ISJ Theoretical & Applied Science, 10 (102)*, 943-958.
13. Chemezov, D., et al. (2021). Reference data of pressure distribution on the surfaces of airfoils having the names beginning with the letter A (the second part). *ISJ Theoretical & Applied Science, 11 (103)*, 656-675.
14. Chemezov, D., et al. (2021). Reference data of pressure distribution on the surfaces of airfoils having the names beginning with the letter B. *ISJ Theoretical & Applied Science, 11 (103)*, 1001-1076.
15. Chemezov, D., et al. (2021). Reference data of pressure distribution on the surfaces of airfoils having the names beginning with the letter C. *ISJ Theoretical & Applied Science, 12 (104)*, 814-844.
16. Chemezov, D., et al. (2021). Reference data of pressure distribution on the surfaces of airfoils having the names beginning with the letter D. *ISJ Theoretical & Applied Science, 12 (104)*, 1244-1274.
17. Chemezov, D., et al. (2022). Reference data of pressure distribution on the surfaces of airfoils (hydrofoils) having the names beginning with the letter E (the first part). *ISJ Theoretical & Applied Science, 01 (105)*, 501-569.
18. Chemezov, D., et al. (2022). Reference data of pressure distribution on the surfaces of airfoils (hydrofoils) having the names beginning with the letter E (the second part). *ISJ Theoretical & Applied Science, 01 (105)*, 601-671.
19. Chemezov, D., et al. (2022). Reference data of pressure distribution on the surfaces of airfoils having the names beginning with the letter F. *ISJ Theoretical & Applied Science, 02 (106)*, 101-135.
20. Chemezov, D., et al. (2022). Reference data of pressure distribution on the surfaces of airfoils having the names beginning with the letter G (the first part). *ISJ Theoretical & Applied Science, 03 (107)*, 701-784.
21. Chemezov, D., et al. (2022). Reference data of pressure distribution on the surfaces of airfoils having the names beginning with the letter G (the second part). *ISJ Theoretical & Applied Science, 03 (107)*, 901-984.
22. Chemezov, D., et al. (2022). Reference data of pressure distribution on the surfaces of airfoils having the names beginning with the letter G (the

third part). *ISJ Theoretical & Applied Science, 04 (108)*, 401-484.

23. Chemezov, D., et al. (2022). Reference data of pressure distribution on the surfaces of airfoils having the names beginning with the letter H (the first part). *ISJ Theoretical & Applied Science, 05 (109)*, 201-258.
24. Chemezov, D., et al. (2022). Reference data of pressure distribution on the surfaces of airfoils having the names beginning with the letter H (the second part). *ISJ Theoretical & Applied Science, 05 (109)*, 529-586.
25. Chemezov, D., et al. (2022). Reference data of pressure distribution on the surfaces of airfoils having the names beginning with the letter I. *ISJ Theoretical & Applied Science, 06 (110)*, 1-7.
26. Chemezov, D., et al. (2022). Reference data of pressure distribution on the surfaces of airfoils having the names beginning with the letter J. *ISJ Theoretical & Applied Science, 06 (110)*, 18-25.
27. Chemezov, D., et al. (2022). Reference data of pressure distribution on the surfaces of airfoils having the names beginning with the letter K. *ISJ Theoretical & Applied Science, 07 (111)*, 1-10.
28. Chemezov, D., et al. (2022). Reference data of pressure distribution on the surfaces of airfoils having the names beginning with the letter L. *ISJ Theoretical & Applied Science, 07 (111)*, 101-118.
29. Chemezov, D., et al. (2022). Reference data of pressure distribution on the surfaces of airfoils having the names beginning with the letter M. *ISJ Theoretical & Applied Science, 10 (114)*, 307-392.